

POLITECNICO DI MILANO

Corso di Laurea magistrale in Ingegneria Biomedica
Scuola di Ingegneria Industriale e dell'Informazione



Circulating tumor cells and early cancer detection: toward a
high throughput Lab-On-Chip dynamic filtering of a blood
sample

Relatore: Prof. Guglielmo LANZANI

Correlatore: Dott. Luigino CRIANTE

Tesi di laurea di:

Filippo STORTI

Matr. 837159

Anno accademico 2016/2017

Contents

Sommario	13
Abstract.....	15
Introduction	16
1.1 Circulating Tumor Cells (CTCs)	18
1.2 CTCs: clinical utility and applications.....	23
1.3 CTCs detection: Non-microfluidic technologies	28
1.4 CTCs detection: Microfluidic Technology and lab-on-chip approach	32
1.5 Figures-of-merit for CTCs detection topic	34
1.6 LOCs: overview	35
1.7 Immunoaffinity-based methods	36
1.8 Label-free methods	40
1.9 Label-free approach: dielectrophoresis (DEP)	41
1.10 Label-free approach: magnetophoresis	42
1.11 Label-free approach: Acoustophoresis	44
1.12 Label-free approach: inertial hydrophoresis	45
1.13 Label-free approach: Filtration	47
1.14 Label-free approach: Deterministic Lateral Displacement (DLD)	50
1.15 Main project and aim of the thesis.....	58
Materials and methods.....	63
2.1 PDMS: a brief overview	63
2.2 Femto-laser micromachining fabrication.....	65
2.3 Femtosecond Laser Irradiation, followed by Chemical Etching (FLICE) technique 66	
2.4 Modification of the substrate properties: hints of theory.....	66
2.5 Chemical etching	68
2.6 Chemical etching: parameters.....	72
2.7 Microfluidic devices fabrication	73
2.8 Designing and control: SCA software	74
2.9 Writing: femtosecond laser micromachine	75
2.10 Femtolaser micromachine: laser source.....	76
2.11 Femtolaser micromachine: optical beam handling line	76

2.12	Femtolasar micromachine: beam focusing	76
2.13	Femtolasar micromachine: 3D sample movement system.	77
2.14	Tests instrumentation and materials	77
Experimental activities		80
3.1	SCA: device design.....	80
3.2	Femtolasar: writing procedure	83
3.3	Femtolasar: writing parameters	85
3.4	Devices realization.....	87
3.5	Tests: sample preparation	94
3.6	Tests: procedure	95
3.7	Test: simplifications.....	97
Results		98
Discussion and conclusions		107

List of figures

Figure 1.1: Histograms showing the top ten causes of death (A) globally in 2015 and (B) in high-income economies in 2015. It could be noticed that cancer hold a relevant place in the global ranking (A) and it is even more present in the ranking of high-income economies, where, summing up the different types of cancer, the count of deaths reaches 105 per 100 000 population (B). [1].....4

Figure 1.2: Schematic of epithelial cells, showing the main differentiation properties disrupted by EMT: apico-basal polarity, epithelial phenotype, cell to cell junctions.....6

Figure 1.3: CTCs, EMT/MET and cancer progression: a schematic of the reversible EMT model for cancer progression. Invasion involves epithelial cells losing their polarity and detaching themselves from the basement membrane through EMT activation. Metastasizing cells then directly enter the circulation. Circulating tumor cells then travel to distant sites and exit the bloodstream. Once they extravasate they may proliferate and reverse back to an epithelial phenotype to form macrometastases.(**Friedlander et al 2013**).....7

Figure 1.4:

- A) Schematic of the size proportion between big CTCs and blood cells (WBCs and RBCs)
- B) schematic of EMT process showing CTCs phenotypical heterogeneity.....9

Figure 1.5: Blood Sampling (A) versus Surgical Biopsy (B): the latter involves much more complex instrumentation, starting from the needle – specially designed depending on the application- and following with the navigation system, which allows the needle to reach deep organs in the body.10

Figure 1.6: Kaplan-Meier plots showing CTCs count per 7.5 ml of blood versus survival in Breast Cancer (A) and in Colorectal cancer (B). the higher the number of CTCs found in the blood sample the lower the Survival Probability of the patient. (**Andree et al_2015**).....12

Figure 1.7: CellSearch™ System components. (1) CellSave Preservative tubes, in which blood is collected and stabilized for up to 96 h at room temperature, allowing the samples collection and the subsequent analysis in distant places. (2) Automated

CELLTRACKS®AUTOPREP® System for the immunomagnetically cell enrichment and staining. (3) CELLTRACKS ANALYZER II® System for the selected cells automatic image generation.16

Figure 1.8 Number of publications regarding microfluidic chips related to CTCs versus CellSearch™ one. It could generally be noticed a growing trend of the research world attention to this topic and, specifically, to the microfluidic technology. (**Jackson et al_2017**)17

Figure 1.9: Gilupi CellCollector™ system: a 20-mm long gold-coated catheter tip of the stainless steel Seldinger guidewire, functionalized with hydrogel labelled with EpCAM antibodies, in direct contact with blood circulation.(**Saucedo-Zeni et al_2012**).....17

Figure 1.10: Schematic of Gilupi CellCollector™ functioning (A) and real example of application of Gilupi System (B).....20

Figure 1.11: Scheme of one of the possible CTCs analysis subdivision by implied techniques.22

Figure 1.12: Immunoaffinity-based LOCs. Positive selection methods: (A) Silicon microposts (diameter of 100 μm and spacing of 50 μm) whose surface has been functionalized with antibodies increase the surface to cell contact area, increasing the capture efficiency. (B) Herringbones structures create a chaotic flow in the channel to increase the collisions between target cells and the functionalized surfaces. (C) Ferromagnetic microbeads targeted CTCs are attracted on the bottom of the chip through a magnet, the non-interesting hematologic cells are flushed away then the cancer cells are released. (D) Magnetic beads attached on the CTCs surface allow the direct deviation of the target cells from the mainstream by applying a magnetic field (E) Silicon antibodies-functionalized nanopillars create a sort of “wood” in which the CTCs are trapped. Negative selection methods: (F) the CTC-I-chip: After a first preparation step in which WBCs are labelled with magnetic beads, the sample will be processed by three stages: a lateral displacement stage will separate RBCs from the main stream, the a hydrofocusing path will put remaining cells in a row and, finally, an applied magnetic field will deviate the leukocytes in a waste output, leaving – theoretically – only CTCs in the stream.....23

Figure 1.13: DEP LOCs. (A) 3D DEP lateral displacement. The electric field is applied in a V-shaped microchannel. Such that the cell displacement could take place on the walls; each cell reaches a precise point on the wall, according to its type (**Cheng et al_2015**). (B) Commercial DEP system, called ApoStream™, which exploits the dissimilarities in the frequency-dependent dielectric properties of the different cell types.(**Gupta et al_2012,Jackson et al_2017**)29

Figure 1.14: Label-free magnetophoretic LOC for breast blood circulating cancer detection. (A) Conceptual block diagram of the device functioning; the analysis process is divided in two steps: RBCs removal by a Paramagnetic Capture Mode cell microseparator and CTCs identification through Electrical Impedance Spectroscopy. (B) PCM microseparator: a ferromagnetic nickel wire is incorporated along the length of the microchannel. When activated, It attracts the RBCs on the central section of the microchannel, thus allowing the output separation in three outlets: outlet 2 collects RBCs, while 1 and 3 gather nucleated cells (WBCs and CTCs). (**Han et al_2006**)30

Figure 1.15: Acoustofluidic Lab-on-chip. (A)Acoustophoresis general concept: after the acoustic pressure node the cells are dislocated in bands across the microchannel, thus allowing the separate collection. (B) Acoustofluidic device for CTCs isolation composed by 3 steps. The first is the pre-alignment step through two acoustic wave nodes to put in two rows the input cells. Then, through inlet b a cell-free fluid, with a different acoustic impedance, is injected in the chip. This fluid pushes all the cell sideway on the walls, before the acoustic separation is met. The analytes with less lateral displacement from the chip walls are discarded through outlet 1. A third acoustic wave node constitutes the concentration step; its goal is to better focus the isolated cells and direct them towards the outlet 3. The fee-cell liquid is discarded through outlet 2. (**Antfolk et al_2015**).....32

Figure 1.16: Vortex HT chip: an example of straight channel interrupted by expansions of the section of the channel (Reservoirs) (**Dhar et al_2016**).....33

Figure 1.17: Spiral chip technology: it exploits the interactions between inertial forces and centrifugal forces, that overlapping within the chip generate the so called “Dean vortices”, which allow a separation in size on the cross-sectional area of the channel. (**Warkiani et al_2014**)34

Figure 1.18: CTCs filtration devices: (A) filtration membrane to capture circulating cells: to use this type of approach is needed a post-analysis recovery step and a pre-analysis cell fixation step, to prevent lysis. (B) solution to adapt membrane filtration: the blood sample is injected through the inlet 1 and aspirated through a syringe from the outlet 2. CTCs are blocked on the membrane and can be immune-stained and further analysed through fluorescence microscopy.(**Yousouff et al_2015**).....35

Figure 1.19: Filtration devices: (A) MOA capture platform: the rooms created between the pillars entrap the CTCs, but not the othe blood cells due to their smaller size- In the second zoom, anti-epcam functionalized microbeads were attached to the CTCs surface in order to increase the cpture efficiency of the system (**Kim et al_2012**). (B) triangula-shaped pillars used to detect and block CTC clusters in whole blood, for further analysis.(**Sarioglu et al_2015**).....36

Figure 1.19 B: Schematic of DLD geometry, resuming the principal parameters to defying it. (**Kruger et al_2014**).....37

Figure 1.20: Schematic of the basic functioning principle of Deterministic Lateral Displacement: (A) particles with radius (a) greater than the critical radius (R_c) follow the direction defined by the micro-post array, while the trajectory of particles with smaller radius ($a < R_c$) is imposed by the initial streamline (B) schematic of the streamlines: the cells larger than the critical diameter (D_c) deviate their path towards the next streamline at each obstacle met. (**Wyatt Shield et al_2015, Davis et al_2006**).....38

Figure 1.21: Different pillar shapes: (A) Circular, squared and I-shaped were studied in a RBC-separation problem from the whole blood, resulting that I-shaped had a greater efficiency (**Zeming et al_2012i**) (B) triangular shaped pillars were applied in the CTCs detection problem, reaching good recovery values and extremely high throughput. (**Loutherback_et_al_2012**).....40

Figure 1.22 Lateral displacement obtained by a combination of two flows and a pillar matrix, characterized by lateral gaping varying in size and no row shift. (**Park et al_2016**).....41

Figure 1.23: DLD chip used for CTC separation from blood. (A) Schematic of the chip: it presents one inlet for the whole blood and three outlets. CTCs are deviated at the centre of the chip and enriched at the middle outlet, while blood cells, smaller in diameter, flow following the main stream towards the external outlets. (B) Zoom showing the main streamline and the so called “bumping mode”, that is the typical flow of particles with diameters greater than D_c . (C) Zoom showing the ideal output condition: CTCs at the centre of the chip and the other blood cells on the external sides. (D) The device is characterized by a length of 35 mm and a width of 3.5 mm, as it can be seen by comparison with a coin.....42

Figure 1.24: CTC i-Chip as an example of DLD integration on a platform to perform RBCs separation from a blood sample. The picture shows the three stages of the device: hydrodynamic cell sorting by DLD, inertial hydrofocusing and magnetic displacement. It is also shown the operative modes of the chip: positive selection or negative selection. **(Jackson et al_2017, Karabacak et al_2014)**.....43

Figure 1.25: Block diagram of the three-steps CTC identification and isolation device.....46

Figure 1.25 (A): Step 1. The whole blood is taken as input and, through a dynamic filtering, RBCs are separated and discarded. The remaining CTCs and WBCs are taken as input in Step2.....47

Figure 1.25 (B): Step 2. WBCs and CTCs exiting from Step 1 are aligned on a row one behind another in preparation for Step 3.47

Figure 1.25 (C): Step 3. The aligned cells exiting from Step 2 are taken in input. The Raman Spectroscopy will discriminate CTCs from WBCs according to their different composition and count them. WBCs are discarded, while CTCs could be enriched for further analysis...48

Figure 2.1: Schematic representation of sealing procedure.....51

Figure 2.2: Schematic of the non-linear processes: (A) multi-photon absorption. (B) Tunneling ionization. (C) Avalanche ionization.....54

Figure 2.3: Resume of the structural modification laser-induced obtainable in fused silica, through femtolaser technique. (1) Weak anisotropic index variations: this modification of the material structure is not sufficient to provide to the chemical etching step a favourable

substrate for material subtraction. (2) Nanogratings generation: structural modifications can be inducted at any height within the sample, allowing volume irradiation (3) Material ablation: the related laser beam working parameters allow only a superficial processing of the sample.55

Figure 2.4: Schematic representation of the nanogratings generation phenomenon. In the case represented, \vec{W} is perpendicular to \vec{E} , thus the generated nongratings are parallel oriented to the writing direction.....56

Figure 2.5: Schematic representation of the relation between polarization (\vec{E}), writing direction (\vec{W}) and nanogratings generation in determining the etching-rate.....57

Figure 2.6: Microfluidic channels HF etch-rate in function of the pulse energy and writing polarization. (\blacktriangle) radiation electric field (\vec{E}) direction perpendicular to writing one (\vec{W}) (\bullet) \vec{E} 45° oriented with respect to \vec{W} . (\blacksquare) $\vec{E} \parallel \vec{W}$ Taylor et al_2008.....57

Figure 2.7: conical shape effect due to the isotropic behaviour HF solution.....58

Figure 2.8: Ultrasound sonication set-up for KOH etching.....60

Figure 2.9: SCA interface. (1) Command window; (2) Command list; (3) Executive commands; (4) 3D graphics for the design visualization; (5) Laser hardware parameters selection; (6) Estimated time of writing.....61

Figure 2.10: Schematic of a femtosecond laser system for used silica sample writing.....62

Figure 2.11: Microfluidic pump system. (A) OB1 controller, the 4-channel flow control system. (B) Schematic of the connections in an experimental set-up.....65

Figure 2.12: Figure showing the experimental set-up.....66

Figure 3.1: Example of complex geometry definition in SCA software, not only the line profiling its elaborated, but also the structure position becomes cumbersome.....68

Figure 3.2: example of the creation of a complex and asymmetrical structure. (A) Design of the desired shape through an external software. (B)The desired writing parameters are selected. (C) 3D structure achievement by superimposition at different Z of the planar figure

imported. The space between the subsequent plans is also a project parameter. It can be chosen to make the volume more densely or sparsely written: (C) three plans; (D) many plans.69

Figure 3.3: Example of “patching” design to obtain a performance increase in the etching process. (B) and (C) laser written examples of patches.....70

Figure 3.4: Section of femtolaser micromachine. (A) AutoFocus automated system for the transparent sample surface identification. (B) Writing laser beam during a fabrication process.....72

Figure 3.5: Low stage accelerations (20 mm/s²) (A) versus high stage accelerations (200 mm/s²) (B).73

Figure 3.6: (A) schematic of the particular case of DLD presented in the relative introduction section. (**Park et al_2016**) (B) Schematic of the working principle of the first chip generation implemented in this project.75

Figure 3.7: first generation of devices: the open to the surface pillar matrix chamber. (A) schematic of chip sealing. (B) the chip sealed.76

Figure 3.8: Embedded pillar shapes, fabricated with FLICE technology: (A) the ongoing HF etching in the combined approach HF for large non-detailed volumes and KOH for small and precise volumes. (B). Pillars after etching in top and side view.....77

Figure 3.9: microspheres showing the tendency of depositing themselves on the bottom of the chip.78

Figure 3.10: Embedded pillar matrix chip: (A) Geometry of the pillar chamber: the only useful separation barrier has turn out to be, from the experimentations, the array highlighted in figure. (B) Simulation showing a significant decrease in flow through the pillar matrix: this area of the chip resulted not only not useful for the separation purpose but also counterproductive for the fluidodynamic behaviour of the chip. (C) Simulation showing a simplified geometry that highlights the “shadow” area that the flow forms in front of the pillars.79

Figure 3.11: (A) Trapping-zone effect due to the circular shape of the pillars composing the “discriminant barrier” of the device. (B) Optimized geometry, showing the introduction of the “patch” writing method. (C) Simplified simulation showing the slightly reduced shadow-zone effect.80

Figure 3.12 Connectorization: polymeric UV glue fixing to fasten the tube to the chip. (A) Tube cross section, external diameter: 360µ m, internal diameter: 150 µm.82

Figure 4.1: first generation chip characterized by pillar chamber open to surface. (A) top view: the pillar diameters showed a good homogeneity. (B) Side view: the pillars were uniform along the Z axis.86

Figure 4.2.1: Complex and small shapes (~ 35 µm) were obtained with a good precision degree embedded in the glass substrate.87

4.2.2: Post-etching figure of the optimized chip version: (A) Very good precision was obtained in the reproducing of the software design. The gap size, the critical dimension of the chip – since if the separation is successful or not – has been designed to let pass only RBCs so values could be acceptable if in the range: 10 µm – 15 µm. The obtained mean gap size was $13.41 \pm 1.56 \mu\text{m}$87

Figure 4.3 A: Figure taken in real-time during the tests of a buried device. (A) Test with a solution of only small particles (10 µm): the device is correctly deviating in the waste outlet the small particles. A negligible number of them go in the target outlet -i.e. the wrong outlet.....88

Figure 4.3 B: Figure taken in real-time during the tests of a buried device. Test with small and large particles: the large particles are well separated from the small ones and rightly directed toward the correct outlet. Few small particles, as noticed in the previous tests, go in the wrong direction.....89

Figure 4.4: Graphs of the amount of time to process 0.5 ml of water at different constant inlet pressures (Up) and the relative throughput (Down) for (A) the pillar matrix chip and (B) the chip referred to as the “optimized version”.91

Figure 4.5: Throughput: optimized chip versus pillar matrix. (O) Optimized chip and (*) pillar matrix.95

List of tables

Table 1.1: Synopsis of the blood cells and circulating tumor cells dimensions and their overlapping.....	8
Table 1.2: summary of the main applications of circulating tumor cells detection, seen as a new generation of biopsy, named “Liquid Biopsy”.....	14
Table 1.3: Resume of the Lab-on-Chips main advantages over the currently in use laboratories bench-top techniques.	20
Table 1.4: Synopsis of the critical characteristics for the new generation of Lab-on-Chips..	21
Table 1.5: figures of merit currently used in the literature of the circulating tumor cells isolation research field. (Jackson et al_2017,Ferreira et al_2016)	22
Table 1.5 B: synopsis of immunoaffinity-based LOCs for CTCs detection and isolation. It could be noticed how either the sensitivity and the capture efficiency variate due to the different used cell lines. (Jackson et al_2017).....	26
Table 1.6: advantages of label-free LOCs technologies in the CTCs isolation from the whole blood problem.....	27
Table 1.7: Synopsis of label-free methods performances for CTC and other cell detection. (Jackson et al_2017 , gupta et al 2012,liu et al 2013, louterback et al 2012, beech et al 2012...).	44
Table 4.1: Resuming of the processing behaviour of the created devices, showing the maximum throughput reached for each geometry and the “free” volume - i.e. the volume, within the chip, not occupied by the pillars; it is calculated with respect the total volume of the device.....	93

Sommario

Al giorno d'oggi il cancro rappresenta una delle principali cause di morte nel mondo. In questo campo, è stimato che circa il 90% delle morti per cancro sia dovuto allo sviluppo di metastasi. Negli ultimi anni, quindi, il mondo della ricerca ha focalizzato la sua attenzione su questa malattia. In particolare, un gruppo di cellule, definite come cellule tumorali in circolazione (CTC) hanno dimostrato di aver particolari peculiarità che potrebbero essere utilizzate nella lotta al cancro. Queste cellule, una volta distaccate dalla massa tumorale, penetrano nella circolazione sanguigna e sembrano essere alla base del processo di diffusione metastatica. Molti studi hanno, inoltre, dimostrato una significativa utilità clinica del processo di detezione di queste cellule come ad esempio: la predizione di scarsa prognosi, il rilevamento precoce del cancro, il monitoraggio sia della progressione del cancro che dell'efficacia delle terapie utilizzate per combatterlo. Uno degli aspetti più impegnativi rappresentati dall'identificazione e isolamento di queste cellule è dato dalla loro rarità: è stato dimostrato, infatti, che possono essere presenti in un numero di 1-1000 per ml di sangue, mentre i conteggi delle altre cellule del sangue (leucociti ed eritrociti) sono dell'ordine di 10^6 - 10^8 . Questo, in aggiunta alla necessità di tecniche di analisi ad alta efficienza e alto throughput, hanno portato la microfluidica ad essere molto attiva in questo campo. Per questo motivo, nei laboratori del CNST@IIT di Milano, è stato concepito un grande progetto di ricerca per la realizzazione di un Nuovo dispositivo microfluidico che soddisfi tutti gli attuali requisiti. Le parole chiave per la creazione di un dispositivo che possa realmente trovare applicazione in campo clinico, e quindi, dare una spinta alla detezione precoce del cancro e alla lotta contro di esso, possono essere riassunte in: basso costo, alta efficienza, alto throughput, e, soprattutto, completamente label-free. Il progetto affronterà questa sfida, sfruttando i vantaggi di una strategia integrata, divisa in tre principali sezioni. Il primo blocco si occuperà del filtraggio del sangue preso in ingresso, per rimuovere da esso quanti più eritrociti sia possibile, migliorando così il tempo di analisi degli step successivi. I globuli bianchi e le CTC rimanenti, che usciranno dal blocco di filtraggio dinamico, saranno quindi poste in riga -una dietro l'altra - per permettere alla terza sezione di identificare in modo selettivo le cellule tumorali. Questo ultimo step, tuttavia, non deve essere pensato solo come passaggio di mera selezione e conteggio: implementa, infatti, una spettroscopia Raman delle particelle in ingresso. Questo fornirà una maggiore quantità di

informazioni sulle cellule tumorali: non solo, infatti, sarà in grado di distinguere tra CTC e altri tipi di cellule ma sarà anche capace di caratterizzare ogni cellula, assegnandole uno spettro della sua composizione chimica. In aggiunta, le CTC hanno anche dimostrato una grande eterogeneità anche all'interno dello stesso tipo di cancro: questo metodo di analisi innovativo, quindi, potrà aiutare anche nell'identificazioni di tali sottogruppi.

Questa tesi, quindi, rappresenta il primo passo verso la creazione di un dispositivo lab-on-chip, opto-microfluidico e completamente integrato in un substrato di vetro per la rilevazione label-free di CTC nel sangue. In particolare, affronterà la sfida di implementare la prima sezione del progetto presentato sopra, cercando di sfruttare tutti i vantaggi offerti dall'innovativa tecnica di micromachining tramite femtolaser, seguito da etching chimico (FLICE). Tra questi uno dei più interessanti è fornito dalla capacità di generare complesse strutture 3D – con quasi nessuna limitazione nella forma e nella dimensione – integrate in substrati di vetro con un'accuratezza micrometrica. Verranno, inoltre, presentate nuove soluzioni per migliorare questa tecnica, al fine di raggiungere fabbricazioni più efficienti e precise di chip microfluidici.

Abstract

For this reason, in the CNST-IIT facility of Milan, it has been conceived a big research project for the realization of a new microfluidic device that addresses all the up to now requirements. The key-words in order to create a device that could really be applied in the clinical routine, and thus, push forward the early cancer detection and the cancer struggle can be resumed in: low cost, high efficiency, high throughput, and, especially, completely label-free. The project will face this challenge taking advantage of a three steps integration strategy. The first step will filter the whole blood sample in input to remove from it as many erythrocytes as possible, thus enhancing the analysis time and the efficiency of the subsequent stages. The white blood cells and circulating tumor cells, coming out from this dynamic filtering, will be put in a row -one behind the other – to allow the third step to selectively identify the tumoral cells. However, this last step should not be thought of as a mere selection and counting passage: it implements, indeed, a Raman spectroscopy of the input particles. Thus, will give a greater amount of information about tumoral cells: it will not only be able to discriminate between CTCs and the other types of cells but it will also characterize each cell, assigning to it the spectrum of its chemical composition. Furthermore, CTCs have shown a great heterogeneity, also within the same cancer type: this innovative analysis method, thus, could help also to identify sub-groups in CTCs.

This thesis represents, thus, the first step toward the creation of a lab-on-chip, opto-microfluidic and glass embedded device for the label-free CTC detection in a blood sample. In particular, it will face the challenge of implementing the first stage of the above-mentioned project, trying to exploit all the advantages offered by the innovative femtolaser micromachining followed by chemical etching (FLICE) technology. Among these, the most interesting characteristic is the capability of generating complex 3D structures -with almost no limitation in shape and dimension - buried in a fused silica substrate with a micrometric accuracy. Furthermore, it will propose new solution to improve this technique, in order to implement a more efficient and precise realization of on-a-chip microfluidic devices.

Chapter 1

Introduction

The last century innovations in medicine field have led, particularly in the last decades, the research on a path of completely new challenges. Since the life span has been increased, new threats to human health have emerged. A relevant part of the whole world mortality can be explained by pathologies that could be defined as “long term” ones, all of them showing the same behaviour: a “silent” rising, which doesn’t particularly affect the health of the subject, a development period, which creates, in a variable way, symptoms for the subject and eventually the impairment of some vital functionality that definitely leads to the subject death. In recent times, therefore, moving the focus on the rising of these diseases became one of the emerging needs. The capability to early detect the signals of the presence of these pathologies could bring a step further the battle against the latter. In this “category” of pathologies cancer can be surely referred to as a holder of a prominent place.

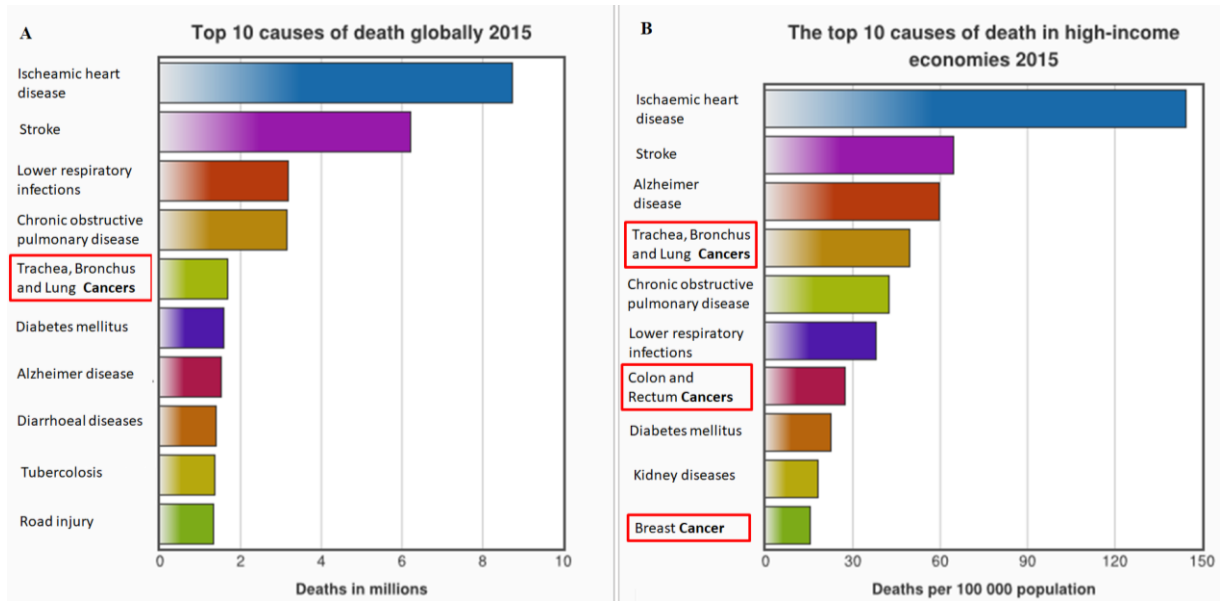


Figure 2.1: Histograms showing the top ten causes of death¹ (A) globally in 2015 and (B) in high-income economies in 2015. It could be noticed that cancer hold a relevant place in the global ranking (A) and it is even more present in the ranking of high-income economies, where, summing up the different types of cancer, the count of deaths reaches 105 per 100 000 population (B). [1]

Simplifying the origin process which leads to the development of a tumoral mass, it could be said that, for multiple and complex reasons, a small group of cells of a given organ, at a certain time, changes its normal behaviour, starting to work against the normal functionality of the hosting organ. Since the earlier steps of the tumoral growth some of these cells penetrate the circulation system and their final goal is to find a new place where they could give rise to a new neoplasia. This is the basic process lying behind the birth of metastases, and the cells in charge of doing that are called: Circulating Tumor Cells (CTCs).

¹ Graphs obtained from the World Health organization (WHO) site:

1.1 Circulating Tumor Cells (CTCs)

This definition encompasses a high number of different types of cells, also showing different phenotypes and different genetic expressions. The main common point is the goal of these cells: infiltrate themselves in the circulation system and find a new place where to set a suitable niche to favor the growth of a new tumoral mass. This process is thought to be at the basis of the creation of metastases, which is considered as the leading cause of cancer-related death [2,3], and it's called epithelial to mesenchymal transition (EMT). The EMT follows few simple steps which are supposed to well explain the aggressive behaviour of the cancer progression. The transition involves the epithelial cells of the primary tumor: first of all, it sees the loss of the epithelial markers of these cells, then the acquisition of mesenchymal markers. This involves the disruption of the cell to cell junctions and the disruption of the apico-basal polarity. With the latter term is defined that property of this type of cells to have extremity areas, within the cell, morphologically differentiated according to the orientation with respect to the environment out of the cell (top or bottom). So, these cells present different types of organelle - and different types of membranes - whether they confine with the outside of the body or the lumen of internal cavities (apical) or connective tissue distant from the lumen (basolateral). The loss of this property, hence, means also the loss of the functional specialization of the cell. The last step is the remodeling of the cytoskeleton of the cells, giving them a greater deformability [4].

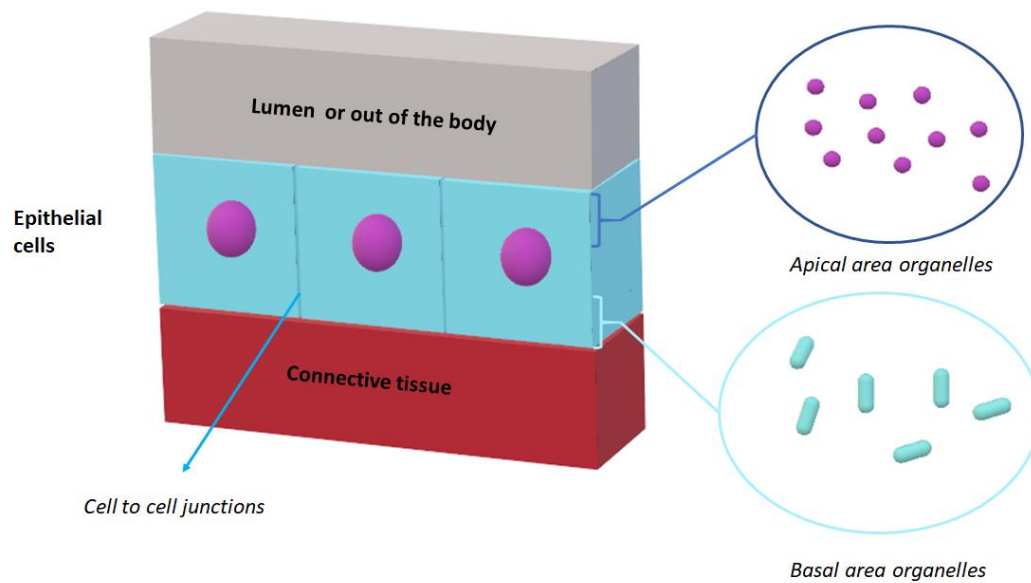


Figure 2.2: Schematic of epithelial cells, showing the main differentiation properties disrupted by EMT: apico-basal polarity, epithelial phenotype, cell to cell junctions.

In this way, the cells that undergo EMT are in a mesenchymal state, i.e. undifferentiated, and free to move, thus allowing the penetration of the circulatory system vessels. Some studies have shown another interesting capability of EMT: its contribution to drug resistance [4]. Thus, supporting the hypothesis that EMT could really facilitate cancer progression. The key factor in this process is its reversibility. In fact, if the intravasated cells manage to survive in the circulation and reach distant places from the original site, i.e. the primary tumor, through the inverse mechanism, called Mesenchymal to Epithelial Transition (MET), they could infiltrate new tissues. Once CTCs have pervaded the new tissue, by means of MET they recover their epithelial properties and can start growing a new tumoral mass, through stimulation of angiogenesis [2,3] It's important to underline that this mechanism doesn't happen immediately: the tumoral cells that invaded new organs could remain "silent" for long periods of time. For example, in breast cancer these cells could lie dormant in site for even over a decade [5].

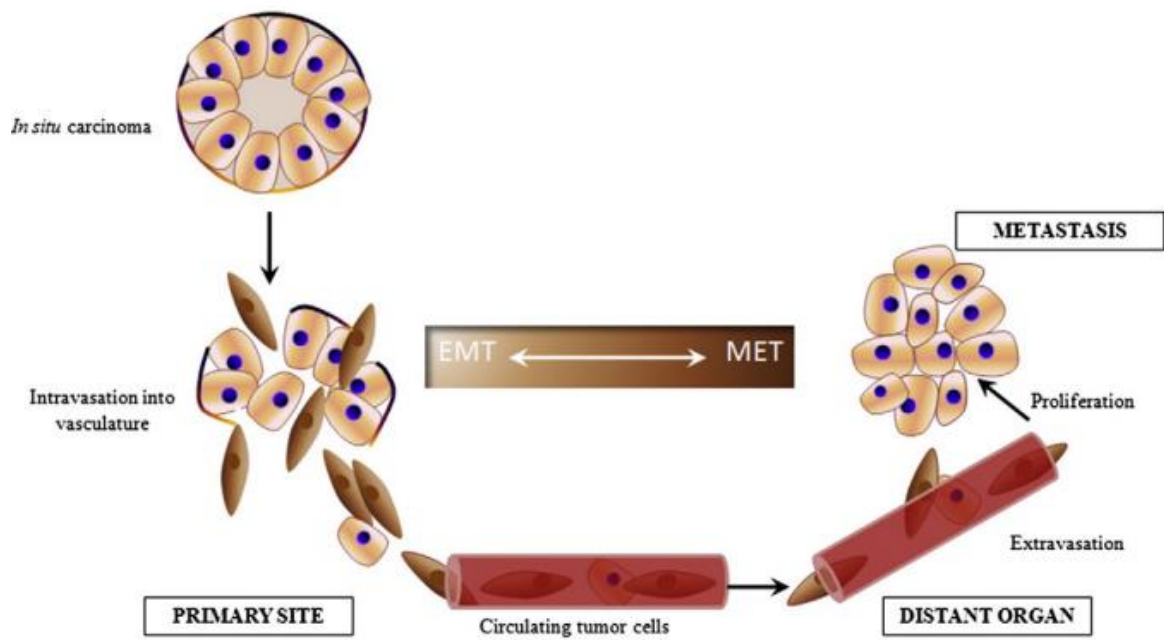


Figure 1.3: CTCs, EMT/MET and cancer progression: a schematic of the reversible EMT model for cancer progression. Invasion involves epithelial cells losing their polarity and detaching themselves from the basement membrane through EMT activation. Metastasizing cells then directly enter the circulation. Circulating tumor cells then travel to distant sites and exit the bloodstream. Once they extravasate they may proliferate and reverse back to an epithelial phenotype to form macrometastases.[6]

This knowledge suggest that this type of cells encloses very useful information both on real-time and potential future progression of the neoplasia, implying that their detection, enrichment and characterization could be critical in the next steps of the cancer struggle. This has turned out to be a real challenging task for several reasons. First of all, this peculiar family of cells is distinguished for its extremely rare frequency in the blood stream. They were found to show a recurrence of 1-10 CTC per 1 ml of blood, when this volume typically encloses 6×10^6 leucocytes, 2×10^8 platelets and $x 10^9$ erythrocytes [7],[8],[9],[10],[11]. Then, has also been shown a relevant morphological differentiation within and between patients, leading also to extensive heterogeneity in biological properties [7],[12]. Though in literature has been demonstrated that CTCs present generally a greater size with respect to the other blood cells - red blood cells (RBCs) and white blood cells (WBCs) - [3],[13],[14] it has also been found that their dimension, spanning a wide range - from $17 \mu\text{m}$ up to 52

μm –, overlaps with some of them [15]. The difference in dimension is a good discriminant between RBCs and CTCs, due to the typical erythrocyte diameter of 6 - 8 μm ; the comparison with leucocytes is, instead, not so critical and shows an overlapping region. WBCs can be separated in 2 subpopulations, granulocytes and agranulocytes. Granulocytes – such as neutrophils and eosinophils – span from 15 μm to 17 μm while agranulocytes vary widely: small lymphocytes from 7 to 10 μm , large lymphocytes from 14 to 20 μm and monocytes from 15 μm up to 25 μm [15].

Furthermore, some studies have evidenced the existence of subpopulations, exhibiting different genetic expression and different invasiveness. This differentiation could be related to the varying degree of epithelial and mesenchymal characteristics expressed by CTCs, due

	Cells	Size [μm]	Overlapping
RBCs	Erythrocytes	6 - 10	No
WBCs	Granulocytes	15 - 17	Yes
	Small Lymphocytes	7 - 10	No
	Large Lymphocytes	14 - 20	Yes
	Monocytes	15 - 25	Yes
CTCs	CTCs	17 - 52	/

Table 1.1: Synopsis of the blood cells and circulating tumor cells dimensions and their overlapping

to the dynamical and continuous nature of the EMT process [4]. This could lead to a stratification of the level of aggressiveness. For example, the biphenotypic ones - circulating cells that express both epithelial and mesenchymal markers- are supposed to be the potentially most offensive cells in the metastatic outgrowth [16]. Has been put in evidence that the EMT status, which reflects on the phenotypic expression of CTCs, it's dependent on the cancer subtype [17],[18] and the stages of the disease [17]. There is also the possibility that another order of differentiation exists, within the same phenotypic group of cells: not all the mesenchymal cells express a peculiar membrane protein – Programmed Death-Ligand 1 (PD-L1) – and those who express it may be correlated with clinical parameters [4],[19].

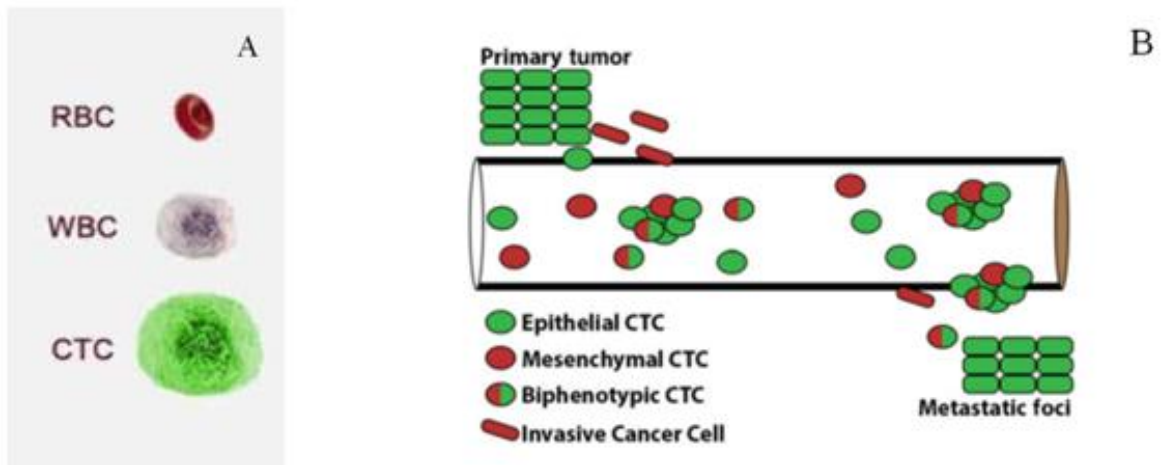


Figure 3.4:

- A) Schematic of the size proportion between big CTCs and blood cells (WBCs and RBCs)
- B) schematic of EMT process showing CTCs phenotypical heterogeneity.

1.2 CTCs: clinical utility and applications

One of the pillars of the cancer diagnosis and therapy efficiency monitoring is nowadays represented by tissue biopsy. This conventional clinical protocol encompasses some different analysis techniques: surgical biopsy, radiologically guided biopsy or endoscopic biopsy. The surgical approach uses a specially designed needle to sample tissues and cells from human body organs, by direct puncturing them. For several reasons, this procedure is complex and expensive. First of all, it is an invasive technique and may expose patients to clinical risk; then it needs highly qualified personnel - included an expert pathologist, in charge of making the diagnosis – and not trivial instrumentation. At the same fashion, radiologically guided and endoscopic biopsy require expensive equipment and expert personnel [1].

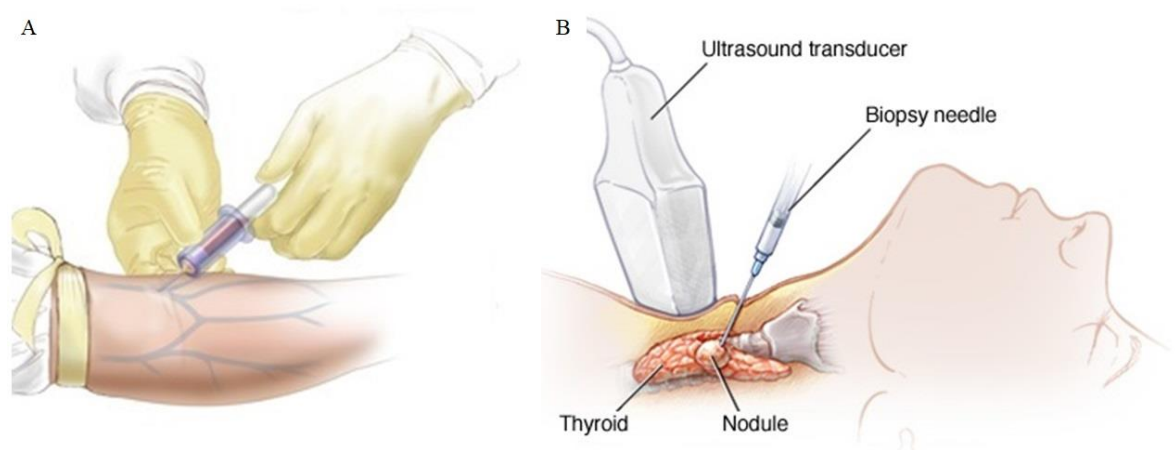


Figure 1.5: Blood Sampling (A) versus Surgical Biopsy (B): the latter involves much more complex instrumentation, starting from the needle – specially designed depending on the application- and following with the navigation system, which allows the needle to reach deep organs in the body.

Furthermore, these diagnostic methods, in addition to their complexity and the risk of adverse events, give a snapshot in time of the cancerous mass and are subjected to a localization bias, due to the spatial tumour heterogeneity. They require also that the tumoral masses have already developed up to significant dimensions to be detected and reached by the needle. So nowadays there is the need to find new techniques, which can be introduced in the clinical routine, less invasive, capable of detecting the changes in the molecular

composition of the cancer cells after exposure to therapy -allowing the monitoring of its efficiency - and not spatially and temporally limited [20]. Besides, it should be necessary to be able to identify the disease presence, even since the earlier stages – i.e. when the tumoral mass is composed only by a group of few cells -, allowing to achieve an advantage, even of years, on the currently used diagnosis techniques [21], [2].

These features could be provided by a recent approach, referred to as “Liquid Biopsy”. This new method is based on the analysis of the “trails” left by tumoral masses in the bloodstream, including: Circulating Tumor Cells, circulating free DNA – nuclear and mitochondrial DNA released both passively and actively in the circulation by tumoral cells [22] - and exosomes – membrane-bound phospholipidic vesicles (200-300 nm) actively secreted by tumoral cells [1]. Focusing on CTCs, these cells are already known by time – they were first noticed in 1869 [10] and, at present, many studies have been conducted on their biophysical, functional and morphological properties. Though the need to shed more light on their subgroup differentiation and their involvement in the complex mechanism of tumorigenesis, many steps have already been taken on the relevant role that they could play in the clinical field. Firstly, it has been investigated if it could be established a relationship between the count of cells in a given blood volume and the prognosis of the patient. Either the cells number, either the blood amount has been identified in order to give significant result: one of the most used combination of these parameters was found to be 5 CTCs in 7,5 ml of peripheral blood. This threshold could be considered as a gold standard since it has been used in the studies that allowed the only approval of a commercialized CTCs detection system – the CellSearch™ - for metastatic breast, prostate and colorectal cancers by US Food and Drug Administration (FDA) [7],[23],[9],[24],[25]. This number of cells was taken as a discriminant value to distinguish between two patients “states”, referred to their prognosis: favourable – with less than 5 CTCs in 7.5 ml of blood - and unfavourable – with equal or more than 5 CTCs / 7.5 ml of blood. It has finally been demonstrated that this threshold was significantly correlated with a poor patient outcome, independently on the time point in which the analysis was taken - i.e. before the starting of a new treatment, during the therapy or after the end of the treatment. The count of CTCs has been correlated with two prognostic indices: the overall survival (OS) – described as the time elapsed between the blood draw and the death of the patient - and the progression free survival (PFS) – the time intercurrent between the blood collection to progression or death [26]. It was shown that patients, categorized as

unfavourable, presented a shorter OS and PFS, thus meaning that a count of more than 5 CTCs is a significant poor patient outcome predictor [9],[24],[27],[26],[28]. This result was obtained for several types of cancer diseases, such as: metastatic breast cancer, lung cancer, colorectal cancer, castration resistant prostate cancer, bladder cancer, pancreas cancer, head and neck cancer, ovarian cancer, neuroendocrine cancer and hepatocellular cancer, [29] esophageal cancer, squamous cell carcinoma of the oral cavity, gastrointestinal cancer, testicular germ cell tumors[23].

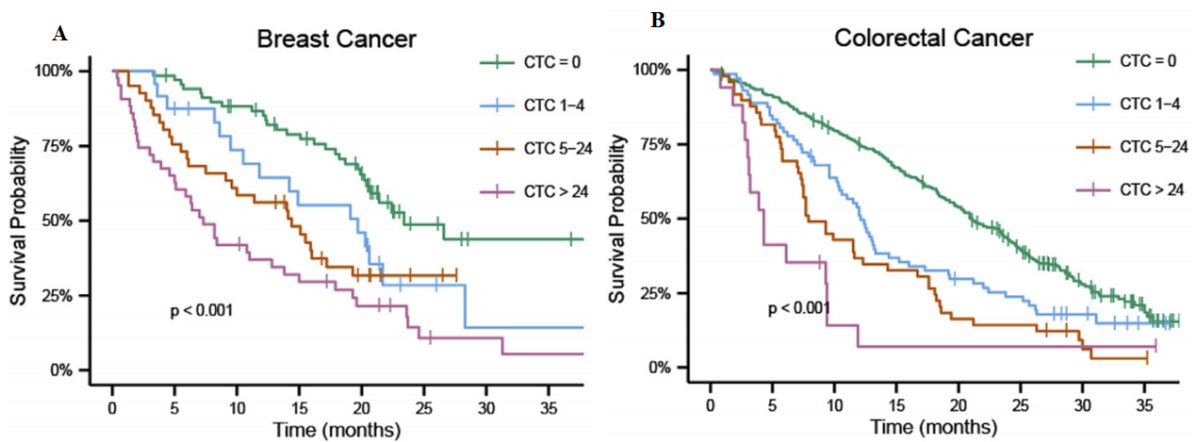


Figure 1.6: Kaplan-Meier plots showing CTCs count per 7.5 ml of blood versus survival in Breast Cancer (A) and in Colorectal cancer (B). the higher the number of CTCs found in the blood sample the lower the Survival Probability of the patient [29].

In addition to its prognostic value, CTCs has been also investigated as an indicator of therapy efficiency. The basic hypothesis is that, if the treatment is acting successfully on the tumoral masses, the number of cancerous cells in the circulation should decrease. The results validated this hypothesis showing that patients, which changed their “state” from unfavourable to favourable during the treatment, presented a greater overall survival [23],[7],[27],[24],[26]. Thus the circulating cells count could give information about tumor progression and therapy efficiency in a fast and less invasive way compared to sequential biopsies [10]. Furthermore, some studies have highlighted that this kind of analysis has the potential to have a higher prognostic value compared to the conventional imaging techniques [10],[30] and, most importantly, has the capability to early detect the metastatic spread of the tumoral mass, overcoming the limitation in the spatial resolution of the imaging analysis [25]. This could lead also to more efficacy in the treatment choice: it has been shown that it

could notice the development of metastases – and so the cancer progression – 3-4 weeks after the start of a new therapy versus the 8-12 weeks necessary to the imaging methods to detect the same, thus allowing a promptly change of the inefficient treatment [9]. The most interesting result was obtained studying the relationship between the presence of CTCs and lung cancer in patients affected by Chronic Obstructive Pulmonary Disease (COPD), considered as a risk factor in development of lung cancer. Patients with different stage of COPD were screened both using low-dose Computer Tomography (CT) spiral scan technique and blood filtering for CTCs detection. The 3% of COPD patients showed a significant presence of CTCs while the CT scan failed to point out the existence of tumoral masses. These patients have been submitted to an annual surveillance by CT-scan screening, which detected – in all cases – lung nodules after 1-4 years from CTCs detection. This early detection allowed promptly resection of the nodules and follow-up conducted 16 months after surgery, both by CT-scan and CTCs detection, showed the absence of new tumoral masses and no cancerous cells in the blood stream. Interestingly, the yearly CT-scan - for 5 years after the start of the study - has demonstrated that no lung nodules were developed by the remaining 97% of COPD patients in addition to non-smoking healthy control subjects and smoking with no pathologies subjects [21]. Thus, this study highlighted the relevance of CTCs analysis as an early cancer detection method which can be used as a screening technique for subjects that present higher risk of developing malignancies, i.e. showing factors as family history, smoking and non-healthy habits or age. This could simplify the process of cancer check-up and detection, and the associated costs, by separating the screening approach in two phases: the application of complex, invasive and time requiring methods should be done only in a second step, after the verification of the presence of CTCs in the circulation – taken as the first step – which could be performed frequently, due to its minimally invasive features [31]. Moreover, the number of cancerous cells found has also been considered as an index of malignancy risk stratification and cancer stage identification: higher the number of counts, higher the risk and the stage [32]. So far, the liquid biopsy approach applied to CTCs has been described as a continuous method, whose strength is the being a fast, minimally invasive, simple technique that gives real-time information about tumor and metastases progression, therapy efficiency, patient prognosis and diagnosis. The power of this technique is that it can be used also in a batch approach - i.e. allowing, besides an on-line analysis, also a downstream study -, extracting even more information. Thus,

another challenging application of these cells is currently being studied, no more involving only the number of counts. Following therefore the liquid biopsy batch approach - i.e. the enrichment of the analyte of interest for a subsequent downstream analysis - these cells could be useful not only for their presence in circulation but also, and maybe mostly, for the enclosed knowledge inside them. **Molecular, i.e. protein, expression characterization, RNA transcriptional profiling and genetic sequencing in DNA of the harvested cells could provide the means to link genetic data to new understanding of the complex mechanisms of drug resistance, opening the way to a precision medicine, based on the concept of finding the best therapy and drugs for the single patient, relying thus primarily on the information extracted from his own cells and his own disease - i.e. moving toward a personalized medicine [25],[33],[34],[7],[35].**

Applications	References
Early cancer detection	[21]
Independent predictor for patient prognosis	[27],[9],[24]
Real-time index for therapy efficacy	[33]
Monitoring of cancer residuals	[35]
Monitoring cancer progression or stages	[31]
Malignancy risk stratification	[35]
Personalized medicine	[34]

Table 1.2: summary of the main applications of circulating tumor cells detection, seen as a new generation of biopsy, named “Liquid Biopsy”.

1.3 CTCs detection: Non-microfluidic technologies

Since several technologies have been developed during the last decades, in this section will be reported only the commercialized systems approved by US-FDA and European Union. The first approach to solve the CTCs isolation and collection was a technique based on the biological properties of the tumoral cells. This method, to which we could refer as the “labelled method”, exploits the evidence that CTCs have shown in many studies: the genetic expression of precise epithelial marker – Epithelial Cell Adhesion Molecule (EpCAM). Thus, “labelled” stays for the selective targeting of cancerous circulating cells through specific antibodies, which bound themselves to EpCAM protein, on the membrane surface of the cells. The golden standard system applying this technique is the already mentioned CellSearch™, which was used as CTCs isolation system in many of the studies that characterized this type of cells in the last decade. The system consists of a series of components to implement a basically two-steps process after the blood sample collection: sample preparation and sample analysis. The first module adapts the blood specimen using ferrofluids – solutions containing magnetic nanoparticle functionalized with EpCAM-specific antibodies – in order to label the target cells. The analysis consists in applying a magnetic field to attract only the labelled cells and wash away the waste. The analytes such enriched are stained with molecular-specific fluorescent dyes, then the specimen is arranged on a cartridge where the cells are place in one focal plan against a glass surface. Therefore, the cartridge is scanned by a dedicate fluorescent microscope and the software automatically generates images of all events presenting predetermined criteria. Finally, a trained operator is assigned to the selection of the events according to the CellSearch™ CTC definition, i.e. presenting features as oval morphology, a visible nucleus, positive staining for cytokeratine and negative staining for CD45 – a dye used to select leucocytes [36],[9],[27][37].



Figure 1.7: CellSearch™ System components. (1) CellSave Preservative tubes, in which blood is collected and stabilized for up to 96 h at room temperature, allowing the samples collection and the subsequent analysis in distant places. (2) Automated CELLTRACKS®AUTOPREP® System for the immunomagnetically cell enrichment and staining. (3) CELLTRACKS ANALYZER II® System for the selected cells automatic image generation².

Despite US-FDA approval, the system is not currently recommended by associations in oncological field – such as American Society of Clinical Oncology (ASCO) and National Comprehensive Cancer Network (NCCN) - neither its clinical routine use has been widely diffused. Furthermore, it presents critical limitations: first of all, during the decade of its operativity, other systems – for the most part microfluidic ones – have proved to be able to reach a higher cell purity in the enrichment, processing lower volumes of blood – passing from 7.5 ml to 1-2 ml. Following, it suffers from the disadvantages of the immunoaffinity technology- which will be discussed in the next section- and lastly the enrichment of CTCs is affected by a high WBCs contamination. For these reasons, it could be noticed that in the past ten years the topic of microfluidic technology applied to circulating cells detection has shown an explosive growth compared to the CellSearch™ one, related to the same purpose [25].

² <https://www.cellsearchctc.com/>

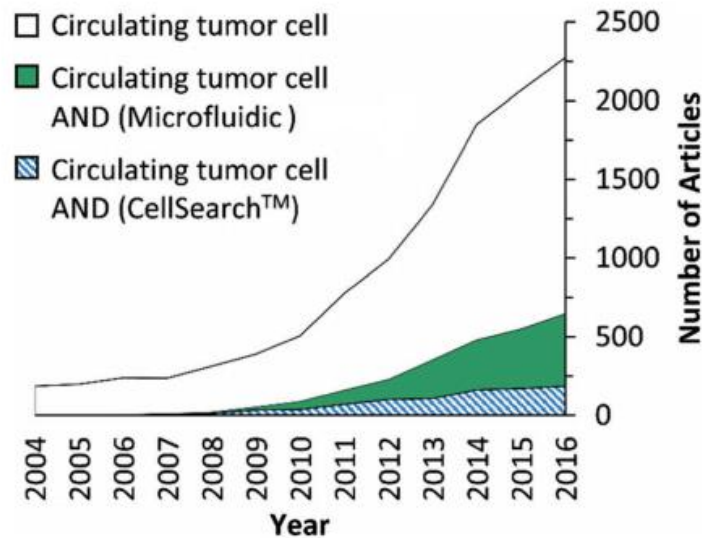


Figure 1.8 Number of publications regarding microfluidic chips related to CTCs versus CellSearch™ one. It could generally be noticed a growing trend of the research world attention to this topic and, specifically, to the microfluidic technology [25].

The next non-microfluidic technology described, was approved by European Union, and could be categorized as a completely different approach – even if based on the same collection principle -from the previously described technology. The CellSearch™, indeed, was an *ex-vivo* immunomagnetic technique, while Gilupi CellCollector™ system is

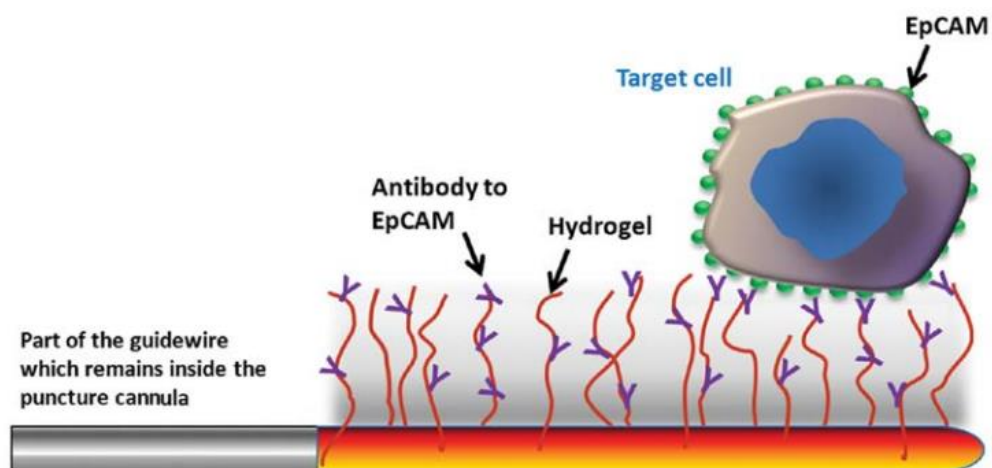


Figure 1.9: Gilupi CellCollector™ system: a 20-mm long gold-coated catheter tip of the stainless steel Seldinger guidewire, functionalized with hydrogel labelled with EpCAM antibodies, in direct contact with blood circulation [71].

classifiable as a *in vivo* immunoaffinity system. It consists in a structured medical Seldinger guidewire (*fig. 1.9*) whose surface has been functionalized with a hydrogel labelled with EpCAM antibodies. The Gilupi CellCollector™ system could be considered as a medical device – since ISO guidelines for class IIa medical devices were verified - whose functioning is similar to that of a simple catheter-tip. The guidewire is inserted in the blood stream of the patient (*fig.1.10*), here the functionalized tip works as a collector of CTCs, thanks to the bounds created between the antibodies and the EpCAM molecules on the cell surface. Before the cells analysis can be carried out, it is necessary to label the tip *ex vivo* with CD45 – a membrane glycoprotein expressed by the leukocytes – antibodies and fluorescent staining.

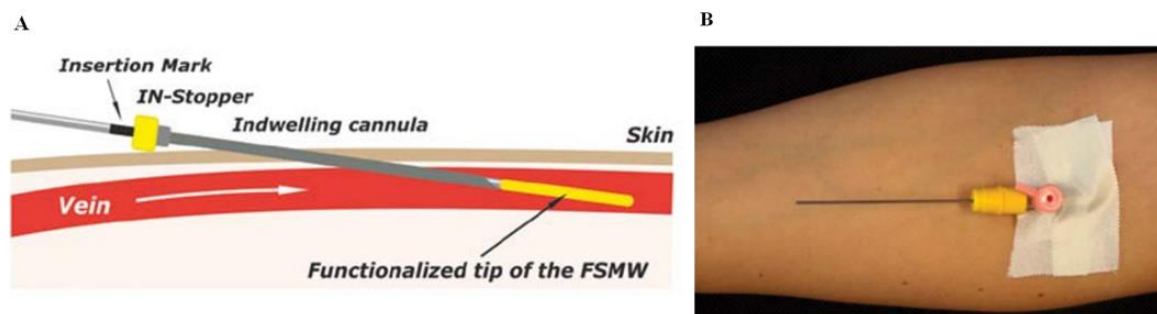


Figure 1.10: Schematic of Gilupi CellCollector™ functioning (A) and real example of application of Gilupi System (B) [71]

As well this system suffers from some limitations: basing its collection principle on the use of antibodies is affected - as the CellSearch™ - by the immunoaffinity issues, then, being the capture efficiency is very low, this requiring large volumes of blood to be processed - up to 1-1.5 liters - and, therefore, increasing analysis time [25].

As was described in the first subchapter CTCs may fall under that heterogeneous grouping of cells named as “Rare cells”, due to their extremely low frequency in the blood stream (1-3000/ml) versus a background of blood cells of the order of 10^7 - 10^9 counts per ml of blood [25]. This, in addition to the heterogeneity of the CTCs, hampers their detection and suggests that large processing volumes are non-optimal for this purpose. Furthermore, to give the chance to the “Liquid Biopsy” approach to spread in the clinical routine it is necessary that the system is as integrated as possible, low-cost, highly sensitive and specific, with high throughput and needs low analyte volumes - i.e. ensuring shorter processing times, and,

among these, the most challenging feature: be completely label-free. Thus, to meet this requirements, research moved its focus toward microfluidic systems (*fig . 1.8*)[35],[1] .

1.4 CTCs detection: Microfluidic Technology and lab-on-chip approach

Microfluidic could be defined as the science and engineering system that, exploiting networks of channels and structures with dimensions from a few micrometres ($10^{-6}m$) up to a millimetre ($10^{-3}m$), can manipulate and control with high precision small amounts of fluids – in the range of microliters ($10^{-6}L$) to picoliters ($10^{-12}L$)[1]. This multidisciplinary strategy sees its main use in taking advantage of the principles of physics, engineering, chemistry, science materials and biotechnology and integrating them in a single platform, which reproduces – reduced on a micrometre scale – the bench-top procedures usually found in laboratories; thus creating the so called “Lab-on-Chip” (LOC) devices. Thanks to the recent progresses in fabrication technologies it has been possible to create a series of microfluidic components – such as: actuators, valves, mixers, separators, pumps [1] or integrated laser sources [38] - that have allowed the implementation of such complex high-performance tools. In addition to such elements, the shift of the analyser toward the same order of magnitude, or at most of one order greater, of the analytes has given to these devices some intrinsic features (*Table 1.3*) that well fit the purpose for which they were created. Microfluidic systems, therefore, presents characteristics as great sensitivity, high specificity, capabilities to reach a high throughput and the need of small analyte volumes - thus, a shorter sample processing time. These properties, summed up to the devices integrated nature, bring to the creation of platforms with an improved potential for automation and control, disposability, the ability to perform a one-step process of sample loading, separation and analysis and lower costs, giving to this recent technology the right potential to hold a significant place in the future of *in vitro* analysis [35],[1],[25].

Microfluidics advantages over bench-top technologies	
1.	Higher sensitivity
2.	Greater Specificity
3.	Small processing volumes: both reagents and analytes
4.	Multidisciplinary ³ integration over the same platform
5.	Improved automation and control abilities
6.	Devices disposability
7.	Lower costs
8.	Potentially shorter analysis time
9.	One-step process of sample loading, separation and analysis

Table 2.3: Resume of the Lab-on-Chips main advantages over the currently in use laboratories bench-top techniques.

For all these reason, during the past years, several microfluidic devices have been developed with the aim of isolating, enriching and directly analysing circulating tumor cells. However, these approaches still show some limitations, among the main ones it could be noticed the difficulty to reach a high throughput – due to the devices small capacities and the low pressures to which the chips can be subjected - and a still too long analysis time when considerable volumes are processed, while maintaining a good sensitivity and specificity. Thus, new generation microfluidic chips should fulfil some requirements, in order to increase the applicability of these devices in the clinical routine. These requisites include an enhanced overall sensitivity and specificity, requiring a shorter processing time for CTCs detection, capture and identification, the need to simplify the operating procedures and to find new solutions to increase both the pressure both the throughput applicable to the device. Last but not least, to reduce batch to batch variations [35].

³ Integration of microfluidics, optics, electronics and magnetic field technology.

	Feature	References
1.	Improved sensitivity	[35],[25]
2.	Improved specificity	[35]
3.	High Throughput	[15]
4.	Short analysis time	[15]
6.	Reduced batch-to-batch variations	[35]

Table 2.4: Synopsis of the critical characteristics for the new generation of Lab-on-Chips

1.5 Figures-of-merit for CTCs detection topic

In the circulating tumor cells isolation field, over the last years, have been defined some performance parameters in order to achieve the possibility of quantitatively comparing the different technologies developed by separate studies and quantitatively defining the limits to overcome to improve the same technique.

Figures of merit	Definition	Measurement unit
Recovery	Efficiency in CTCs selection: number of tumor cells captured divided by the actual number of tumor cells	%
Purity	Ratio of CTCs to the total number of cells in the isolated amount	%
Throughput	Volumetric rate for processing blood samples	ml/h
Clinical sensitivity	The technology's ability to correctly identify patients with the disease	%
Clinical specificity	The technology's ability to avoid false positives for subjects without the disease	%
Clinical yield	The median number of CTCs isolated from patients with a defined cancer type and stage	CTCs counts/ml
Cell viability	Percentage of CTCs that are still alive following enrichment	%

Table 1.5: figures of merit currently used in the literature of the circulating tumor cells isolation research field [25],[39].

1.6 LOCs: overview

In order to give a clearer overview on the LOCs techniques applied to the CTCs isolation case, it could be made a substantial dichotomy in the analysis methodologies, identifying two main ones: immunoaffinity-based and label-free techniques. Each of these categories could in turn be divided according to the separation targets – for immunoaffinity-based – or the physical property- for label-free methods (*fig.1.11*)

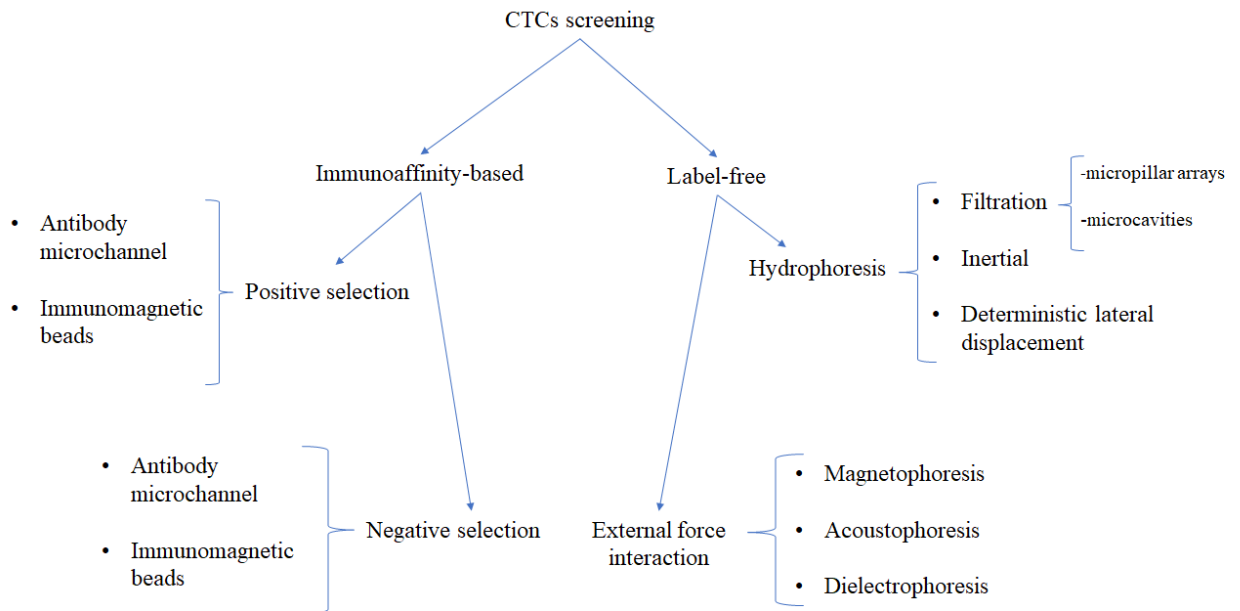


Figure 1.11: Scheme of one of the possible CTCs analysis subdivision by implied techniques.

1.7 Immunoaffinity-based methods

The cells capture principle at the basis of these techniques is the same described for the CellSearch™ and Gilupi systems. Basically, antibodies specific for determined surface proteins expressed by the target cells on their membranes are used to label those cells, which then are captured or deviated. It is possible to identify two sub categories, depending on the target cells selected.

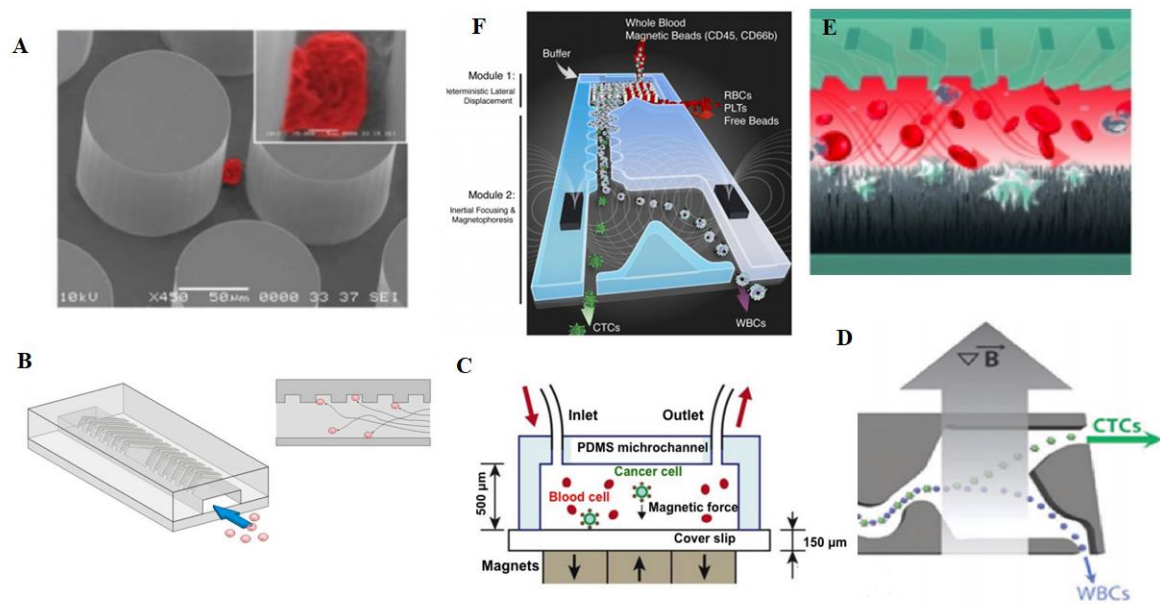


Figure 1.12: Immunoaffinity-based LOCs. Positive selection methods: (A) Silicon microposts (diameter of 100 μm and spacing of 50 μm) whose surface has been functionalized with antibodies increase the surface to cell contact area, increasing the capture efficiency. (B) Herringbone structures create a chaotic flow in the channel to increase the collisions between target cells and the functionalized surfaces. (C) Ferromagnetic microbeads targeted CTCs are attracted on the bottom of the chip through a magnet, the non-interesting hematologic cells are flushed away then the cancer cells are released. (D) Magnetic beads attached on the CTCs surface allow the direct deviation of the target cells from the mainstream by applying a magnetic field (E) Silicon antibodies-functionalized nanopillars create a sort of “wood” in which the CTCs are trapped. Negative selection methods: (F) the CTC-I-chip: After a first preparation step in which WBCs are labelled with magnetic beads, the sample will be processed by three stages: a lateral displacement stage will separate RBCs from the main stream, the a hydrofocusing path will put remaining cells in a row

and, finally, an applied magnetic field will deviate the leukocytes in a waste output, leaving – theoretically – only CTCs in the stream [1],[25],[40],[41].

The first, the positive selection, involves the direct labelling of CTCs, through a specific antigen for the epithelial molecule (EpCAM) expressed by tumoral cells – belonging to carcinomas of lung, colorectal, breast, prostate, head and neck, and hepatic origin [40] – and not by hematologic cells. One subgroup technique of this category uses magnetic microbeads, whose surfaces has been functionalized with the targeting antibodies; thus, once the microbeads are bound to the circulating cells, they can be deviated, by applying a controlled magnetic field, in the right output or in a collection area. The other principal subgroup, under the category of positive selection, is the microchannel based capture. This approach exploits the surface of the internal walls of a microfluidic path, by covering them with cancer cells specific antibodies. In such way, the target cells are captured and the “waste” cells are flushed away by the flow, then only in a second moment the cancer cells could be dislodged and enriched for further analysis. To optimize the surface to cell contact and thus the capture efficiency, other, from a simple straight microchannel, complex geometries have been studied, including: sinusoidal and herringbone channels and complex structures as silicon microposts (100 μm in diameter and 50 μm in spacing) and silicon nanopillars. Positive selection methods generally present a throughput of 1-1.5 ml/h and are characterized by a generally elevated efficiency, a generally low purity, except for the sinusoidal chip and a very high sensitivity (*Table 1.4*). Though, this result is due to the nature of the capture: using specific antibodies, indeed, allows to get high sensitivity values only for the cells that belong to a specific cancer line. Thus, this could be considered a great advantage, in case the cancer type is known, but, since in most of the cases – and, surely in a potential application as early cancer detection – it is not, it may result as a big disadvantage. Therefore, this could be considered as a limitation of these methods, requiring a priori knowledge on the type of cancer or at least making some hypothesis about that [1],[25]. Another critical point of this approach is constituted by an intrinsic property of CTCs, namely their high heterogeneity – even in the same cancer type cells. This could mainly be due to the EMT transition to which circulating tumor cells are subjected; this process leads the cells to a loss of their epithelial marker – i.e. the target of the specific antibodies – in the transition to a mesenchymal state. Furthermore, it could be considered as a dynamic process

that could verify in different times for cells belonging to the same tumoral mass zone. [4]. Thus, the result is that not all the circulating tumor cells in the bloodstream can be detected by this method [42]. The last issues can be reduced by using “antibodies cocktails”, which comprehend different cancer types and membrane proteins antigens [43]. Though, also the use of specific antibodies in a certain way could be seen as a limitation; because, in one case, it requires a preliminary step to the real analysis to let the functionalized microbeads to bind to the target cells, in the other, it limits the throughput, due to the low flow rate needed to ensure the interaction between the cells and the functionalized walls. So, in the perspective of the “Liquid Biopsy”- i.e. the creation of a device that allows simple, fast and almost *in situ* analysis of the blood sample [35]– either the low throughput and the blood sample preparation can be considered as non-optimal for this kind of application. The second approach of the immunoaffinity-based methods is the negative selection and it has been thought to resolve the epithelial markers related issues. In this technique, indeed, the antibodies targets are no more the cancer cell, but the membrane proteins present only on leukocytes surface. Thus, before the real isolation of CTCs, a step of purification from red blood cells is needed. This could be performed in different ways; among the most used, there is the erythrocytes lysis in a pre-analysis sample preparation stage, otherwise an on-flow filtering to deviate red blood cells from the main stream [41], through a technique called Deterministic Lateral Displacement (DLD), which will be deeply discussed in the next sections. As far as the actual detection of cancer cells is concerned, the techniques are similar to the positive selection approach. In the first case, the immunoaffinity will detain only WBCs and the flow will take away the CTCs, while in the second, microbeads are bounded to leukocytes to deviate them in a waste output [1]. One interesting application of this technology is given by the CTC- I-chip, which integrates three stages on the same platform: a DLD stage to filter red blood cells, a hydrofocusing stage to put the cells in a row and a magnetic field application stage to obtain the separation between leukocytes and CTCs. This technique, after the labelling procedure, reaches moderate throughputs (8 ml/ h), a good efficiency, a moderate purity and a medium-high sensitivity (*Table 1.4*). Besides the limitations due to the need of a sample preparing step, described for the positive selection, this kind of approach -i.e. not label-free - is affected by the fact that not all the cells in the blood, that are not RBCs or WBCs, are tumoral cells; an example of this could be given by

Epithelial Circulating Cells (ECT). Thus, the purity of the achieved enrichment cannot reach high values [1],[25],[35].

Capture technique	Device Geometry	Recovery [min-max]	Purity [min-max]	Sensitivity [min-max]	Throughput
Positive selection (Immunoaffinity)	Microposts array	$74 \pm 5\%$ - $80 \pm 6\%$	$34 \pm 8\%$	90%- 100%	1 ml/h
	Sinusoidal Channel	$64 \pm 4\%$ - $93 \pm 5\%$	~90%	63% -100%	1.5 ml/h
	Nanopillars array	$65 \pm 5\%$ - 95%	ND	0% - 96 %	1 ml/h
	Herringbone	$3 \pm 1\%$ - $97 \pm 1\%$	0.77% - 14%	41% - 93%	1 -1.5 ml/h
Negative selection (Immunoaffinity)	CTC i-chip	$11 \pm 3\%$ - $99 \pm 4\%$	0.02% – 43%	29% - 90%	8 ml/h

Table 1.5: synopsis of immunoaffinity-based LOCs for CTCs detection and isolation. It could be noticed how either the sensitivity and the capture efficiency variate due to the different used cell lines [25].

Note on the table construction:

The table was built by taking the minimum and the maximum values for the figures-of-merit found in literature. Those values refer to different tests performed on diverse cancerous cell lines- i.e. different cancer types.

Aside from the issues affecting the immunoaffinity-based methods described up to now, it could be noticed one more: the use of antibodies contributes, over and above the increase in analysis time, also to the increase of the costs of the entire procedure. Thus, to search for the creation of a low-cost and high-performances devices, that could be inserted in the clinical routine, it should be necessary to address other solutions. These could be easily represented by approaches that do not base their identification strategy on the genetic marks of tumors,

thus implying a reduction in costs and a widening of the detectable cancer type spectrum, without loose in efficiency. Those approaches are known as label-free technologies.

1.8 Label-free methods

The category name of this methodologies is not only explicative of the technique used to isolate circulating tumor cells but also of its main aim: the identification of cancerous cells without a priori labels – i.e. knowledge – of the sought cancer type. This approach, indeed, should be able to identify any type of malignancy, basing its investigation on physical properties common to all cancer cells [44]. These properties could be subdivided in two groups, according to the force to which are subjected: size, deformability, density and shape are submitted to hydrophoresis, while cells dielectric properties – such as membrane capacitance and cytoplasmic conductivity [42]– obey to dielectrophoresis. Exploiting the intrinsic features of the cancer cells, these methods could have the possibility to overcome the limitations typical of the immunoaffinity-based approaches. Besides the non-dependence from surface protein specific antibodies, label-free techniques have shown relevant advantages: high throughput, faster processing, lower costs, the possibility to directly scan the sampled specimen, without the need of a pre-analysis sample preparation stage, and the completely absence of chemical bindings that could alter the biophysical properties of the target cells and thus their viability [43].

Advantages	
1.	No labelling
2.	Potential detection of all types of cancer
3.	High throughput
4.	Low costs
5.	No pre-analysis sample preparation
6.	Absence of chemical binding with the target cells
7.	Avoiding selection bias resulted from cell targeting

Table 1.6: advantages of label-free LOCs technologies in the CTCs isolation from the whole blood problem

1.9 Label-free approach: dielectrophoresis (DEP)

This technique is based on the principle by which cells, subjected to a non-uniform electric field, behave as electrical dipoles. Thus, exploiting the interaction by this induced cell polarization and the spatial gradient of the electric field, it is possible to make each kind of cell experience a unique net electrical force and, hence, move them. The magnitude of this force depends on several factors, such as the cell membrane properties, cell size, cytoplasmic properties, strength and frequency of the applied electric field and fluid medium properties. As far as the latter properties are concerned, dielectrophoretic methods can be divided in two categories: Positive DEP and Negative DEP. The first occurs in the case that cells present a greater polarizability than the surrounding medium and, thus, the cells will be attracted towards the regions of higher electric fields and retained at the electrode surface. In the other case - namely, if the cells are less polarizable than the suspending medium – they will move to the regions of lower electric fields and then be eluted by the flow [1]. Regarding the CTCs isolation problem, this technique takes advantage of the existing differences between cancer and normal cells. In comparison to the latter, indeed, tumor cells show different surface morphological features in the lipid bilayer membrane and greater sizes, thus resulting in a different net electric force acting on these cells and in a distinction among the different cell types. This method is characterized by a good capture efficiency but is limited by a low throughput (*Table 1.7*), which is necessary to allow to the cell displacement by the DEP force and a low purity of the enriched sample. Furthermore, to reach higher performances, it is advisable a sample preparation step, in a pre-analysis phase, to remove RBCs from the specimen [42], [25]. To overcome the low-throughput limitation it has been studied a new geometry which allows a 3D DEP lateral displacement, increasing the throughput up to 2.5 ml/h, at expenses of barely microfluidic chip dimension – i.e. 13 cm long microchannel [45]. Another issue for a reliable application of this method could be found in the dielectrophoretic force high sensitivity to buffer conditions -e.g., salt concentration [46].

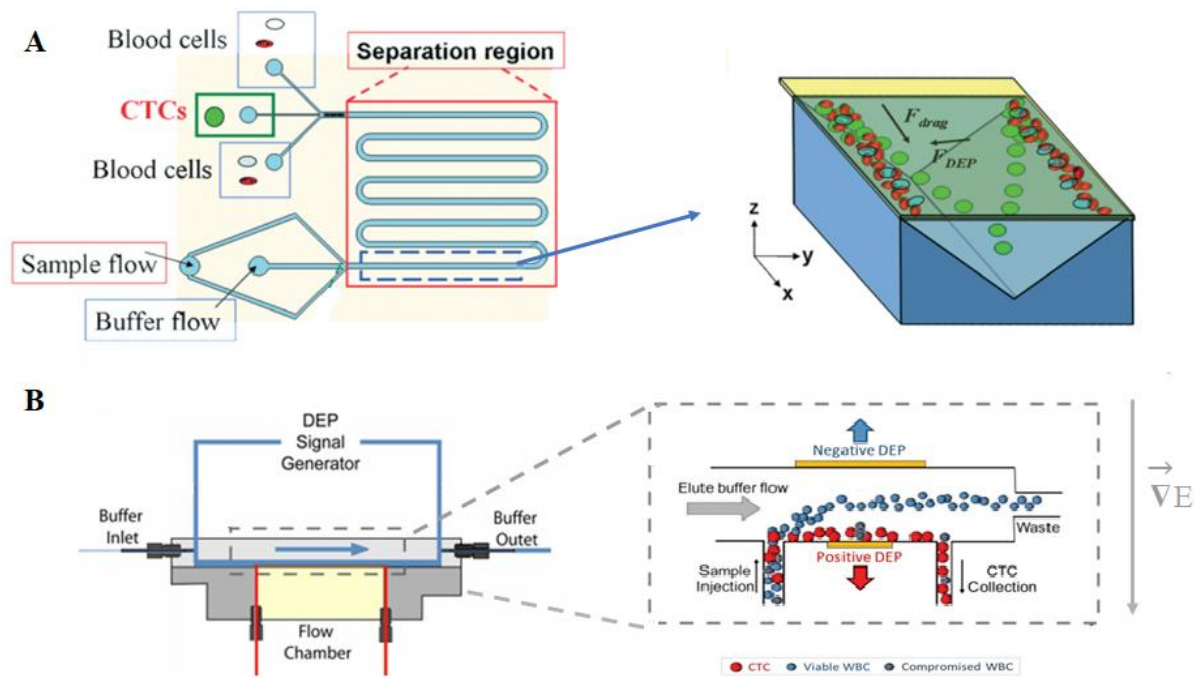


Figure 1.13: DEP LOCs. (A) 3D DEP lateral displacement. The electric field is applied in a V-shaped microchannel. Such that the cell displacement could take place on the walls; each cell reaches a precise point on the wall, according to its type [45]. (B) Commercial DEP system, called ApoStream™, which exploits the dissimilarities in the frequency-dependent dielectric properties of the different cell types [47], [25].

1.10 Label-free approach: magnetophoresis

This method differs from the immunomagnetic one, described in the previous section, by the fact that exploits intrinsic magnetic properties of the cells, without the need for any labelling agent. The technique algorithm could be compared to the immunomagnetic negative selection one: CTCs, indeed, have not shown sufficient magnetic properties to interact with a magnetic field. Conversely, it has been found that deoxygenated RBCs are paramagnetic - i.e. attracted toward the source of a magnetic field -, while oxygenated RBCs and WBCs are diamagnetic, namely deflected from magnetic field source [46]. Thus, a label-free magnetophoretic system will isolate CTCs by applying a magnetic field to separate from the main stream RBCs and WBCs. An interesting application could be represented by the Paramagnetic Capture Mode (PCM) magnetophoretic microseparator, used as the first step

in an integrated microdevice for breast circulating cancer cells (BCCs) in the blood to separate from the blood RBCs and thus isolate nucleated cells (WBCs and BCCs). The second stage of the microfluidic device contemplated a micro-scaled electrical impedance spectroscopy (μ -EIS) to discriminate CTCs among WBCs and residual RBCs. The method showed a high recovery rate (94.8%) but it's mainly limited by the extremely low throughput (2.5-20 μ l/h), needed to reach high capture efficiency values (*Table 1.7*) [31].

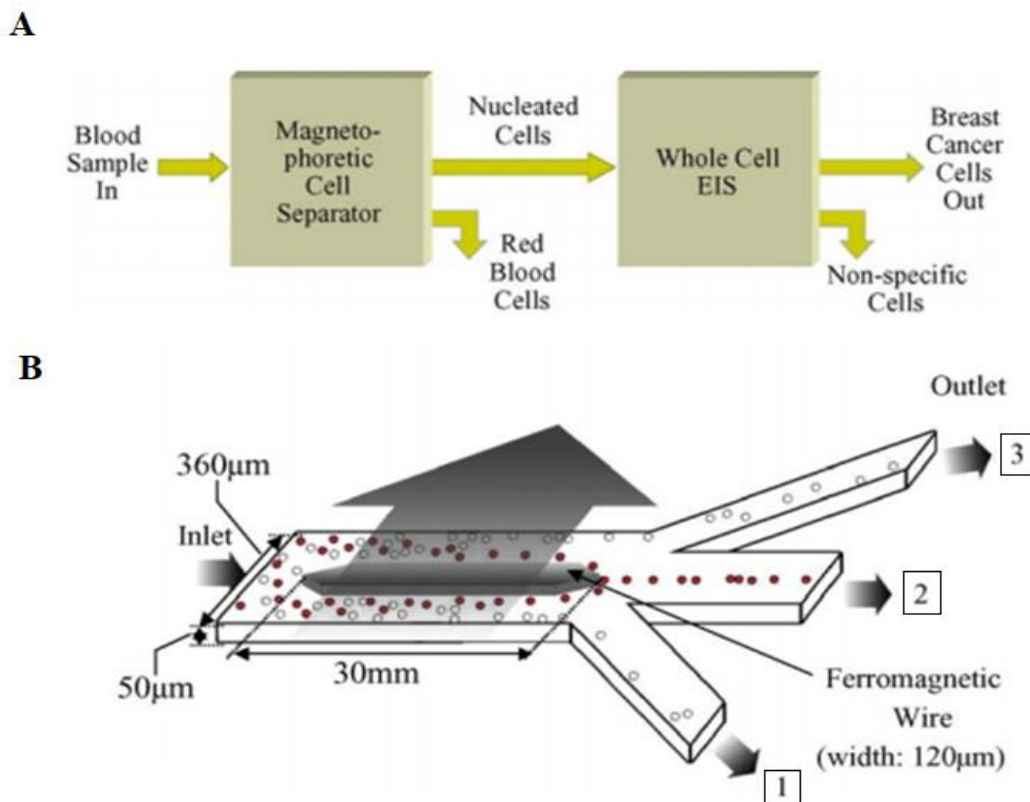


Figure 1.14: Label-free magnetophoretic LOC for breast blood circulating cancer detection. (A) Conceptual block diagram of the device functioning; the analysis process is divided in two steps: RBCs removal by a Paramagnetic Capture Mode cell microseparator and CTCs identification through Electrical Impedance Spectroscopy. (B) PCM microseparator: a ferromagnetic nickel wire is incorporated along the length of the microchannel. When activated, It attracts the RBCs on the central section of the microchannel, thus allowing the output separation in three outlets: outlet 2 collects RBCs, while 1 and 3 gather nucleated cells (WBCs and CTCs)[31].

1.11 Label-free approach: Acoustophoresis

As magnetophoresis and dielectrophoresis this technique exploits the interaction between a net force, generated by an external applied field, and the physical properties of the analytes contained in the microchannel. In the acoustophoresis, high intensity sound waves interact with the walls of the microchannel, generating pressure gradients that push cells into specific spatial location; in this way, a standing wave profile is created within the microchannel and the cells are moved toward high-pressure nodes or anti-pressure nodes by radiation forces. The parameters that influence the magnitude of these forces are the volume, the density and the compressibility of the cells, the surrounding medium and the wavelength of the acoustic wave. Thus, cells with greater density and compressibility greater than the surrounding fluids will migrate towards the pressure nodes, depending on their size. Aside from greater dimensions, it has also been shown that CTCs present different deformability from WBCs and RBCs, thus allowing the application of this method to the cancer cell separation problem [46] In this way, after crossing the pressure nodes, bands of cells - grouped by deformability, density and size - will be created across the microchannel and thanks to the flow laminarity, their positions will be hold until the different outlets. In literature, it has been shown that this technology presents good recovery rates, high purity of the enriched analytes and medium-high throughput (*Table 1.7*). The main lack of this method could be individuated in the still undocumented and fragmentary knowledge about CTCs compressibility properties [46].

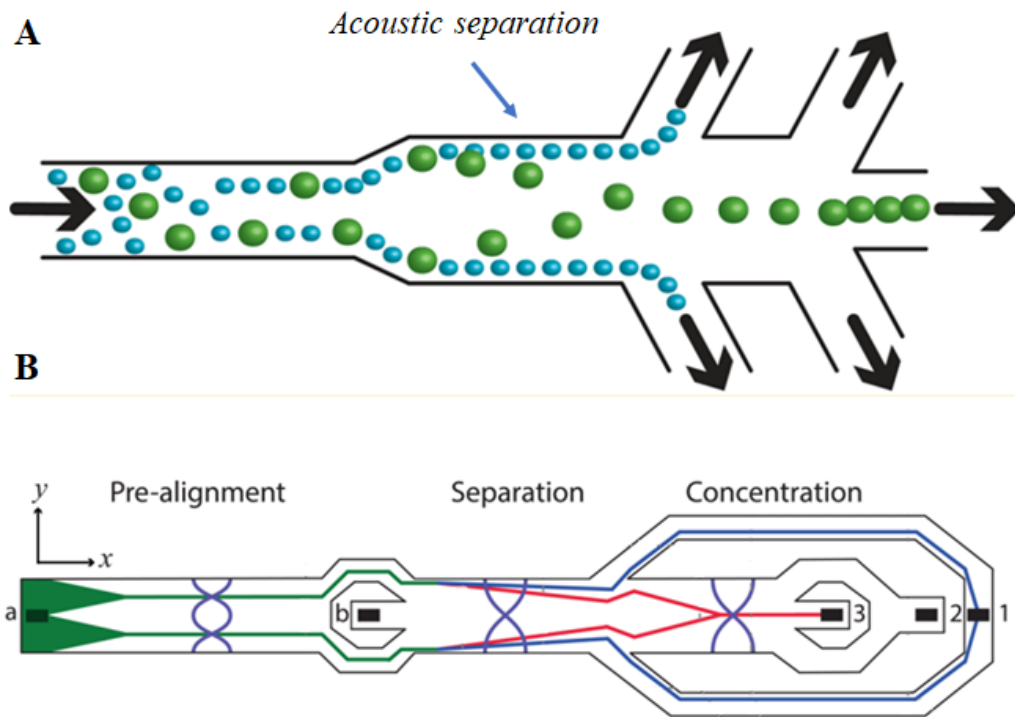


Figure 1.15: Acoustofluidic Lab-on-chip. (A) Acoustophoresis general concept: after the acoustic pressure node the cells are dislocated in bands across the microchannel, thus allowing the separate collection. (B) Acoustofluidic device for CTCs isolation composed by 3 steps. The first is the pre-alignment step through two acoustic wave nodes to put in two rows the input cells. Then, through inlet b a cell-free fluid, with a different acoustic impedance, is injected in the chip. This fluid pushes all the cell sideways on the walls, before the acoustic separation is met. The analytes with less lateral displacement from the chip walls are discarded through outlet 1. A third acoustic wave node constitutes the concentration step; its goal is to better focus the isolated cells and direct them towards the outlet 3. The fee-cell liquid is discarded through outlet 2 [48].

1.12 Label-free approach: inertial hydrophoresis

This kind of method differs from the previous ones by the fact that no external force is involved. The basis of hydrophoresis technique, indeed, exploits only chip geometry and dimension to separate cells, mainly by size, in some cases also by deformability. It is possible to identify two kinds of different inertial approaches. The first involves geometrically straight channels that for all their length repeat, with the same distance step, present abrupt

expansions of the channel section, creating trapping reservoirs. Fluid shears, thus, create transverse inertial migration of cells. Once the cells reach the reservoir's area, larger cells are trapped by vortex generated in the reservoirs, while smaller-sized cells are flushed toward the outlet. Then by reducing the flow it is possible to recover also the entrapped large cells.

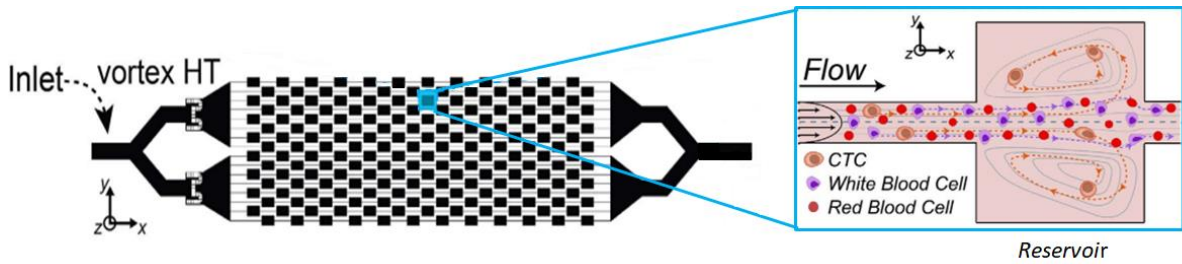


Figure 1.16: Vortex HT chip: an example of straight channel interrupted by expansions of the section of the channel (Reservoirs) [49].

The second approach, conversely, draws inspiration by the commonly bench-top used technology for blood centrifugation: it uses, indeed, curved micro-channels. In this chip configuration, centrifugal forces overlap with the inertial forces creating the so called “Dean Vortex” – i.e. a double recirculation in the transversal section of the channel. The strength of this recirculation depends on a parameter, called “Dean number”, defined by the hydraulic channel radius and the radius of curvature. These two forces in the spiral channel, therefore, generate a transverse cell migration according to its size. At an equilibrium point, the separated cells are positioned at a precise distance along the channel cross-section [14],[1].

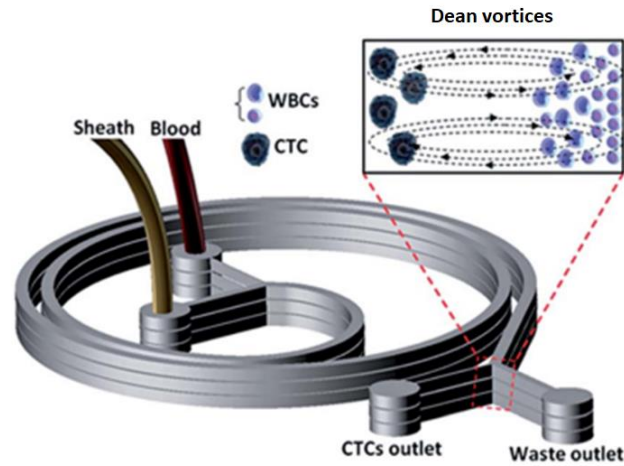


Figure 1.17: Spiral chip technology: it exploits the interactions between inertial forces and centrifugal forces, that overlapping within the chip generate the so called “Dean vortices”, which allow a separation in size on the cross-sectional area of the channel [50].

The spiral geometry shows good values of recovery rate, but low purity and medium-low throughput. It has to be noticed that this method could be applied either on the whole blood or on the RBC-lysed blood; in the second manner, both the throughput and the purity considerably improve (Table 1.7). As far as the straight channel method is concerned, it presents a moderate recovery rate, high purity value and very high throughput (Table 1.7). For the efficiency rate, it’s worth noting that the system has low one – around 20% - but if more cycles of analysis are performed - i.e. taking the output again as input for the chip - it could reach high one – around 83% [49]. The main limit of this method is that performance – mainly efficiency and throughput - are destabilized when flow populated densely with cells are processed [46].

1.13 Label-free approach: Filtration

This technique represents one of the most conceptually simple solutions for CTC isolation. It is based mainly on the greater sizes of the cancerous cells versus hematologic cells. Thus, two types of filtering systems can be created: the first involves the use of micropore drilled membranes; conversely, the second method uses micro-post arrays to entrap the circulating cells, or clusters of them, in the spacing between pillars [25]. For the membrane filtering devices, the critical parameter to control is the size of micro-pores; usually chosen as lower

than 10 μm . Thus, the drilled membrane allows the passing-through of the cells with size smaller than the micropores diameter. (*Table 1.7*) These methods have showed high recovery rates and very high throughputs but still lack of good purity values (*Table 1.7*). One of the most critical issues is given by the problem of clogging; this could be minimized by the use of cross-flow injector to flush away cells that block the pores – thus, complicating the chip geometry - or by lysing RBCs in the blood sample before the microfluidic analysis. However, apart from particular geometry solutions, a recovery step is needed to enrich the isolated cells and proceed with further analysis; furthermore, another extra-device step is often used: a fixative wash to prevent cell lysis during filtration [46] .

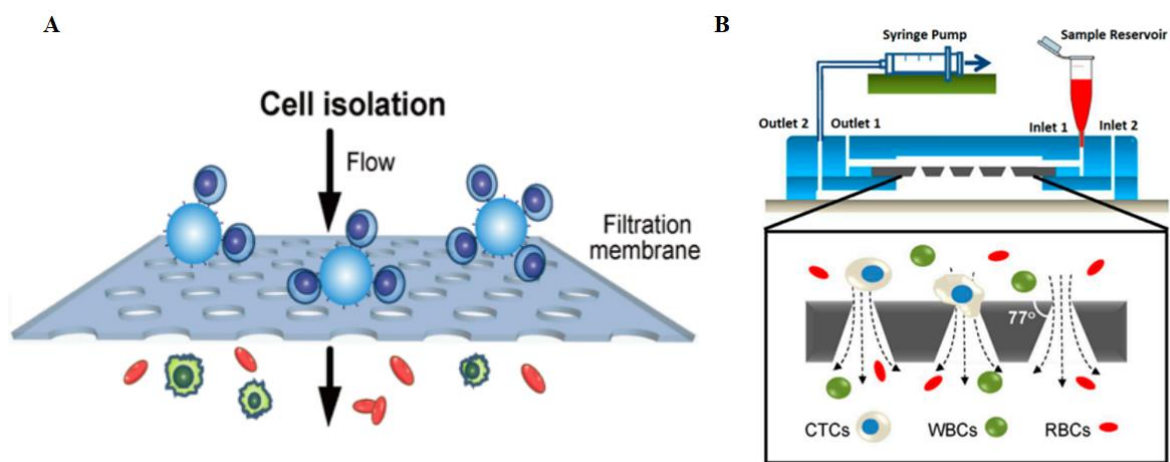


Figure 1.18: CTCs filtration devices: (A) filtration membrane to capture circulating cells: to use this type of approach is needed a post-analysis recovery step and a pre-analysis cell fixation step, to prevent lysis. (B) solution to adapt membrane filtration: the blood sample is injected through the inlet 1 and aspirated through a syringe from the outlet 2. CTCs are blocked on the membrane and can be immune-stained and further analysed through fluorescence microscopy [46].

The use of micropillars to enrich CTCs is known as Multi-Obstacle Architecture (MOA) capture and it is important not to confuse it with Deterministic Lateral Displacement. In the former case, indeed, the purpose of the micro-structures inserted in the channel is to entrap specific target cells, according to their dimension. The spacing and the geometry of the pillars are studied in such a way to allow the passage of smaller cells, while cells greater in size are blocked. This technology has been applied both for CTCs and CTCs clusters -i.e. micro-emboli of CTCs (≥ 2 CTCs) grouped together that have been associated with increased metastatic potential and poor prognosis but are even rarer than single circulating cells [25]

(fig.1.18). This approach presented high efficiency rates but moderate throughput (Table 1.7). For the single CTC MOA capture it should be noticed that the method used in label-free mode showed low recovery rate (~20%); thus, this value has been increased by labelling CTCs with anti-EpCam coated microbeads in order to increase the size of the cells and reduce their deformability [51].As the membrane filter methods, also these approaches are affected by the need of a sample preparation stage or a post-isolation step to allow the recovery of the enriched cells. This could be considered as a critical limit because it prevents the possibility to integrate on the same platform a following CTC analysis or counting step.

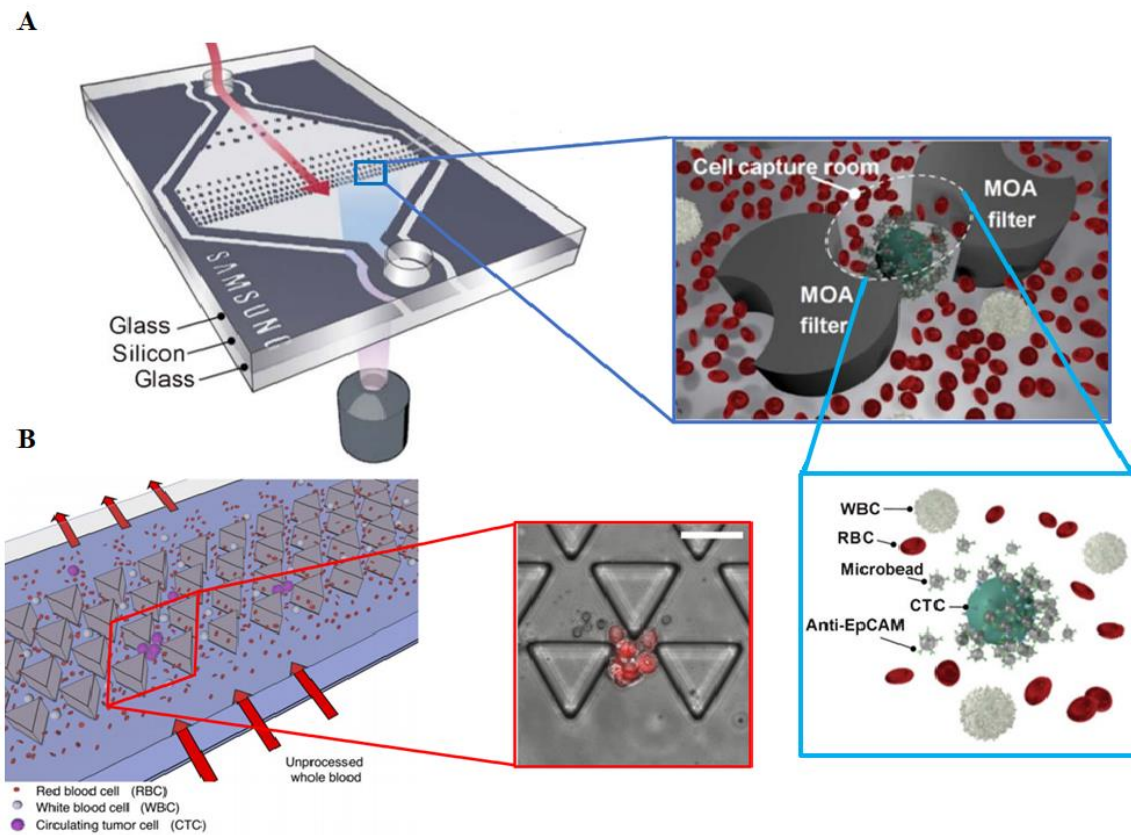


Figure 1.19: Filtration devices: (A) MOA capture platform: the rooms created between the pillars entrap the CTCs, but not the other blood cells due to their smaller size- In the second zoom, anti-epcam functionalized microbeads were attached to the CTCs surface in order to increase the capture efficiency of the system [51]. (B) triangula-shaped pillars used to detect and block CTC clusters in whole blood, for further analysis [52].

1.14 Label-free approach: Deterministic Lateral Displacement (DLD)

This kind of method could be considered as a particular case of filtration problem. It exploits the interaction between the flow and different shaped micro-structures – i.e. pillars – within the device. Thus, when the flow forces cells around the obstructing micro-structure, they are differentially displaced according their differences in a the combination of size, shape and deformability (*fig.1.20*). Control over the particle sorting is given by the specific parameters, which define the geometrical disposition of the pillars in the micro-chamber; these are: the critical diameter D_c , the gap between pillars G , the shift angle between two subsequent pillars α , the row shift d and the centre-to-centre distance λ (*fig.1.18*).

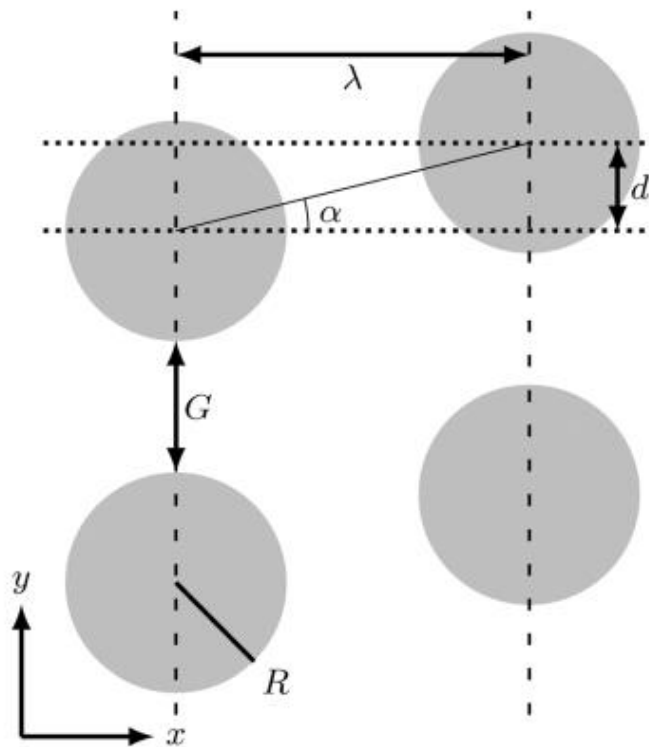


Figure 1.19: Schematic of DLD geometry, resuming the principal parameters to defying it [53].

It is also possible to define other two parameters: the shift row fraction ε and the number of flow stream that carry equal flux, N , respectively as:

$$\varepsilon = \tan \alpha \quad (1)$$

$$N = \frac{1}{\varepsilon} \quad (2)$$

The parameter which sets the behaviour of the chip is the aforementioned critical diameter: cells with a smaller diameter ($\phi < D_c$) will flow along the streamline of the initial flow, while particles with a larger one ($\phi > D_c$) will move towards the next streamline, thus following the direction dictated by the pillar array (fig. 1.20). It is defined as:

$$D_c = 2\beta \quad (3)$$

Where β is the width of the stream line. The equation number (3) could be further approximated, under the condition of non-uniform velocity profile, as:

$$D_c = 2\eta G\varepsilon, \quad (4)$$

where η is a unit-less for the correction of a non-uniform flow profile. Furthermore, in literature it has also been proposed an empirical formula to describe the same quantity:

$$D_c = 1.4G\varepsilon^{0.48} \quad (5)$$

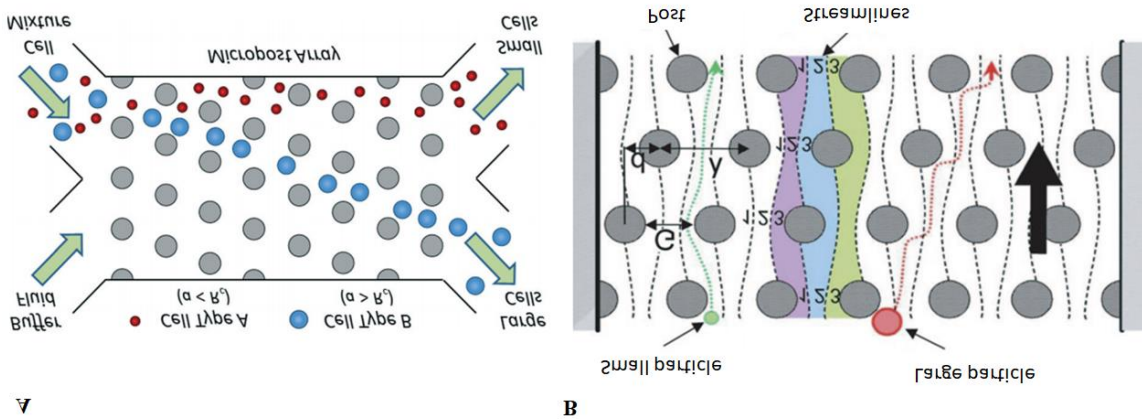


Figure 1.20: Schematic of the basic functioning principle of Deterministic Lateral Displacement: (A) particles with radius (a) greater than the critical radius (R_c) follow the direction defined by the micro-post array, while the trajectory of particles with smaller radius ($a < R_c$) is imposed by the

initial streamline (B) schematic of the streamlines: the cells larger than the critical diameter (D_c) deviate their path towards the next streamline at each obstacle met [54],[55] .

It is also possible to calculate the systemic resistance of the DLD chip due to lateral gap (G). The resistance of the flow in a microfluidic device can be generally calculated as:

$$R = \frac{\Delta P}{Q} \quad (6)$$

Where ΔP stays for the pressure drop and Q for the flow. For a simple rectangular channel, with the assumption that the lateral gap (G) is less than the depth of the channel (E), it can be derived:

$$R_{rectangle} = \frac{12\mu L}{G^3 E} \quad (7)$$

Where μ is the fluid viscosity and L is the channel length. In literature, it has also been calculated the resistance of a circular pillar array with the condition that the gap size is equal to the post size and the row shift fraction is 0.1:

$$R_{circlearray} \approx 4.6 \left(\frac{\mu L}{W G^2 E} \right) \quad (8)$$

being W the width of the arrays.

In literature have been investigated many different pillar shapes, according to the device separation function. Or the RBCs separation from the whole blood it has been found that I-shaped pillars – versus circle or squared ones – granted the best efficiency (*fig 1.21(A)*) [56].

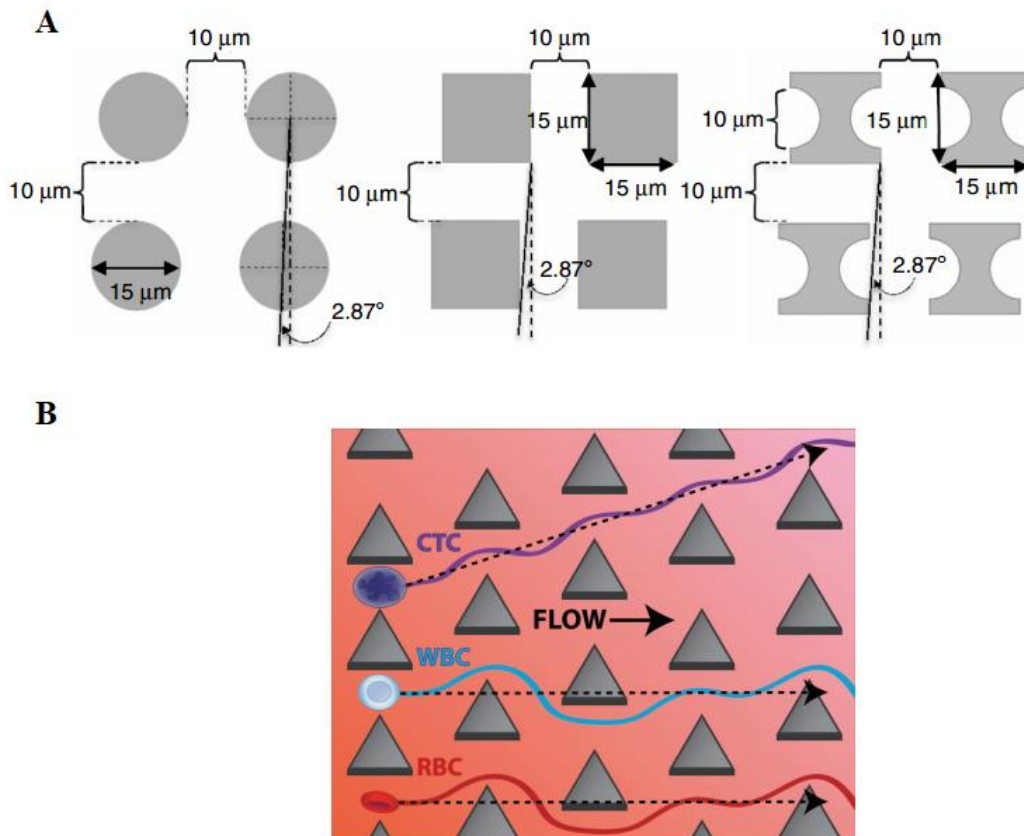


Figure 1.21: Different pillar shapes: (A) Circular, squared and I-shaped were studied in a RBC-separation problem from the whole blood, resulting that I-shaped had a greater efficiency [56] (B) triangular shaped pillars were applied in the CTCs detection problem, reaching good recovery values and extremely high throughput [57].

Triangular shaped, instead, were used in CTCs isolation; in comparison to circular ones, triangle-shaped posts led to greater throughput and improved efficiency. Thus this shape seemed to be more suitable for cell type with large due to the cell minimal deformation at the pillar apex [46].

It should also be mentioned, as a particular case of DLD, a device that exploits a varying distance between pillars in order to better discriminate circulating cells. It represents a particular case because the obtained cell displacement is not deterministically defined by the position of the pillars, but is created by the flow. The chip is composed by a matrix of pillars that – row by row – present different spacing measures: starting from 18 μm and down to 2 μm (fig 1.22).

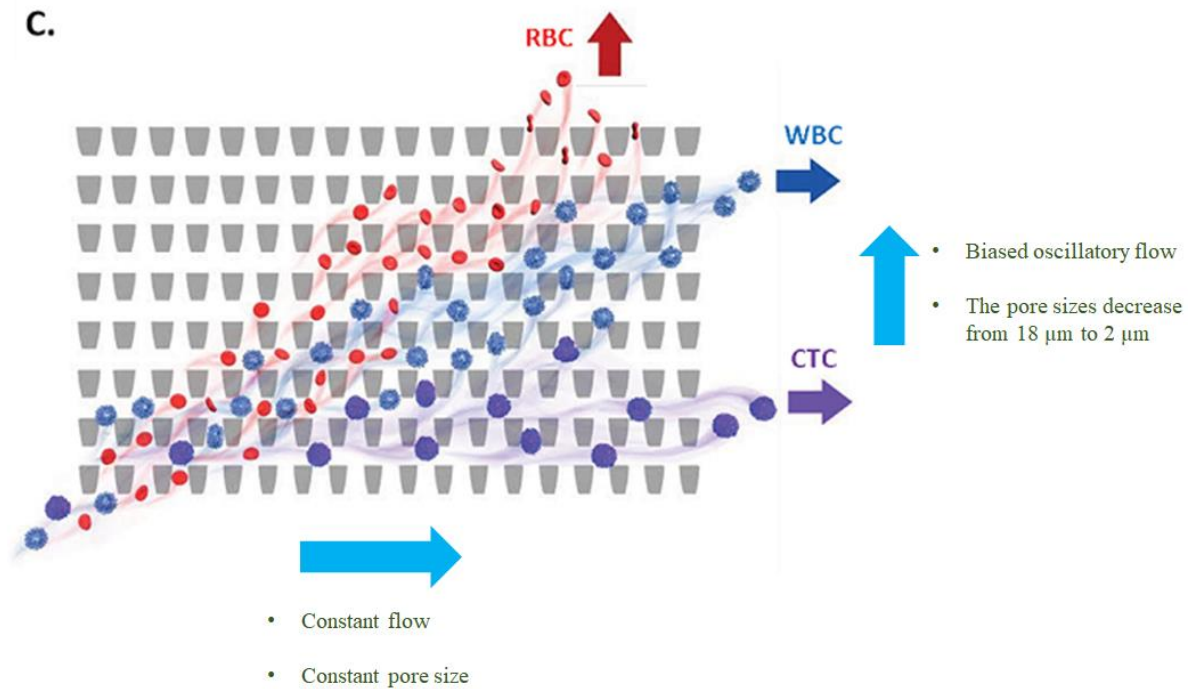


Figure 1.22 Lateral displacement obtained by a combination of two flows and a pillar matrix, characterized by lateral gaping varying in size and no row shift [58].

The working principle is based on the use of two crossed flows. The first, in the horizontal direction, is a constant low, while the second, in the vertical direction, is characterized by a sine waveform of the amplitude. This particular composition of flows allows the cell separation, according to their dimension and deformability. The vertical flow, indeed, will push upward the cells: that ones that have the right dimension – or that, thanks to their deformability, can squeeze themselves enough – will pass through the pillar array; the cells greater in size, conversely, wouldn't pass through the gaps between the pillars. In such a way, larger cells would remain blocked in that gaps, but the oscillatory nature of the vertical flow will invert the stream and will thus release the cells. At the same time, a constant flow will ensure that all the cells -both that passed through the pillar barrier and the blocked larger cells, when free to move - will be flushed towards the outlets. The system obtained is thus capable to reach high values of recovery rates but is affected by a limited throughput; to overcome the latter issue, is thus possible to use more devices run the processing in parallel [58].

DLD-devices are generally characterized by relatively big dimensions, as to reach high levels of recovery this technique requires long paths (fig.1.23) (e.g.: length 35 mm, width: 3.5 mm) [59]. Furthermore, thanks to the deterministic nature of this devices -conversely to the stochastic phenomenon of diffusion – the desired particles trajectories will be maintained even for high pressures and high flows. This property allowed these devices to reach throughput level greater than any other microfluidic chip for cell separation, while maintaining good values o capture efficiency.

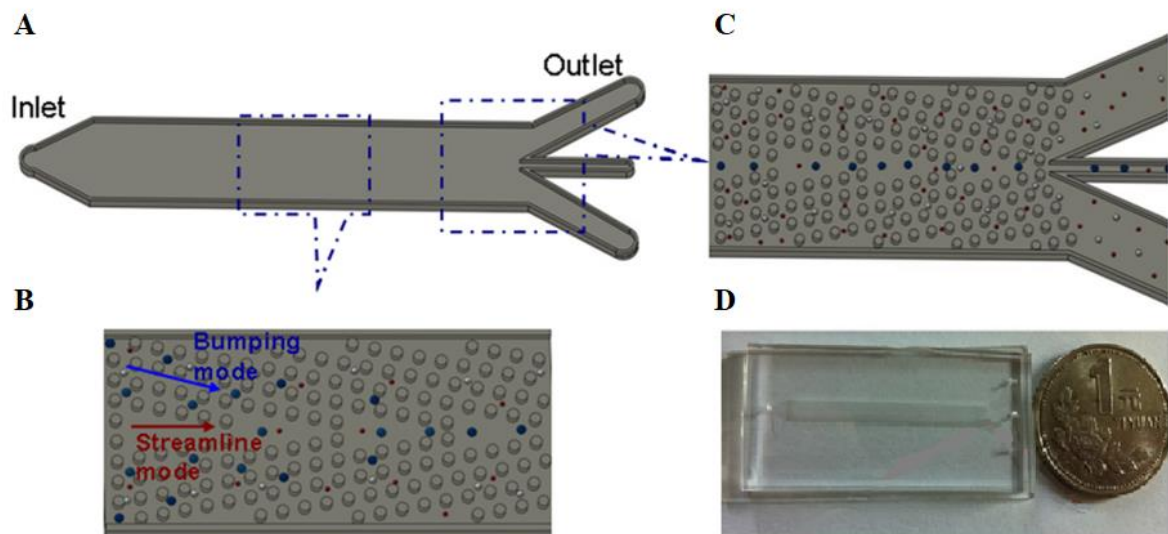


Figure 1.23: DLD chip used for CTC separation from blood. (A) Schematic of the chip: it presents one inlet for the whole blood and three outlets. CTCs are deviated at the centre of the chip and enriched at the middle outlet, while blood cells, smaller in diameter, flow following the main stream towards the external outlets. (B) Zoom showing the main streamline and the so called “bumping mode”, that is the typical flow of particles with diameters greater than D_c . (C) Zoom showing the ideal output condition: CTCs at the centre of the chip and the other blood cells on the external sides. (D) The device is characterized by a length of 35 mm and a width of 3.5 mm, as it can be seen by comparison with a coin.

These properties make this kind of approach really interesting, in particular for applications that involve multiple analysis steps, integrated on the same platform. Regarding the CTCs isolation and identification problem, therefore, this type of technology could be used within the same device as a RBCs removal step, allowing the subsequent steps to focus their analysis only on circulating cells and WBCs. Thus, should increase the capture efficiency of

the whole system and significantly improve the device throughput. A successful implementation of such a chip could be represented by the aforementioned CTC i-chip [41].

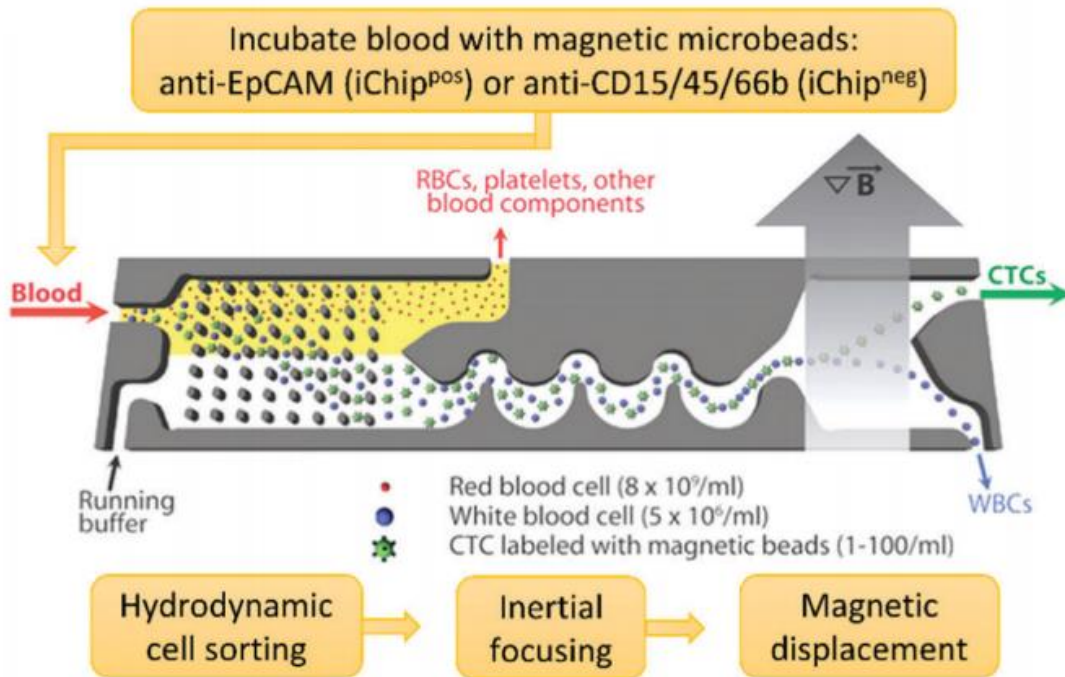


Figure 1.24: CTC i-Chip as an example of DLD integration on a platform to perform RBCs separation from a blood sample. The picture shows the three stages of the device: hydrodynamic cell sorting by DLD, inertial hydrofocusing and magnetic displacement. It is also shown the operative modes of the chip: positive selection or negative selection [25],[41].

Capture technique	Device Geometry	Recovery [min-max]	Purity [min-max]	Sensitivity [min-max]	Throughput
Dielectrophoresis	Apostream™	68 ± 10% - 75 ± 3%	0.1% - 1%	0% - 93%	/
Magnetophoresis	PCM microseparator	94.8%	/	/	2.5 µl/h – 20 µl/h
Acoustophoresis	/	84 ± 2% - 92 ± 1%	~99%	/	6 ml/h
Filtration	Membrane filters	68 ± 8% - 95 ± 3%	0.1%	50% - 100%	200 ml/h-220 ml/h
	MOA (cluster)	41% - 90%	/	31% - 41%	2.5 ml/h
	MOA (single)	20% - 89.7%	/	/	/
Inertial hydrophoresis	Straight channel	8% - 37%	20% - 95%	50% - 88%	24 ml/h
	Spiral channel (Not Lysed)	85%	7% - 9%	100%	3 ml/h
	Spiral channel (Lysed)	71% - 88%	0.1% - 86%	100%	12 ml/h
Deterministic Lateral Displacement	Triangular pillars	80% - 99%	/	/	120 ml/h
	Triangular pillars	91%	/	/	600ml/h
	Circular	90%	97%	/	15 ml/h
	Gap-variable ratchets	77% - 96%	/	/	1 ml/h

Table 1.7: Synopsis of label-free methods performances for CTC and other cell detection. [25],[47],[59],[57],[60]

From the literature, thus, emerges that any new project, involving the creation of a new microfluidic device for the rare cells detection, should overcome precise values of the above-reported parameters. In particular, in order to be captivating for the clinical use, it should be defined a threshold, at least, above 90% for the capture efficiency – i.e. the recovery rate – and a throughput greater than or equal to 7.5 ml/h.

1.15 Main project and aim of the thesis

Analysing the state of art, thus, it becomes clear that the rare cells detection, in particular of CTCs, is currently the frontier research in the early detection, involving even applications in the personalized medicine field. Of course, the attention is focused on slightly or completely non-invasive methods, because of all the attached advantages of this kind of approach. With this in mind, microfluidic platforms well adapted to these requirements and could represent the way to a new generation of CTC-chips that would push-forward the early cancer detection and so, ultimately, the cancer struggle.

For these reasons, in the CNST-IIT facility of Milan, it has been conceived a big research project for the realization of a new microfluidic device that addresses all the up to now listed requirements, taking advantage of a three steps integration strategy (*fig. 1.25*). The main project, thus, will be focused on three critical parameters: low cost, high efficiency and high throughput. Since immunoaffinity-based technique have shown a great capture efficiency but poor throughputs and high costs - due to the reagents -, the proposed platform will be completely label-free and will involve three main processing steps. The view of the project is, therefore, projected toward the creation of an innovative microfluidic device for the high sensitive identification and isolation of circulating tumor cells. As it was already mentioned, microfluidics allows to integrate different physical principle onto the same platform, opening the way to the ambitious combination of multiple techniques – filtration, hydrodynamic flow control and optical detection - not only to push further the research in the biological analysis field but also to make more accessible some medical procedures, that nowadays remain still expensive, invasive and not repeatable with high frequency.

As all the research that aims to the development of a final device, it is necessary to focus an initial point from which to move. This thesis, thus, could be considered as only one piece of

a more complex and challenging “puzzle”, aiming to give not only a solid theoretical basis, but also the related interpretation and application, in order to implement the first steps on the path that, hopefully, will lead the project closer to the final goal.

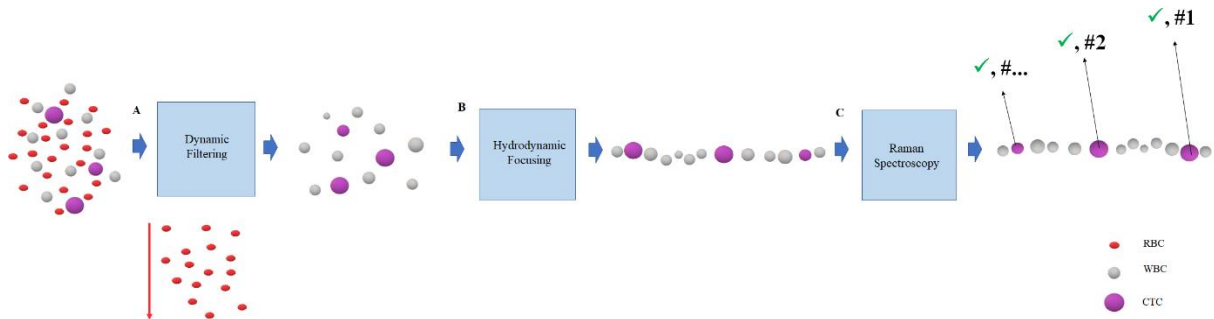


Figure 1.25: Block diagram of the three-steps CTC identification and isolation device.

Making an analogy with the signal theory, one of the main issues in the analysis of rare cells field, as seen in literature [25],[35],[1], is the poor “signal to noise ratio”; this is given by the fact that rare cells represent “one positive event” – i.e. the signal that carries information and that we want to “extract” from the whole blood – over billions of “negative events” – i.e. noise that superimpose to our measurement. Therefore, if we consider each single count as a contribute to the “frequency” of the whole signal, we could think to the target signal as a low-frequency one while the noise shows a high frequency content. Thus, as often happens in biological signal analysis, the first step toward the extraction of information is given by a low-pass filtering. Coming back to the real problem, the “low-pass filtering” nature of the first section of the project – i.e. the dynamic filtering - could be applied by removing - or drastically reducing their number – those cells that are easily identifiable as non-target cells and thus, useless and only time consuming for the device purpose. In this way is improved not only the recovery rate - i.e. the efficiency – of the whole device but also its throughput, because of the reduction of the number of cells to be processed in the subsequent steps. Fortunately, in the whole blood it exists a category of cells, that, principally thanks to their smaller dimensions, could be easily rejected as non-CTC and is represented by the erythrocytes (*fig 1.25 (A)*). In literature, many solutions to separate cells from whole blood have been presented. Though, to satisfy not only the requirements of high efficiency and throughput but also the need of this stage to be capable to interface with the subsequent steps,

the choice of the “optimal” method has fallen on the Deterministic Lateral Displacement (DLD) approach.

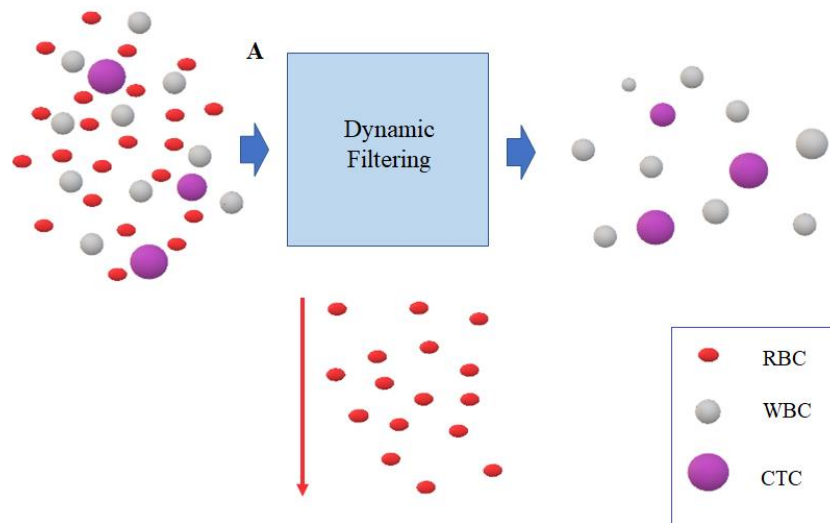


Figure 1.25 (A): Step 1. The whole blood is taken as input and, through a dynamic filtering, RBCs are separated and discarded. The remaining CTCs and WBCs are taken as input in Step 2.

The second step is thought to increase further the efficiency of the detection by stacking one behind the other the cells that exit from the DLD stage, through hydrodynamic focusing (fig.1.25 (B)).

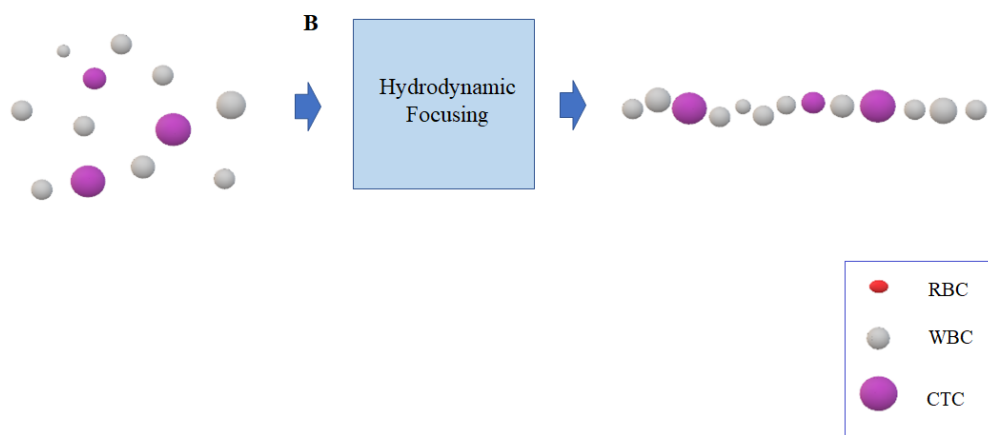


Figure 1.25 (B): Step 2. WBCs and CTCs exiting from Step 1 are aligned on a row one behind another in preparation for Step 3.

This could be seen as a preparations stage to the third step, in which the real discrimination between CTCs and the remaining blood cells – ideally only leukocytes -is implemented (fig.

1.25 (C)). This analysis should be performed by using a monochromatic coherent source of light to strike each single cell and obtain information about its composition – i.e. Raman Spectroscopy. This technique, really innovative for this kind of integrated application, allows to assign to each cell a defined chemical component spectrum, which uniquely distinguishes the type of cell. This feature, thus, not only allows the identification of CTCs but also gives an on-line chemical analysis and the possibility to identify the subgroups, that characterize the heterogeneous nature of these cells, and the type of tumor they belong to. Therefore, this element represents the key to contribute actively to the development of a personalized medicine based on these cells.

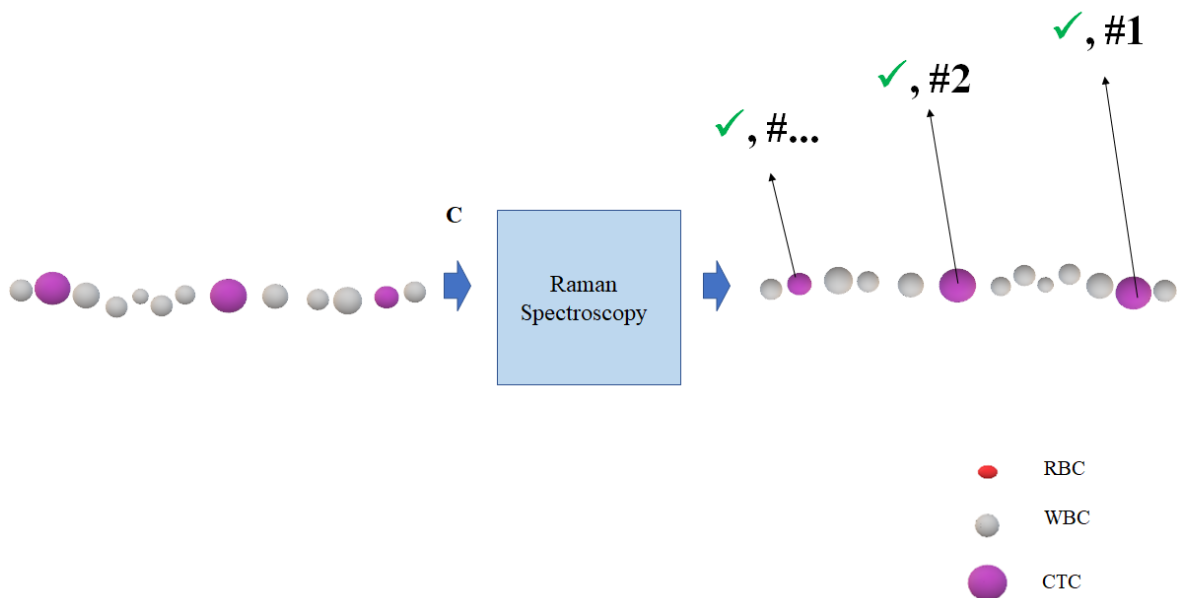


Figure 1.25 (C): Step 3. The aligned cells exiting from Step 2 are taken in input. The Raman Spectroscopy will discriminate CTCs from WBCs according to their different composition and count them. WBCs are discarded, while CTCs could be enriched for further analysis

One of the most challenging aspects of this project is its fabrication method, applied to the realization of a three-step integrated device. The whole system, indeed, is thought to be created using an innovative and fast prototyping technique, the femto-laser micromachining followed by chemical etching, which potentially allows to obtain complex 3D structures in fused silica samples. The choice of glass as unique material to build a cell detection device could also represent a challenge: the relative advantages, both of the technique and of fused silica, will be discussed in the Materials and Methods section.

Eventually, this project of thesis is focused only on the first step of the above described project. In particular, the aim of this study is to verify the feasibility of complex-shaped structures completely buried in glass sample - as the ones defined by the DLD approach, i.e. pillars - and the high-resolution control on their geometrical positioning within the device, their size and their dimensions, by using the femto-laser micromachining fabrication system. Thus, secondary aims could be identified in find geometries of the device that could well fit both the requirements of the first step processing and those imposed by the fabrication technique and, then, the validation of the microfluidic devices obtained as result.

Chapter 2

Materials and methods

The trend in the last years in the microfluidic systems applied to biological sample analysis is to carry out increasingly complex 3D structures at micro-scale level to enhance the devices performances. Obviously, the main limits and challenges are imposed by the choice of the material and its manufacturing technique. In the particular case of CTC capture strategies, many kinds of materials have been used, such as semi-conductors (e.g. silicon), ceramics (e.g. fused silica), polymers (e.g. polydimethylsiloxane (PDMS)) or metals [35],[61] Due to the need of optical transparency, which allows the direct visual monitoring of the chip and the application of optical analysis techniques the choice has narrowed the acceptable options to two of the above materials: PDMS and fused silica – i.e. quartz glass.

2.1 PDMS: a brief overview

Due to its particular features, PDMS has been one of the most used materials for microfluidic devices, obtained by lithography, in the identification and separation of CTCs, particularly in their early development stages. Among these it could be mentioned: optical characteristics – e.g. transparency –, biological compatibility, cost efficiency and the possibility of surface functionalization and integration with other nanotechnologies[35]. PDMS lab-on-chip platforms are created using standard photolithography, either “positive” or “negative”, after the whole designing of the chip structure using computer-assisted technology. The fabrication procedure consists in the superimposition of layers of substrate and photo-resist. Then a metallic mask, reproducing the wanted geometry, or its negative, is used to cover the photo-resist. The sample is then exposed to UV light: according to type of chosen technique – positive or negative – the UV light will harden or melt the photoresist in the exposed areas,

resulting in 3D grooves. The following step is a washing of the formed channels that will leave a fully organized microfluidic chip. The final step consists in the sealing of the obtained chip on a substrate to close the channels and the chambers created (*fig 1.26*) [62].

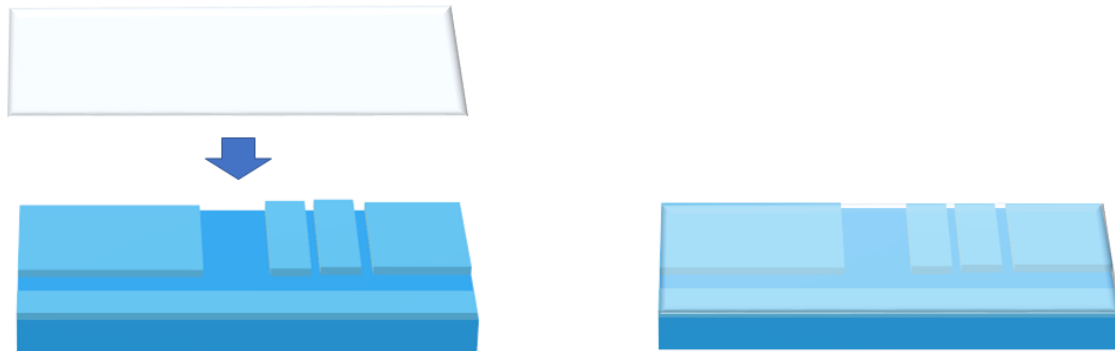


Figure 2.1: Schematic representation of sealing procedure.

Apart from its several advantages, this technique presents some critical limitations. First of all, the lithography technology could be defined as planar: this means that complex structures, varying their section along the z axis – e.g. conic shapes – are difficult to obtain. For the same reason, all the devices need to be created divided in two parts that must be joined together – i.e. sealing - to obtain a working platform. Thus, this method imposes to any device a bond on the maximum pressure of input injection, and, as result, on the whole throughput of the chip, except for particular solution studied to avoid the detachment of the two pieces. Furthermore, PDMS shows to be a flexible material: this could create an issue when the geometry involves small cavities, that, due to the non-rigidity of the material, are deformed when subjected to high pressure. Other critical points of PDMS could be: it is gas permeable, this could be an advantage in oxygen and carbo dioxide transport in cellular studies, but not for the application presented in this study. The passage of gas bubbles - e.g. air – can be problematic: low molecular weight chains in PDMS can leach out into solution, affecting cellular studies. Furthermore, PDMS, as hydrophobic material, is susceptible to non-specific adsorption and permeation by hydrophobic molecules [61]. This issue could be fixed by using a plasma exposure to make the surface hydrophilic: though this procedure will make the manufacturing more complicated [62]. Thus, it couldn't be considered as a totally inert material, which should be ideally for this kind of application.

Eventually, for the chosen application, either the technique and the material show critical issues that suggest the need to turn to different materials and technologies. The main constraint on the choice of the manufacturing process is imposed by the need to obtain a device resistant to high pressure to reach very high throughputs. Consequently, it should be necessary to find a fabrication approach that could allow the development of 3D complex-shaped devices, on the micro-scale, and fully embedded in the substrate – i.e. that not require sealing. These kinds of requirements could be satisfied by an innovative technology for 3D writing, referred as femto-laser micromachining. Moreover, this technique presents a further advantage: it provides the first stages of the research and development field with a fast, flexible and mask-less prototyping technique.

2.2 Femto-laser micromachining fabrication

This represent a direct writing technique, able to modify the material properties exploiting the interaction between the latter and the ultra-short (femto) laser pulses. One of the most common materials used as substrate for this kind of fabrication is fused silica glass. It is well known for its optical characteristics, such as transparency and low background fluorescence, being completely inert - thus, compatible with biological samples-, presenting relatively low non-specific adsorption and being not permeable to gases [61]; furthermore, its rigidity (shear modulus ~ 30 GPa) allows the creation of self-supporting devices. All these features make this kind of material interesting, specially, if related to the creation of platforms for the processing of biological sample. It is also important to emphasize that the transparency of the material is a basic property required for the fabrication technique, described in the next sections, that offers the possibility of machining hollow volumes into transparent materials with a great freedom of geometry in 3D [63].

2.3 Femtosecond Laser Irradiation, followed by Chemical Etching (FLICE) technique

This manufacturing technology is known with several names: selective laser-induced etching (SLE), femtosecond laser assisted etching (FLAE), in-volume selective laser etching (ISLE), and many others [64]. All of them refer to the two-steps fabrication process: 1) permanent modifications of the morphological-physical properties of the substrate, achieved by laser irradiation; 2) selective removal of the modified material through chemical etching.

As already said, FLICE manufacturing technology allows to generate complex 3D structures in a subtractive 3D printing process within fused silica samples. Furthermore, in comparison with photolithography technology, femtolaser micromachining in this kind of applications, gives access to a more rapid, simple and maskless manufacturing process, especially in the prototyping phase of the device. These results could be obtained by setting precise laser writing parameter that allow material modification sufficient to facilitate the subsequent removal of material by chemical etching.

2.4 Modification of the substrate properties: hints of theory

The structural modification of the material is made possible by an optic energy transfer to the electrons, and thus to the lattice, of a laser irradiated material. The underlying process is called *optical breakdown* and it involves, in presence of sufficiently high radiations, *non-linear* phenomena that cause the transition from the valence energy band to the conduction band in transparent materials, otherwise impossible. Among these processes, particularly three could occur:

- 1) multi-photon absorption: due to the absorption of multiple photons by a single electron in the valence band.
- 2) Tunnelling ionization: the high-intensity electric field incident laser impulses lower the Coulomb potential barrier, thus allowing the electron to pass from the valence to the conduction band, through tunnelling effect.
- 3) Avalanche ionization: this phenomenon is created by the interactions between laser light and free charges at the bottom of the conduction band. When the absorbed energy is sufficiently high to overcome the band minimum of at least

E_g - the transparent material energy gap – a second electron could be moved in the conduction band by collision. Thus, two electrons are obtained at the bottom of the conduction band and they could repeat the energy transfer cycle, giving rise to an exponential increase in the population.

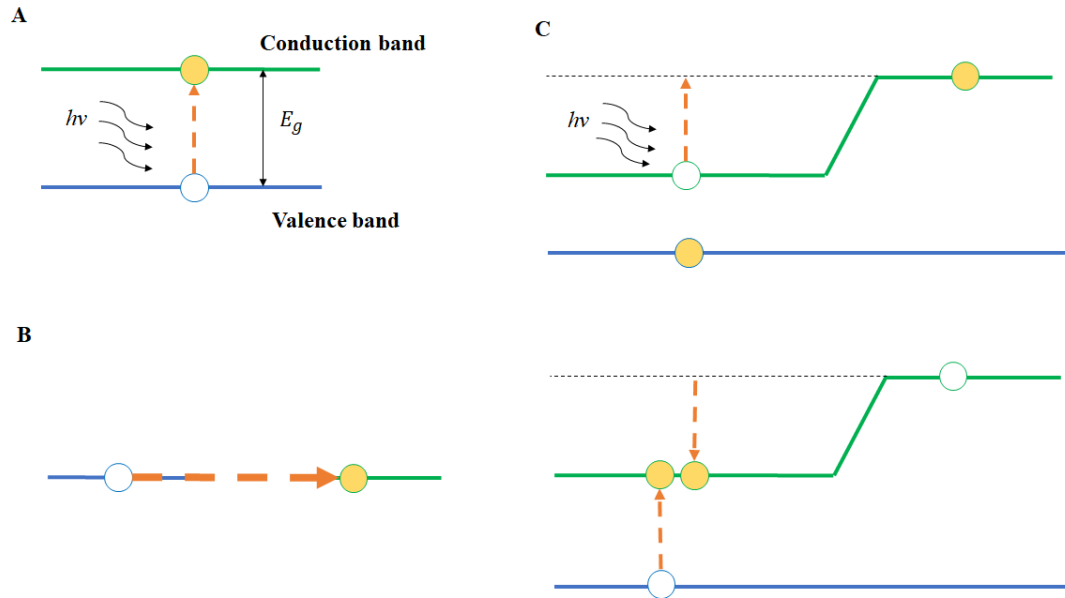


Figure 2.2: Schematic of the non-linear processes: (A) multi-photon absorption. (B) Tunneling ionization. (C) Avalanche ionization.

The permanent damages on the material are due to these non-linear phenomena, though the physical mechanisms that lie behind the modification of the index in transparent materials are, up to now, not well understood. Exceeded the threshold of damage a morphological modification of the material occurs in the laser beam focus point. This change depends both from exposure parameters – such as, energy, impulses time length, repetition rate, writing speed, polarization, wavelength, ...) and the material properties (thermal conductivity, bandgap,...). Varying these parameters, it is, thus, possible to produce three different structural modifications in the material:

- 1) For fluence slightly above the threshold of damage: weak isotropic refractive index variation occurred
- 2) For higher fluency values: nanogratings generation
- 3) For even high fluency values: material ablation

In the practical application for the creation of microfluidic devices, the second structural modification is our laser beam working point. Thus, the fabrication of directly buried 3D structures is allowed.

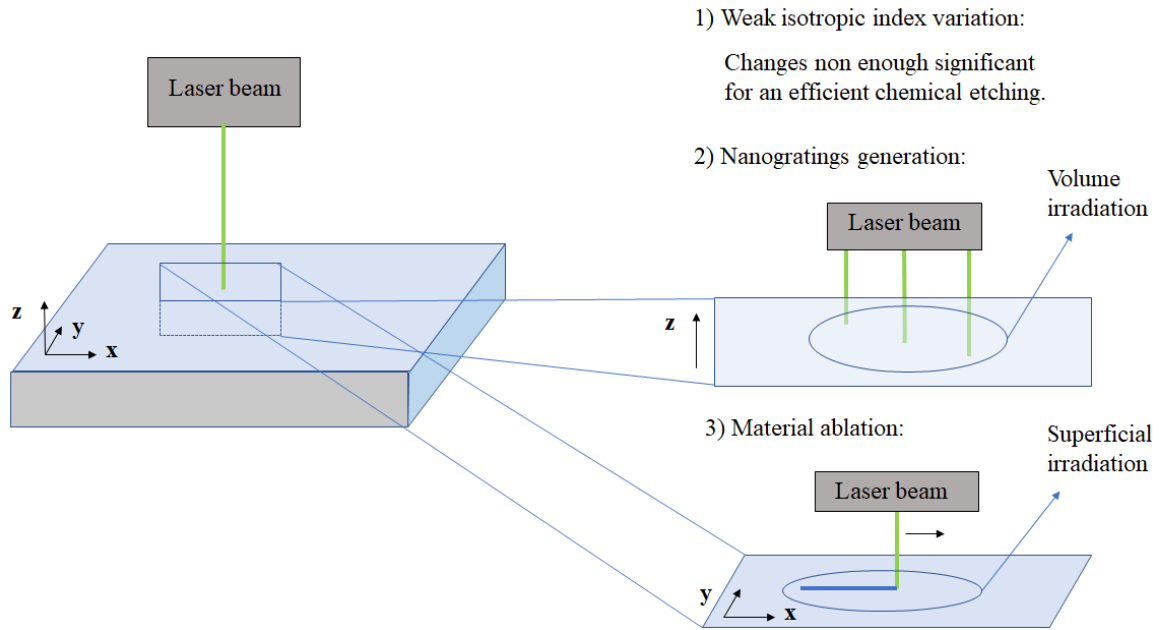


Figure 2.3: Resume of the structural modification laser-induced obtainable in fused silica, through femtolaser technique. (1) Weak anisotropic index variations: this modification of the material structure is not sufficient to provide to the chemical etching step a favourable substrate for material subtraction. (2) Nanogratings generation: structural modifications can be induced at any height within the sample, allowing volume irradiation (3) Material ablation: the related laser beam working parameters allow only a superficial processing of the sample.

2.5 Chemical etching

According to the goal of our fabrication technique, the more interesting variation that occurs, using the second laser regime, is the increase of the etching-rate of the irradiated areas of the material. This condition is obtained in an optimal way by setting the laser writing parameters in order to promote the nanogratings generation, within the material and along the writing direction (\vec{W}). These periodical structures are composed by the alternation - with a defined periodicity of $\sim \lambda/2n$ - of high-density material (light areas) and low-density material (dark areas). It could be observed that these nanostructures are all orientated in an orthogonal way

with respect to the electric field (\vec{E}) – thus, of the used polarization - of the laser writing beam (fig 2.4).

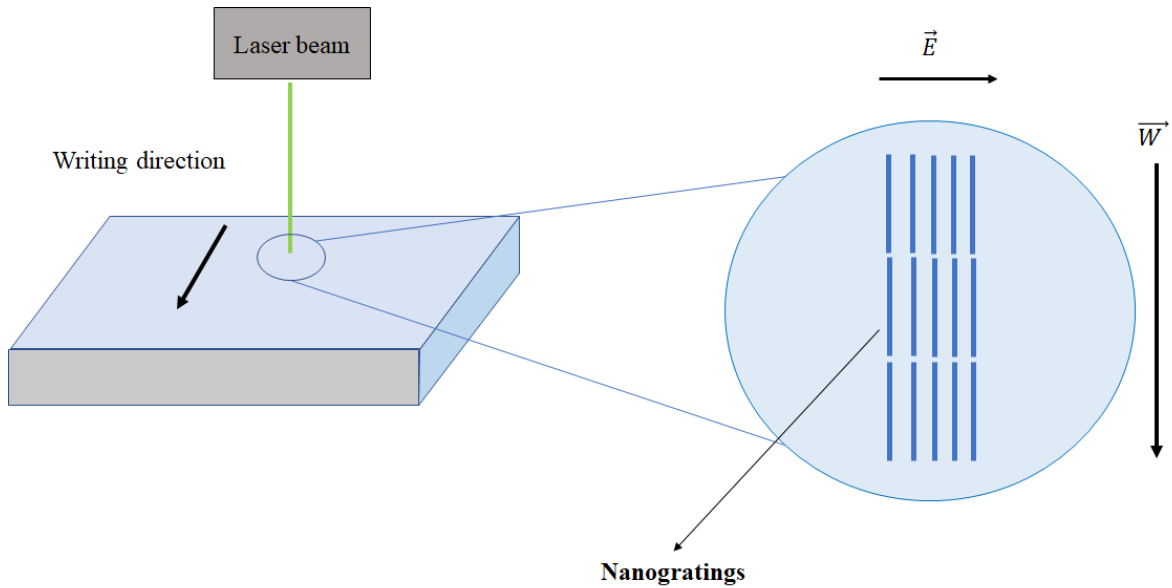


Figure 2.4: Schematic representation of the nanogratings generation phenomenon. In the case represented, \vec{W} is perpendicular to \vec{E} , thus the generated nongratings are parallel oriented to the writing direction.

In particular, it could be observed that when nanogratings are parallel oriented to the writing direction \vec{W} - so that $\vec{E} \perp \vec{W}$ - the such generated nanostructures will positively affect the etching-rate, by helping both the chemical solution and the reaction products diffusion through the irradiated areas of the material. Exactly for this reason the laser writing beam polarization effect – showed in the previous figure - on the formation of these structures is crucial to the success of a favourable etching and, ultimately, to the creation of the device. Conversely if the gratings are aligned orthogonally to the writing direction – i.e. $\vec{E} \parallel \vec{W}$ – the etching will proceed much slower in the structurally modified zones of the material – i.e. where the laser beam has passed (fig. 2.5). The result is a low etching-rate that may compromise the realization of the device, or at least its quality.

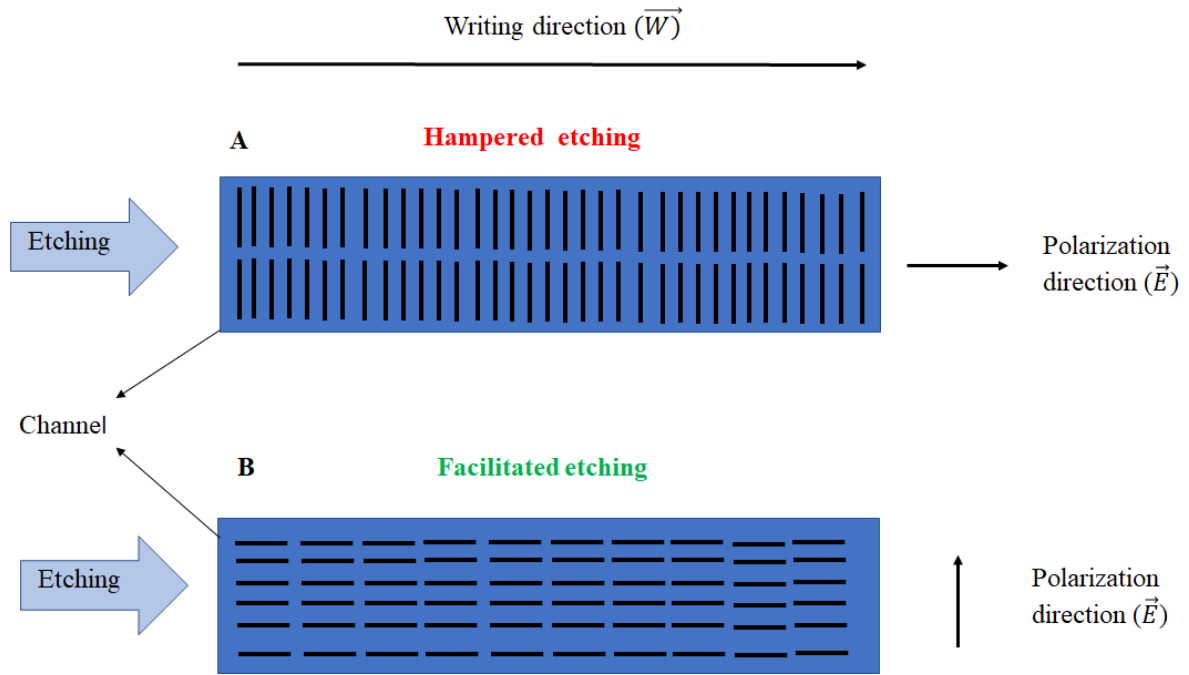


Figure 2.5: Schematic representation of the relation between polarization (\vec{E}), writing direction (\vec{W}) and nanogratings generation in determining the etching-rate.

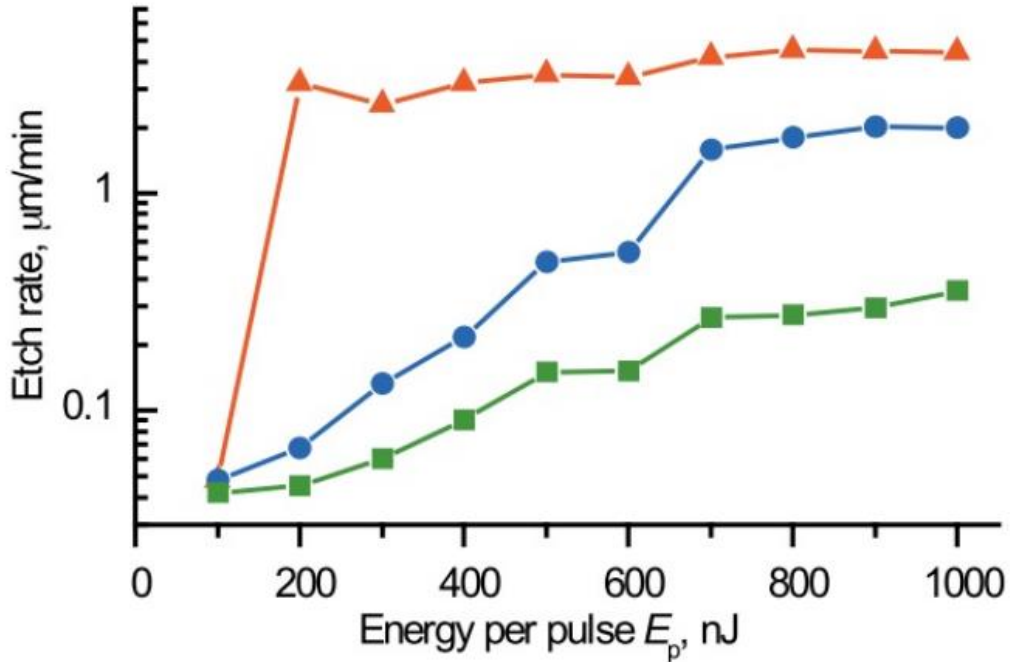


Figure 2.6: Microfluidic channels HF etch-rate in function of the pulse energy and writing polarization. (▲) radiation electric field (\vec{E}) direction perpendicular to writing one (\vec{W}). (●) \vec{E} 45° oriented with respect to \vec{W} . (■) $\vec{E} \parallel \vec{W}$ Taylor et al_2008.

In this kind of application, the hydrofluoric acid in aqueous solution (HF) has found a widespread use as etchant. It has shown that its action is isotropic in the space: the un-irradiated silica is also attacked, but at a much lower rate. The result on the creation of microchannels is a conical shape effect, since the terminations - from which the etching has started – are exposed to the effects of the acid for a longer time [65]. In practice, this is translated in the need for a compensation during the chip designing phase.

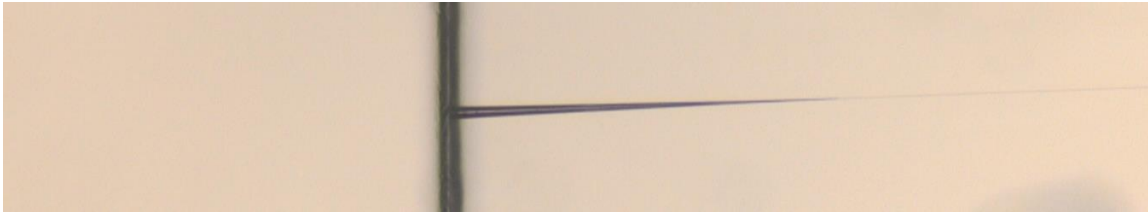


Figure 2.7: conical shape effect due to the isotropic behaviour HF solution.

In order to better compare different types of etchant solution, it has been introduced a quantity called selectivity, it is defined as:

$$(1) \quad S = \frac{l}{h+r_0 r_0}$$

where l is the etched channel length in μm , h is the etching time in hours and r_0 is the etching rate of a non-modified fused silica in $\mu\text{m/h}$ [66]. This parameter could be considered as an etching efficiency index: greater the selectivity, greater is the capability of the solution of removing modified material, while leaving intact – or at least minimally attacking – the un-irradiated areas.

Since HF has presented a construction-limiting behaviour – that is, saturation in elongating channel structures - and, furthermore, showed a not remarkable selectivity [67], the creation of material-integrated hollow volumes with standing structures -i.e. non-modified sections of the material - inside is challenging. This suggested the need to find other chemical solutions with a greater selectivity.

Among these, in the recent years a particular solution has proved interesting properties as etchant agent: the potassium hydroxide aqueous solution (KOH). The principal advantages over HF is the nearly double selectivity and its least saturation behaviour in elongating structures[67]. This is promising in leaving intact particular structures inside material-

embedded chambers, though the considerably small etching rates - as compared to HF acid – limits the removal of larger volumes, that also need to be totally irradiated.

Therefore, to exploit the advantages of both the techniques recently was proposed the combined use of both solutions in two distinct steps, showing successful achievements [65]. With regard to this thesis project, the challenging aspect was the need to remove high volumes of material while leaving inside intact structures – i.e. pillars – with a precise shape and position. Thus, it has been adopted the combined chemical etching in order to exploit the high material aggressiveness of HF acid and the higher selectivity of KOH. In a first moment, large volumes of material were removed by using HF in the chip areas where it was not required a particular precision in fabrication - i.e. tube accesses, channels until embedded structures – and, in a second phase, KOH to finish the device by removing moderate quantities of material in depth in the sample and to maintain the geometry of the planned structures.

2.6 Chemical etching: parameters

For HF acid, it has been used a 20% concentration aqueous solution, inserted in an ultrasonic bath at 35°. The etching was performed under flowing hood, at ARCO-Lab facility of CNST@IIT, due to the high danger represented by the acid.

For KOH, a 10 molar solution in water at 90° was used, along with a magnetic stirrer. The baker containing the KOH solution was then put in a water bath to allow an ultrasound sonication through a sonication tip. It has to be highlighted that this method is quite innovative and, up to now, no concrete achievements are known. Regarding the sonication control, were chosen cycles composed by 7 seconds on over 50 seconds, for all the etching duration.

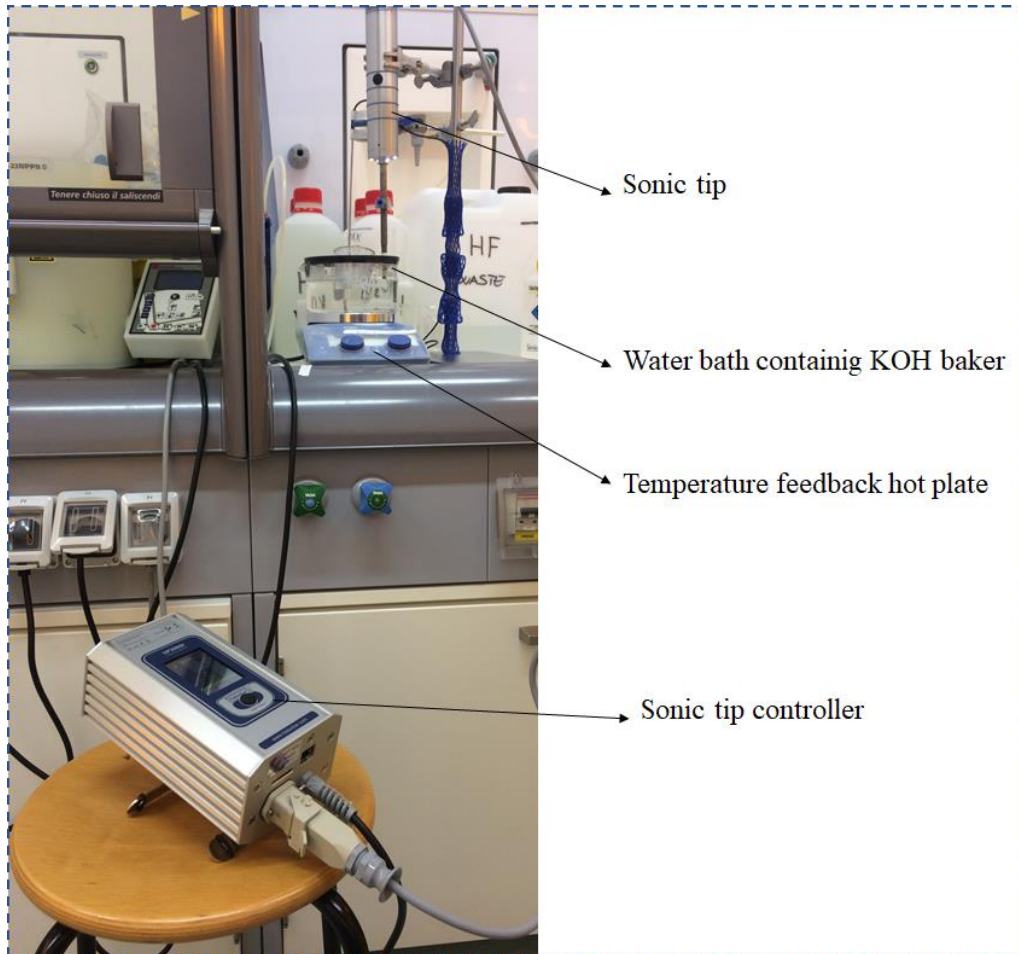


Figure 2.8: Ultrasound sonication set-up for KOH etching.

2.7 Microfluidic devices fabrication

The creation of a working device through this technique is a process that moves along a defined path, requiring basically three principal steps. The first – as the fabrication of a device of any kind – is represented by the designing phase by a 3D design software; the second involves the transfer of the virtually conceived geometries from the software to the hardware -i.e. the fused silica sample -, through the femtolaser micromachine, placed in the facilities of CNST-IIT of Milan. The third and last step is the completion necessary to make the device finally working and is represented by the chemical etching, described above.

2.8 Designing and control: SCA software

This software allows the user to implement two crucial activities for the making device purpose. It provides, indeed, a platform for the design of 3D structures, presented in user-friendly interface (*fig 2.10*) and it also deals with the translation of the user commands into G-code. The laser system, in fact, is computer controlled through G-code low-level programming language. SCA also controls the stage (Fiber-Clide3D, Aerotech), which allows the movement of the fused silica sample – fixed by vacuum suction - in the space with sub-micrometre resolution. The writing set-up, indeed, keeps the laser beam focused in one point and moves the sample along the three axes in order to avoid defects in the beam quality and misalignments. The stage motion is performed precisely, fast and with frictionless, thanks to retroactive engines supported by air bearings.

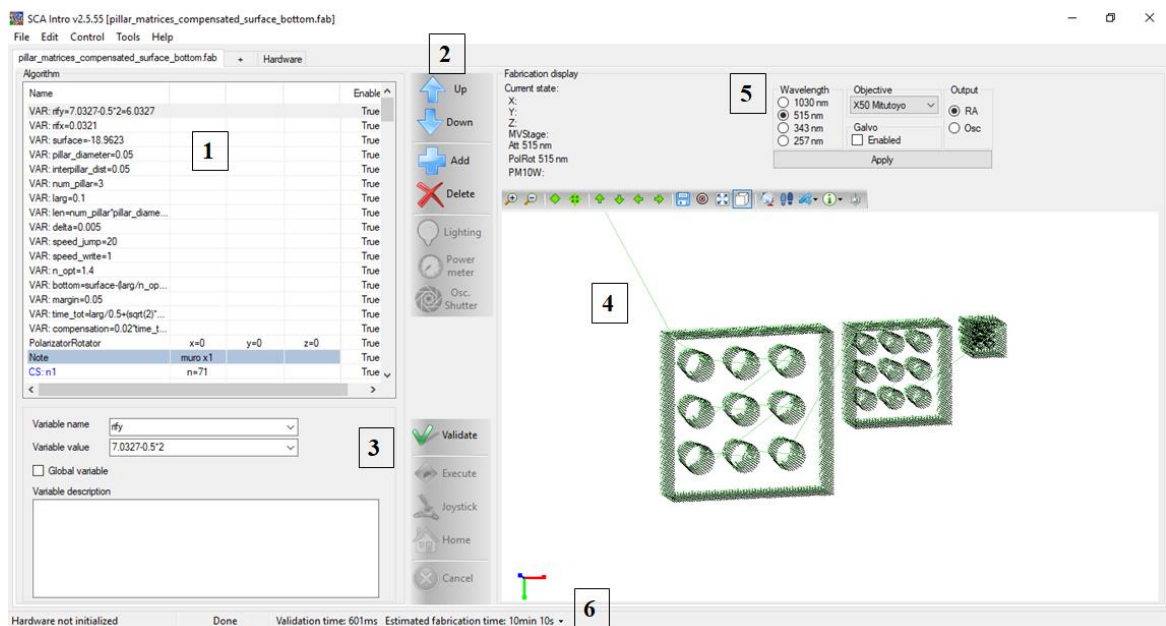


Figure 2.9: SCA interface. (1) Command window; (2) Command list; (3) Executive commands; (4) 3D graphics for the design visualization; (5) Laser hardware parameters selection; (6) Estimated time of writing.

2.9 Writing: femtosecond laser micromachine

The femtolaser writing system has been installed in the laboratories of CNST-IIT of Milan from WOP of Photonics (*Altechna l.t.d.Group*) and specially modified by the FemtoFab-IIT group.

A typical femtosecond laser writing system is composed by few principal components (*fig. 2.11*):

- Laser source
- Optical beam handling line
- Beam focusing system
- 3D sample movement system

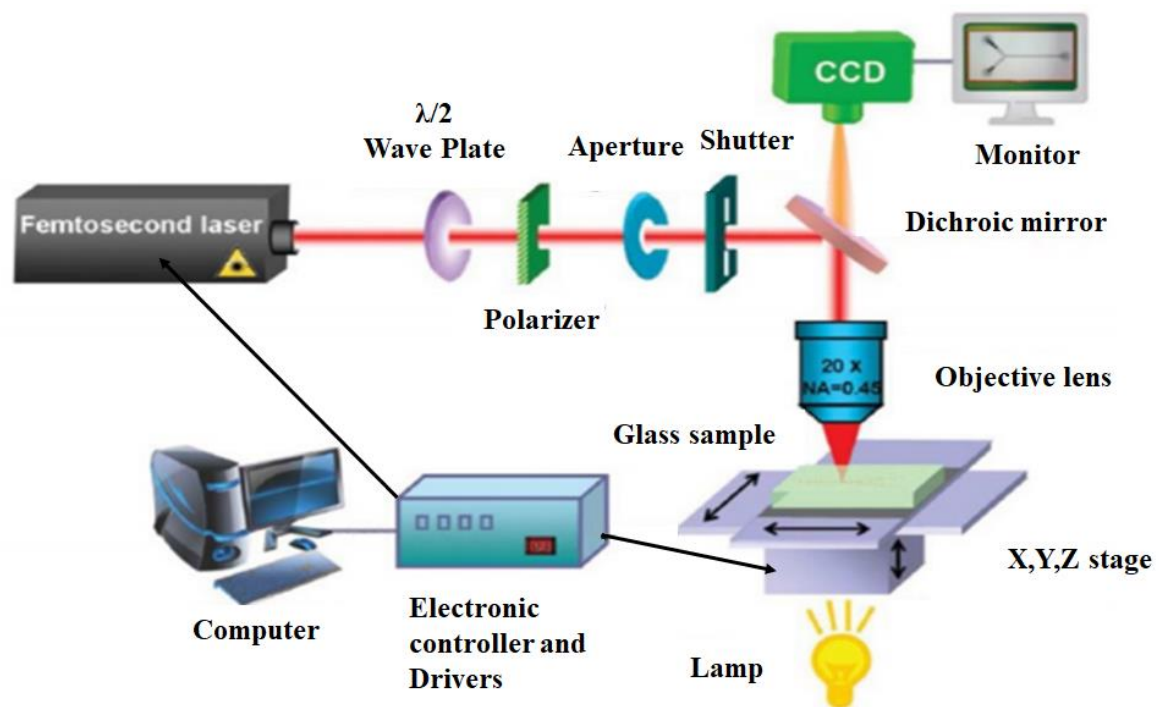


Figure 2.10: Schematic of a femtosecond laser system for used silica sample writing.

2.10 Femtolaser micromachine: laser source

The femtosecond laser pulse source used is a commercial compact system, called *Pharos Light Conversion*. It provides the user with the possibility of varying several parameters, such as, pulse duration (240 fs – 10 ps), repetition rate (1 kHz – 1 MHz), pulse energy (up to ~ 0.2 mJ) and the average power (up to ~ 10 W)⁴ and to exploit the fundamental harmonic (1030 nm). To obtain such short and high-power pulses, a chirped-pulse amplification system is needed, it consists of: a short pulse oscillator, an impulse stretcher/compressor module and a regenerative amplifier. At last, there is also an electronic shutter that allows to modify the repetition rate of the outgoing laser pulses without altering the characteristics of the laser cavity.

2.11 Femtolaser micromachine: optical beam handling line

The laser beam outgoing from the generation system, before arriving on the sample, meets on its path various component, needed for the control of its characteristics. The first among these is the harmonic generator (HIRO, Light Conversion), that takes as input the laser beam fundamental harmonic (1030 nm) and allows the generation of other ones ($2^{\text{a}}\text{H} = 515 \text{ nm}$; $3^{\text{a}}\text{H} = 342 \text{ nm}$; $4^{\text{a}}\text{H} = 257 \text{ nm}$). Other important elements are represented by the power attenuators and the respective polarizers – one for each line – that provide the user with simple and direct control of the beam parameters via software.

2.12 Femtolaser micromachine: beam focusing

In the last section of its path the laser beam needs to be focused in one point to be used for fabrication purposes. The focusing operation is done by an objective lens. The system is equipped with different lenses: 10x, 20x, 50x, 100x. these are specially designed for the reduction of spherical aberrations and the possibility to work at centimetre distances, with a

⁴ information available from the manufacturer company site www.lightcon.com

spot sizes from a few microns (ellipsoid: $3\ \mu\text{m} \times 3\ \mu\text{m} \times 20\ \mu\text{m}$) to sub-microns in the best of the cases.

2.13 Femtolaser micromachine: 3D sample movement system.

See SCA designing section.

2.14 Tests instrumentation and materials

All the tests during this thesis were conducted at the ArcoLab facility, Politecnico di Milano/IIT. The needed instrumentation included:

- Microfluidic Pump System by ElveFlow:

This system was composed by pressure compressor, flow control system, software for the controller, connection tubes and vials (*fig 2.11*)

The OB1 flow controller system is characterized by four outputs: channel 1-2 for low pressures (5 – 200 mbar) and channel 3-4 for high pressures (50 mbar – 8 bar).

The system ensured for low pressure range a pressure stability of 0.005% FS (10 μbar) and or high pressure range 0.006% FS (500 μbar)⁵.

⁵ Information gathered from the ElveFlow site: www.elveflow.com/microfluidicw-control-products/flow-control-system/pressure-controller/

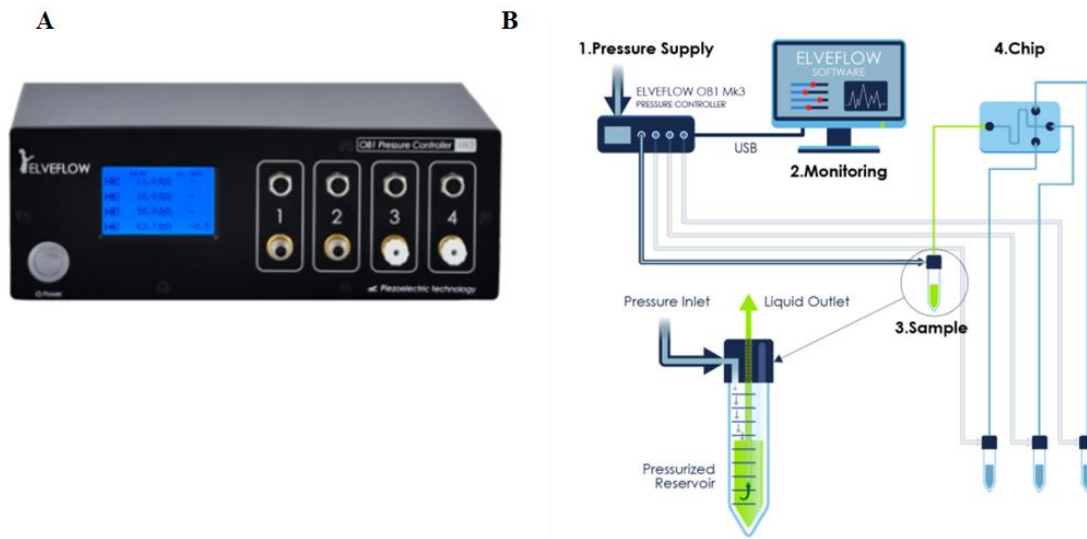


Figure 2.11: Microfluidic pump system. (A) OBI controller, the 4-channel flow control system. (B) Schematic of the connections in an experimental set-up.

- Polystyrene latex microspheres., 2.5 wt% dispersion in water:

The experimental activity included a series of tests which required a distilled water solution containing micro-particles in order to simulate a simplified version of the blood. The used microspheres were spherical in shape, rigid, with not-functionalized surface, fully miscible in water, and presented a mean diameter of 10 μm and 40 μm . The 10 μm simulated RBCs while the 40 μm simulated CTCs, according to the dimension found in literature [15]. The material was chosen on the basis of references[48]. The product has been provided by Alfa Aesar (Heysham, United Kingdom)⁶.

- Optical Microscope:

To perform operations on the devices – such as, connectorization – or to monitor in real time the performing microfluidic test, an optical microscope has been used. The instrument was equipped with a CMOS camera that allowed the computer vision and the image and videos capturing. The system was an Olympus BX51M reflected light

⁶ <https://www.alfa.com/it/catalog/042717>

microscope with trinocular head and high resolution 5x,10x,20x,50x,100xobjectives⁷.

- Filtered solutions:

Any solution, principally distilled water and IPA, that came in contact with the devices has been filtered before. This operation was necessary o avoid the chip clogging by dust, micro-fibers of paper or other micro-particles. The filtering was performed using syringes with specially designed connection for PVDF filters (pore size: 0.22 μm) for water and PTFE (pore size: 0.22 μm) for IPA.

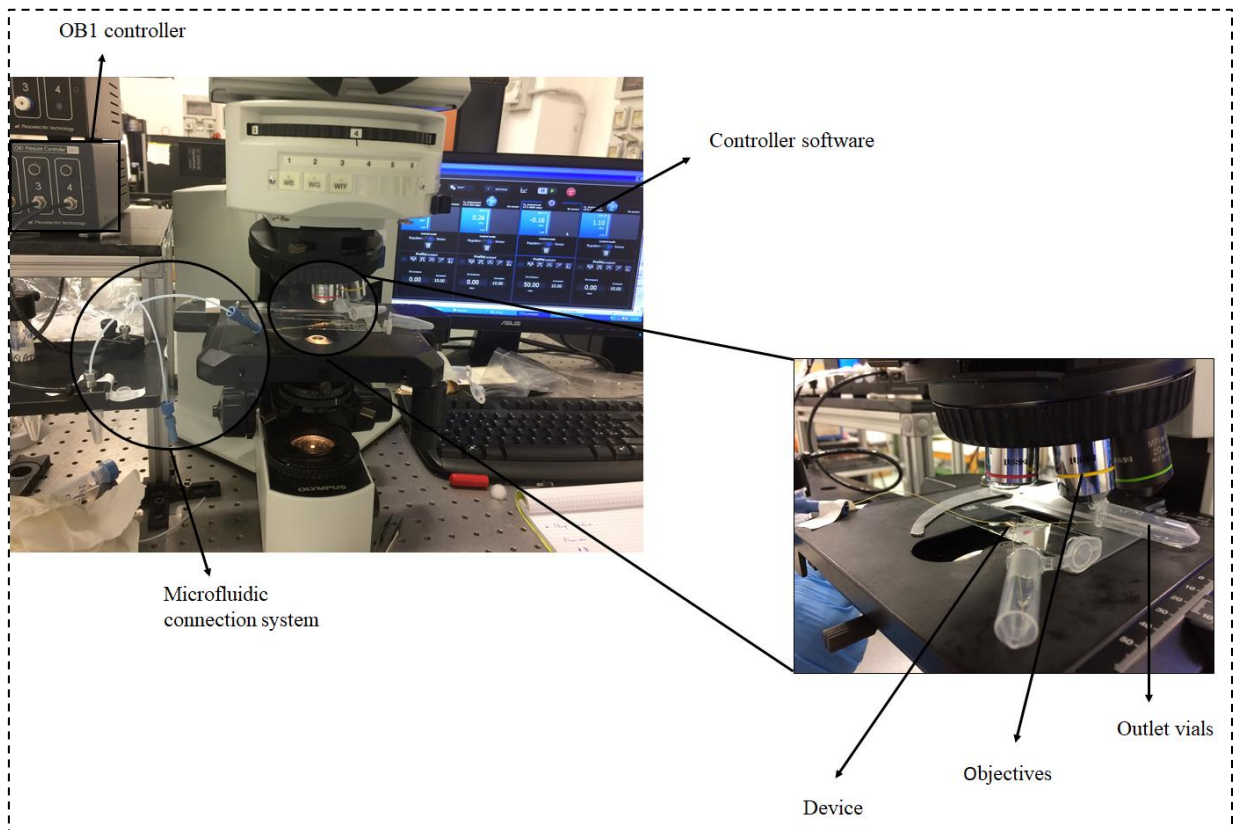


Figure 2.12: Figure showing the experimental set-up.

⁷ <http://www.spachoptics.com/OLYMPUS-BX51M-UM-p/olympus-bx51m-umplfl.htm>

Chapter 3

Experimental activities

3.1 SCA: device design

As described in the material and methods section dedicated to it, this software gives to the user an interface to design potentially any 3D geometry and to communicate it to the laser machine. The designing operation on this software can be executed through two different types of implementations. During this thesis, thus, it has been necessary to find which of the writing modalities could be optimal for the project device realization. The first mode requires the definition of a reference system - either absolute or relative – where the user can define the desired geometries. The profiling of the latter could be achieved by specifying the starting and the ending point, in the linear case, or by defining the analytical law in the non-linear trajectory case. The last operation results to be simple in the case of elementary non-linear functions- such as circumference – but it gets more and more complex as soon as elaborated geometries need to be defined.

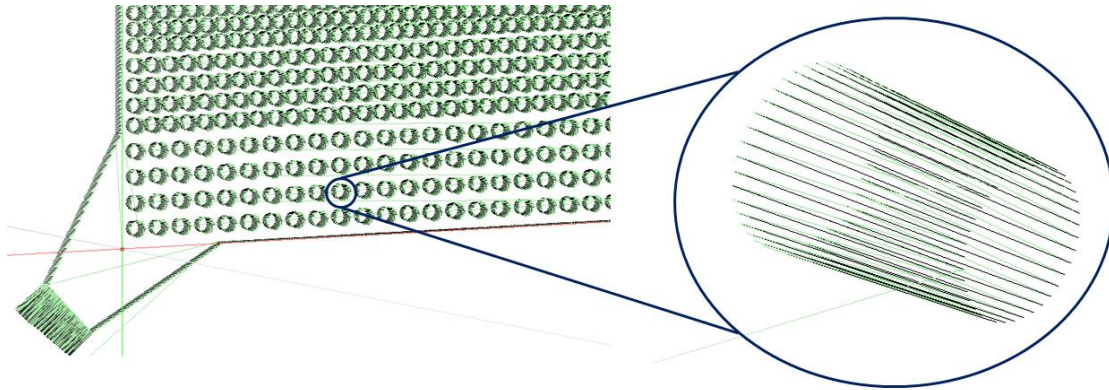


Figure 3.1: Example of complex geometry definition in SCA software, not only the line profiling its elaborated, but also the structure position becomes cumbersome.

The second working modality allows to overcome this limitation. It is based on the 2D design of the desired geometry in an external design software – e.g. AutoCad – that could then be imported in SCA software – as a plotting file (extension: *.plt*) and used to create complex 3 structures. This expedient provides the user with the ability to profile any-shaped contours and to place in a simple way and in any position in the space – within a defined area – the wanted structures (*fig 3.2*). Furthermore, the SCA software allows the user to define important writing parameters that could be determinant for the success of the realization. Among these: the possibility to draw only the contours of the imported shape or to hatch the internal area delimited by the contours, the filling line spacing and the filling line orientation angle. The need imposed by the application is to irradiate an arbitrary volume within the substrate. Thus, writing the structures using the analytical law of the laser trajectories in 3D is complicated and could be limited. The micromachine is able to manage 3D plotting CAD/CAM files (**.stl*), however this type of writing is affected by low resolution – few points per micrometer – and the loss of control over the nanogratings alignment - i.e. over the etching efficiency. For these reasons, it has been developed a new strategy that combined precision and flexibility in 3D fabrications. The procedure to build a 3D structure using this method is quite simple (*fig.3.2*):

- Design of the 2D desired geometry in an external software;
- Conversion of the file in a plotting file (*.plt*);
- Import the plotting file in SCA and selection of the writing parameters;
- Definition of the 3D structure by superimposing at different Z axis points the planar figures imported.

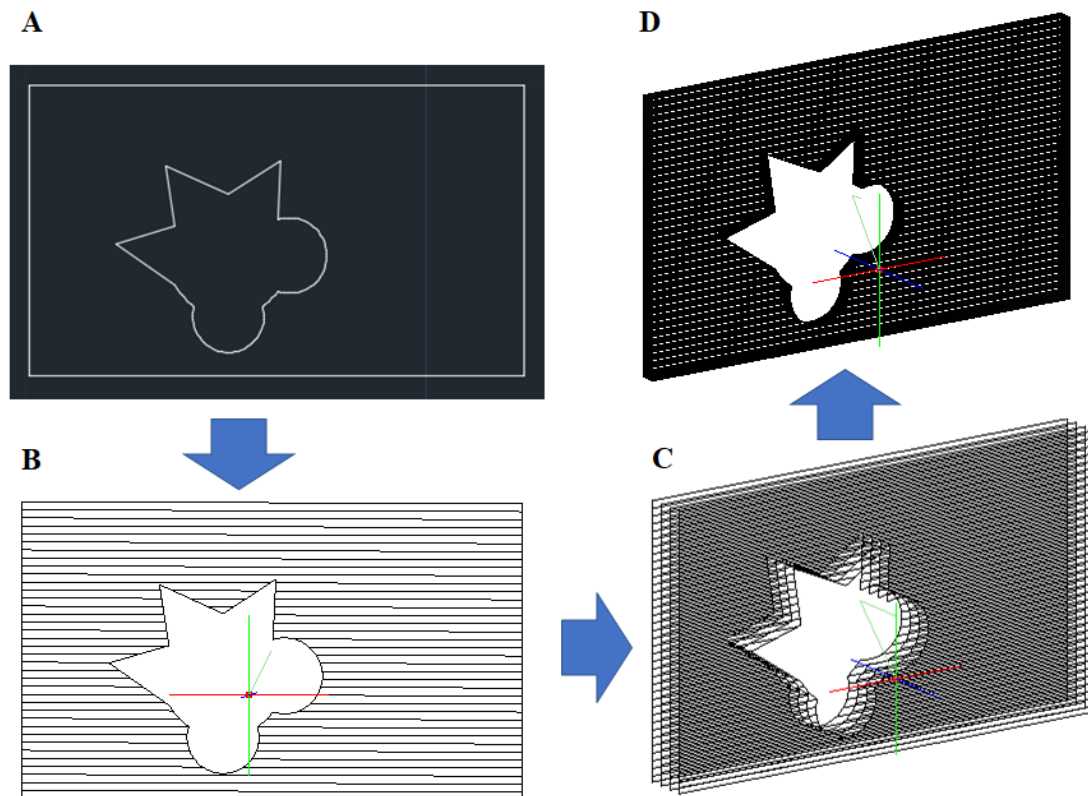


Figure 3.2: example of the creation of a complex and asymmetrical structure. (A) Design of the desired shape through an external software. (B) The desired writing parameters are selected. (C) 3D structure achievement by superimposition at different Z of the planar figure imported. The space between the subsequent plans is also a project parameter. It can be chosen to make the volume more densely or sparsely written: (C) three plans; (D) many plans.

There is also the possibility to further improve this technique. As described in the materials and methods section, the writing and the polarization direction play a fundamental role in the achievement of good outcomes from the etching procedure. Thus, it is possible to optimize this approach by dividing the original planar figure in different sections – or “patches” – by choosing, for each different area, the writing parameters. Therefore, parameters such as the filling lines orientation angle and the polarization can be chosen in order to help the etching process along the writing lines. In this way, it could be possible to reach improvements in the quality of the contours definition and of the spacing between structures within the final device, allowing the any-shaped 3D structure realization in arbitrary volumes.

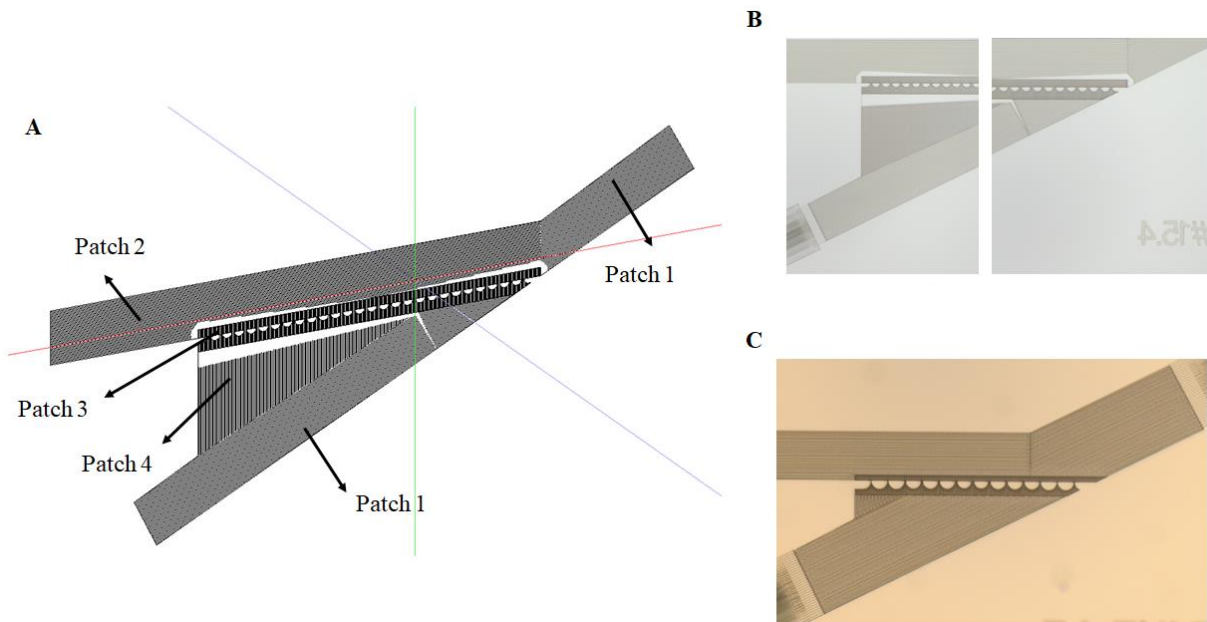


Figure 3.3: Example of “patching” design to obtain a performance increase in the etching process. (B) and (C) laser written examples of patches.

3.2 Femtolaser: writing procedure

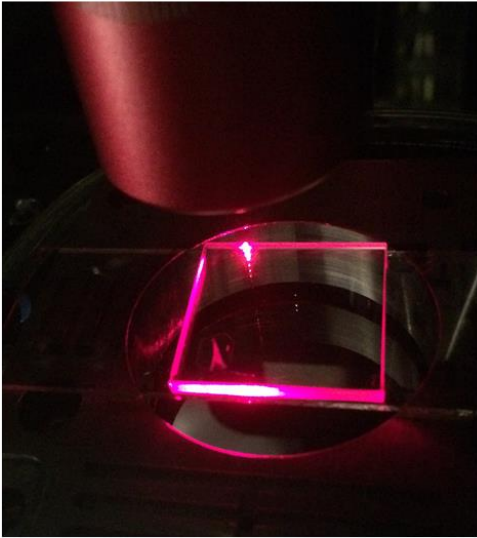
As it is treated in the materials and methods section, the structural modifications in the material that allow the use of this fabrication method for the embedded microfluidic device building application are those referred to as nanogratings. To obtain the generation of this structures in the material, it is thus mandatory to select the right working point of the laser femtomachine. This operation could be achieved by setting some fundamental parameters, that will be treated in the next section as “hardware writing parameters”. Therefore, before each device fabrication process, it has been necessary to accomplish some basic passages to start-up the laser machine and bring it to the desired working point. The procedure could be resumed in the following steps:

- Laser source turn-on;
- SCA software initialization;
- Writing parameters setting;

- Beam alignment;
- Power measurement and settings;
- Search of the sample surface.

The laser source turn-on does not need further explanation. The SCA software initialization is an important operation that allows the communication among the design software, the laser source and the stage – i.e. the 3D sample movement system. Once the initialization is complete, the setting of the writing parameters could be accomplished. This involves the selection of the pulse frequency, the writing wavelength, the lens and the stage accelerations. The beam alignment procedure involves the chosen lens and represents a basic operation necessary to ensure that beam energy deposition processes occur at the desired point. Another important parameter to be set is the writing power. This passage is done by using a power meter that measures the energy of the beam, that, for this operation, needs to not go through the lens. Once the power meter reports the desired power, this value is locked via software. The last step before the starting of the real fabrication involves the identification of the glass sample surface, in order to give a reference point for the writing in the space. This operation could be performed in two ways: manually by the user, thanks to a vision system implemented by a CMOS camera (μ Eye), positioned before the lens, or by using the AutoFocus automated system. A red laser beam, that impinges on the glass sample, is used to finely scan the substrate surface in Z position, taking advantage from a “Z-scan”-like optical configuration: the reflected signals and their related polarizations are detected by photodiodes. Each acquired signal shows its maximum when the red laser beam spot crosses any interface -e.g. air-glass). The weighted average of all the signals thus obtained provides the Z value corresponding to the detected surface.

A



B

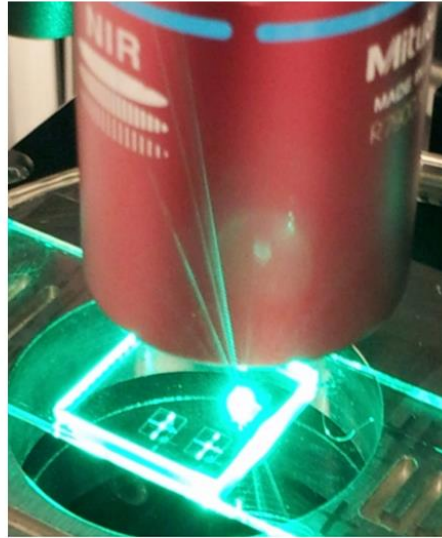


Figure 3.4: Section of femtolaser micromachine. (A) AutoFocus automated system for the transparent sample surface identification. (B) Writing laser beam during a fabrication process.

3.3 Femtolaser: writing parameters

During this project, it has been necessary to find the parameters that seemed “optimal” in order to achieve good quality geometric 3D structures. Among these parameters it could be identified a division in “hardware writing parameters”, which, once identified, were rarely subjected to modifications, and “software writing parameters, which, in turn, have been frequently modified, according to the current fabrication. Among the “hardware writing parameters”:

- Writing power: 200 – 210 mW;
- Objective lenses: 50 x;
- Impulse frequency: 500kHz;
- Wavelength: 515 nm (green light);
- Stage accelerations: 20 mm/s².

As regards the last parameters, it could be interesting to notice that it is significantly smaller with respect the accelerations used for other devices fabrications. This is due to an inertial effect of the stage, when subjected to sudden variations in direction and accelerations within small areas, as it can occurs in our chip fabrication case. (*fig.3.5*)

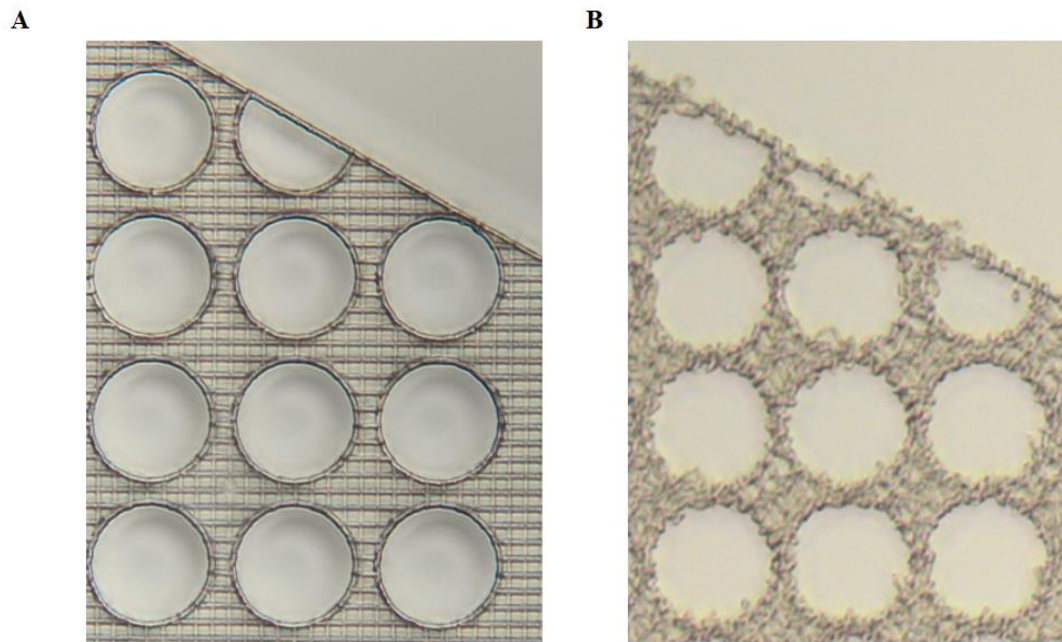


Figure 3.5: Low stage accelerations (20 mm/s^2) (A) versus high stage accelerations (200 mm/s^2) (B).

The acceleration decrease resulted in a significant improve in the contours profiling of the designed shapes, even if it presented a slightly increase in the fabrication time.

As far as the “software writing parameters” are concerned, basically they are the ones described in the SCA designing section:

- filling lines spacing;
- filling lines orientation angle;
- polarization;
- distance in the Z axis between two subsequent planar figures for the 3D structures construction.

The latter parameter defines the amount of volume, in the material, to be irradiated. Thus, is fundamental to determining it in an optimal way to ensure that all the “to-be-removed” volume is irradiated. This is crucial, as described in the materials and method section, for the achievement of a successful etching and, in the end, of the device realization. A too large step between the planar sections, indeed, risks to leave non-modified slices of material in written volume, that could slow down or even completely block the etching process, specially in the KOH-etching case. An optimal range for this parameter was found to be: 6

$\mu\text{m} - 8 \mu\text{m}$. As regards the other parameters they are strictly related to the designed geometry, the precision demand and the spot size of the objective lens used. To give an order of magnitude, for the filling line spacing, it was found that $5 \mu\text{m} - 9 \mu\text{m}$ could be indicated as a good working range.

3.4 Devices realization

From the analysis of the several methods present in the literature for CTC isolation, DLD has demonstrated to have the right potential to fulfil the requirement imposed by the project idea, thanks to its characteristics: very high throughput, high efficiency and label free approach to isolate tumoral cells from the whole blood.

First some considerations are necessary. To avoid the chip sealing issue, our idea is to build a completely buried in the substrate filtering device. From the literature, the realization of a highly selective DLD separation of cells that may differ from a few micrometers requires chip lengths of 20 -35 mm [68],[57],[69] : this lengths for totally embedded structure could be critical. However, the solution lies behind the basic aim of our filtering problem: the new IIT chip project involves the use of the DLD technique (or similar) as a high-throughput solution for the filtering of RBCs from the rest of the cells – namely, CTCs and WBCs – and not for the selection of CTCs. The latter, indeed, present sizes that could be superimposable with the WBCs ones; thus, making CTC identification not so selective, for obvious reasons. Therefore, our aim is to remove RBCs from the blood; consequently, there is the need for a separation system able to discriminate only between 2 groups of cells – the smallest ones (RBCs) from the others (CTCs and WBCs). Thus, one of the first challenges of this thesis was to find a trade-off geometry that could accomplish the isolation task, while maintaining compact dimensions. Drawing inspiration from a particular case of DLD – presented in the relative section in the introduction chapter – in which a composition of two flows was used to perform a filtration and displacement of RBCs, WBCs and CTCs (*fig. 3.6 (A)*), the first geometry was created.

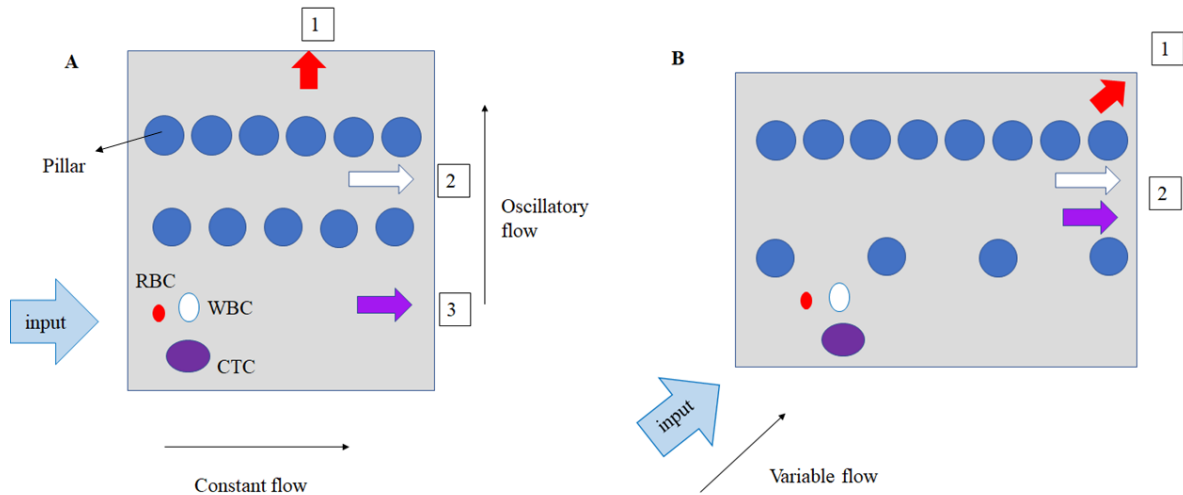


Figure 3.6: (A) schematic of the particular case of DLD presented in the relative introduction section.[58] (B) Schematic of the working principle of the first chip generation implemented in this project.

As the first step of an integrated platform for the CTC analysis, there wasn't the need to straightaway separate also CTCs from WBCs. Thus, it has been possible to simplify the geometry by bringing together the WBCs and the CTCs outputs. A further simplification was introduced by summing the effect of the two flows in one unique flow, inclined of $\sim 45^\circ$ with respect to the pillar matrix. The pillar matrix was defined by placing a series of pillar arrays with spacing gap between pillar around $10 \mu\text{m}$ right before the RBCs output and another series, with spacing of $\sim 50 \mu\text{m}$ right before the target outlet, where WBCs and CTCs should be collected. The $10 \mu\text{m}$ spaced arrays had the task to let pass through only RBCs and rejecting all other particles. The $50 \mu\text{m}$ spaced array was instead leaved to not create a too high hydraulic resistance unbalance between the two areas of the chip and to "guide" the larger particles toward the right output. In order to validate the innovative writing mechanism that we suggested, resumed in *fig. 3.2*, the first test was studied specially to not suffer difficulties and mechanisms related to the etching procedure of embedded structures. For this reason, the pillar fabrication on chip was executed within an open to surface chamber. This was made to ensure the successful pillar structures creation, but presented, as drawback, the crucial limit to be sealed.

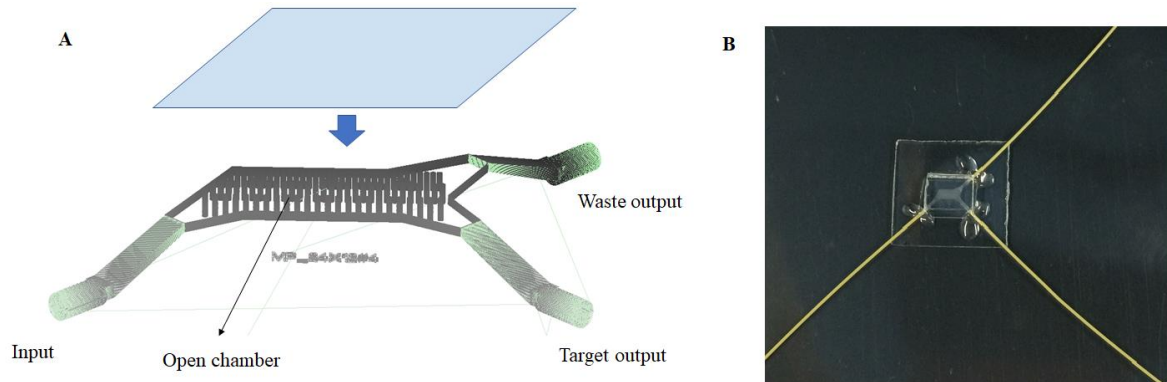


Figure 3.7: first generation of devices: the open to the surface pillar matrix chamber. (A) schematic of chip sealing. (B) the chip sealed.

The sealing, thus, comported two disadvantages: the first, seen from a mere manual point of view, while the second, from an operational one. The encountered manual difficulties in the sealing were related to the small dimensions of the chip (2 mm x 3 mm). The most relevant limitation, although, was detected during the first tests, where the sealing compromised the experimentation accomplishment. This was due to the fact that the sealing procedure didn't allow to reach pressures higher than few hundreds millibars (~500 mbar): at those pressures the cover was no longer holding and leaks from the chip occurred. Despite these problems, this preliminary test was useful to demonstrate an important concept: the fabrication process allows the realization of a precise number of pillars of any shape and any dimension. In this way, to proceed with the development of functioning devices, it has been necessary move toward an embedded realization of the chip, that could allow to avoid the sealing procedure. In order to find some meaningful parameters to accomplish this task, some preliminary writing and etching tests were done. To find the right fabrication and etching parameters and to demonstrate that the embedded creation of small structures was possible, the experimentation focused on the reproduction of some pillar shapes, found in literature. The parameters that could be defined thanks to this test were useful both for the etching procedure and the writing process. Thus, for the etching it has been verified the optimal combination of the HF acid and the KOH solution and was also found a good working sonic-tip duty-cycle. While for the writing phase, were identified some important parameters such as the level of irradiation of the material volume, defined by the filling spacing for the plotter files and the distance between two parallel planar figure plans.

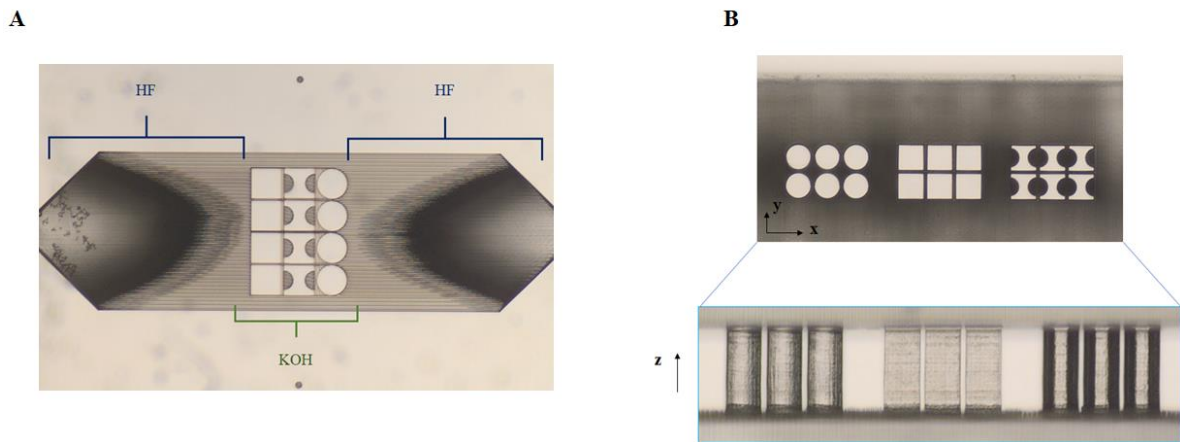


Figure 3.8: Embedded pillar shapes, fabricated with FLICE technology: (A) the ongoing HF etching in the combined approach HF for large non-detailed volumes and KOH for small and precise volumes. (B). Pillars after etching in top and side view.

After performing the tests shown in *fig. 3.8*, the subsequent step was the realization of a completely buried device, with a geometry inspired by that one reported in *fig. 1.22*. Having thus created an embedded device, allowed to correctly accomplish the tests. One of the first observations that derived was regarding the height of the chip chamber. So far, the chamber was $100\ \mu\text{m}$ high and the dimensions of the used microspheres were $10\ \mu\text{m}$ and $40\ \mu\text{m}$; this, in addition to the low velocity profile on the wall – characteristic of the laminar flow – and the internal surface rugosity, generated a stopping effect on the bottom of the chip that could lead to a clogging of the device (*fig. 3.9*).

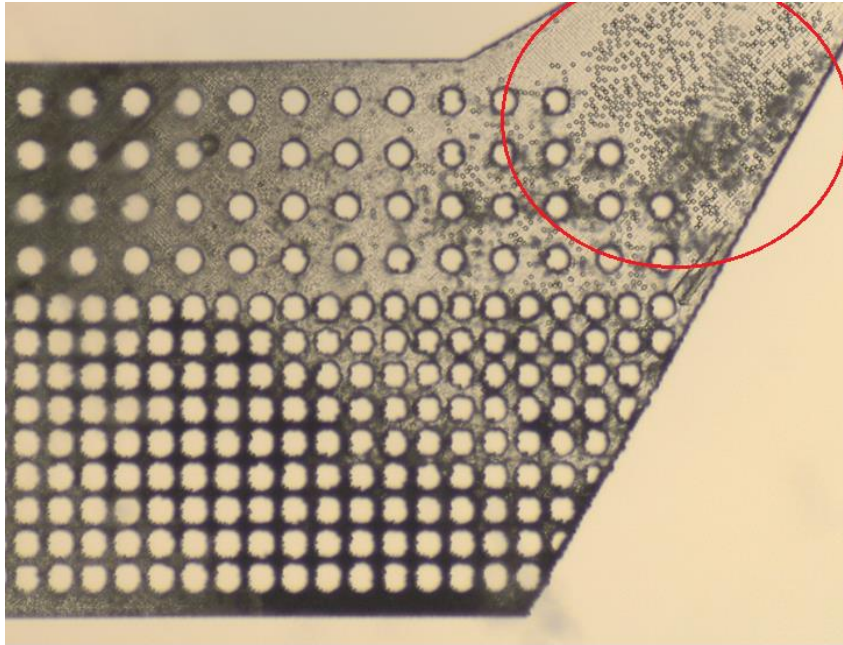


Figure 3.9: microspheres showing the tendency of depositing themselves on the bottom of the chip.

The results reported in *fig.3.9* suggested, thus, to increase the height of the chamber ($200\ \mu\text{m}$) - along with the related rising of the fabrication time - to limit this effect. To avoid the prosecution of the trial-and-error approach, adopted up to this point, we used some simulations - performed using multiphysics modelling software COMSOL - to better understand the functioning of this geometry. Thus, the results led to drastic changes in the geometry. The observations drawn from the simulations could be resumed in:

- presence of a “shadow” area in the flow in front of circular pillars;
- one single array should have been sufficient for the discrimination in size of the two groups of cells (RBCs on one side and WBCs and CTCs on the other);
- the circular pillar created zones that could trap large particles.

Furthermore, the simplified simulation of a pillar chamber showed that the pillars presence increased significantly the flow resistance – as the flow decreased – thus meaning that all the rows behind the “discriminant barrier” could be considered not only non-useful to the separation purpose but also counterproductive for the fluidodynamic behaviour of the chip. All these aspects contributed to the main problem affecting these device: the clogging, which reduced drastically the chip performances in an increasing way, during the test.

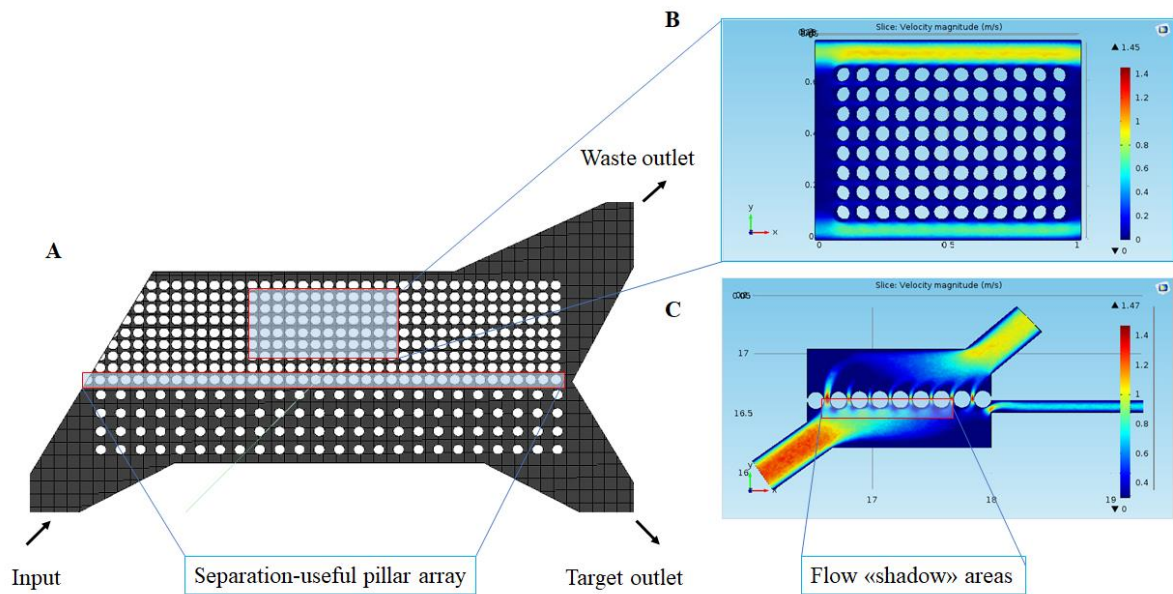


Figure 3.10: Embedded pillar matrix chip: (A) Geometry of the pillar chamber: the only useful separation barrier has turned out to be, from the experimentations, the array highlighted in figure. (B) Simulation showing a significant decrease in flow through the pillar matrix: this area of the chip resulted not only not useful for the separation purpose but also counterproductive for the fluidodynamic behaviour of the chip. (C) Simulation showing a simplified geometry that highlights the “shadow” area that the flow forms in front of the pillars.

The conclusions that were made starting from these points, thus, led to the design of a geometry focused only on a row of pillars. Moreover, this array presented a different pillar shape – i.e. semi-circular shape - in order to reduce either the “shadow” zone area in front of the pillars but especially the “trapping zones” created by circular shape (fig. 3.11(B)).

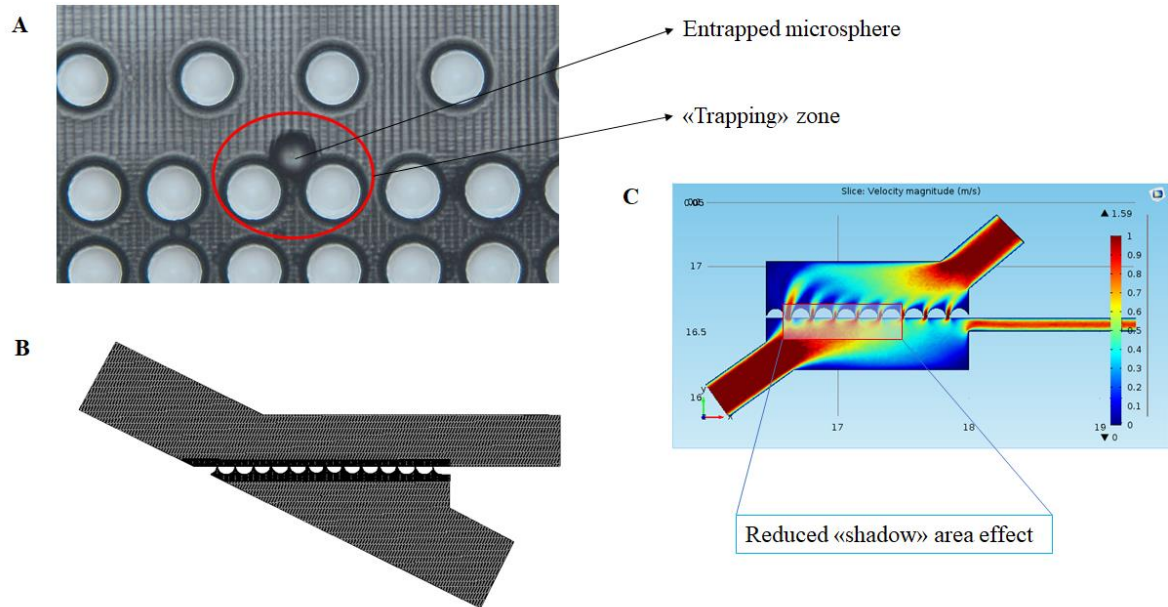


Figure 3.11: (A) Trapping-zone effect due to the circular shape of the pillars composing the “discriminant barrier” of the device. (B) Optimized geometry, showing the introduction of the “patch” writing method. (C) Simplified simulation showing the slightly reduced shadow-zone effect.

The obtained new geometry showed both operational and fabrication-related advantages with the respect of the previous one. The new shaped pillars slightly decreased the “shadow” zone in front of the pillar and resolved the “trapping” issue created by the circular geometry. However, the device showed an increased throughput – displayed in the results section – due to its better fluidodynamic and its increased volume-processing area. This quantity can be defined as the ratio:

$$(2) \quad \text{“free” area} = \frac{nA_p}{A_t} \cdot 100$$

Where n is the total number of pillars – all pillars presented the same radius: $30 \mu\text{m}$ -, A_p is the section area of the pillars and A_t is the total section area of the chip – that can be calculated from the planar figure used in the design phase. Moreover, the fabrication time of the device and the related etching time were reduced by ~ 2 h and ~ 3 h respectively. The fabrication increase in performance could be attributed to the smaller dimensions of the chip – which did not influence the throughput performances –, the optimized geometry and the use of the “patched” writing technique (fig.3.11 (B)).

3.5 Tests: sample preparation

Each obtained device, after the completing of the etching procedure, has been tested through the instrumentation described in the material and methods section. Though, before the starting of the real device testing it has been necessary follow a brief procedure of sample preparation. This operation is called connectorization. This term refers to the manual procedure by which small tubes (external diameter 360 μm ; internal: 150 μm) were inserted in the appropriate accesses, specially created in the glass sample. the procedure involved the following steps:

- Cutting the tubes from the reel;
- Tube insertion into the device;
- Tube fixation in the accesses;
- Chip fixation on a microscope slide.

The tubes were cut using a specially designed cutter, which reduced the occlusion risk by bending and ensure a net slash (*fig. (A)*). The length was defined according to the channel into which the tube should have been inserted, in order to favour the device performance. The lengths were: 7 cm for the inlet, 6-7 cm for the target outlet and 4-5 for the waste outlet. The tube insertion in the device was performed using a micrometric manual stage set-up, assisted by an optical stereomicroscope. After the insertion, the tubes were fixed by using a UV-solidification polymeric glue, which required three cycles of 45 s to become completely solid. Thanks to the femtolaser micromachine fabrication technique, tubes resulted automatically aligned to the chamber centre.

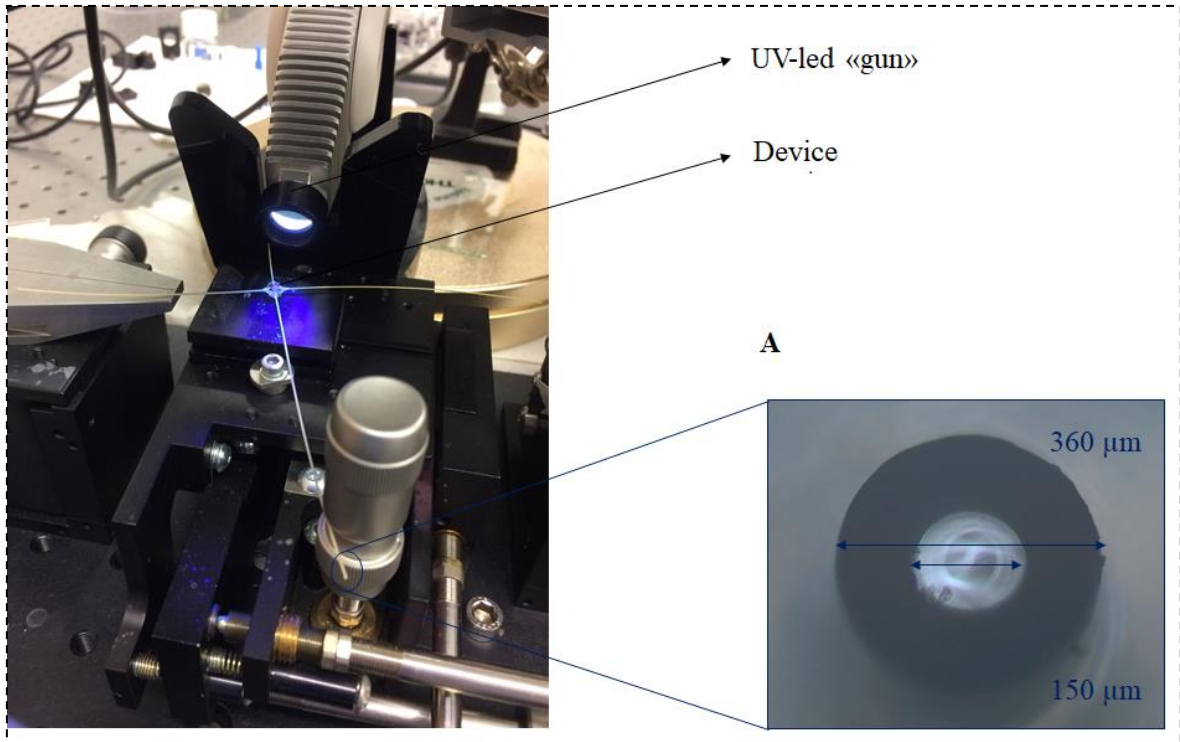


Figure 3. Connectorization: polymeric UV glue fixing to fasten the tube to the chip. (A) Tube cross section, external diameter: $360\mu\text{ m}$, internal diameter: $150\mu\text{ m}$.

The device was finally set on a microscope slide to ensure a transparent stable support for the tests.

3.6 Tests: procedure

Since the aim of all the tested devices, independently from their different geometry, was the same – i.e. reach an acceptable degree of separation between “small” microspheres (diameter $\sim 10\mu\text{ m}$), simulating erythrocytes, and “large” microspheres (diameter $\sim 40\mu\text{ m}$), simulating CTCs – tests were structured in the same fashion. It can be made a distinction between two kinds of tests: the first, was studied to verify the above reported goal, the second kind was done to check a really important parameter of the microfluidic devices, the throughput.

The general structure of the first type of tests could be resumed in four basic steps:

- Air bubbles removal;
- Chip connection to ElveFlow micropump system;
- Testing the chip only with small microspheres;

- Testing the chip with the superimposition of small and large microspheres.

Air bubbles in microfluidics could be a great issue, since they have the capability to physically block the whole chip, thus interrupting its functions. One of the most critical moments for the air bubble entrapment in the chip is the first connection with the micropump system. Therefore, it has been necessary for the successful conduction of the tests, to find an approach to reduce the bubble formation during this phase. One of the methods that turned out to be efficacious was the high pressure (~ 3 bar) injection into the chip of filtered isopropanol (IPA). Between the injection of IPA and the test-solution input was taken in account a pure water flow for a small amount of time - e.g. 30 s – in order to flush away IPA.

The real tests involved the use of microspheres of different size to simulate the cells in blood; to do this, the beads were suspended in filtered distilled water. The first type of test was a simplified version of the separation problem, because it concerned only the use of small size spheres. This has been useful to look at the overall working principle of the created chip and its behaviour in presence of particles in the solution; thus, allowing fluidodynamic-based considerations on the overall geometry. Furthermore, the test could be justified by the fact that the device should practically work also in true negative cases – i.e. when no CTCs are present in the blood. The superimposition of small and large size spheres, instead, has been useful to focus the attention on the discrimination performances of the devices. This means that, thanks to this kind of tests, observations about the shape and position of the structures used for the dynamic filtering -i.e. pillars – were made possible. The drawn conclusion from the tests thus have been necessary to allow a development path in geometry and chip manufacturing technology – i.e. passage from sealing technique to embedded devices.

In order to ensure a high throughput, the devices had to show an elevated mechanical resistance to high pressures. The test involved the use of 0.5 ml vial of distilled water, without particles in solution, for each point of a set of increasing inlet pressures. For each vial, the inlet pressure was kept constant and was measured the amount of time necessary for the chip to process the volume of water. The set of investigated pressures involved for the low-pressure range 50,100,200 mbar and for the high-pressure range from 2 to 8 bar with step of 1 bar.

The results obtained both from the first and the second type of experiments will be illustrated in the relative section in the results chapter.

3.7 Test: simplifications

Since the created devices represent only the first step of the development of a chip for the red blood cell separation, the test simulated a simplified situation in order to better understand the working of the device. It is important to notice that in this preliminary phase specially equipped facilities for the blood experimentation were not necessary. The introduced simplification, thus, referred to the fact that the simulated blood cells did not involve the white blood cells. Though, the work does not lose its meaning because, since the leukocytes are significantly larger in size than erythrocytes, they would not pass through the RBC size based gaps in the devices. Another significant approximation could be found in the rigidity of the spheres and in their round shape. These characteristics go far away from the real situation. Cells – particularly red blood ones – are indeed characterized by well distinguished values of deformability and by non-spherical shapes. This results in a more complex interaction with obstacles on their path, that does not depend only by their size [56],[53]. However, for the aim of this thesis the spherical shape and the non-deformability of the particles were acceptable, since, from their behaviour within the chip, it was made possible the extraction, of information about the right functioning of the device.

The last approximation has been made in both the types of experiments, using distilled water instead of blood. Nevertheless, this choice could be considered reasonable – in the lacking possibility of using real blood samples – as water shows a density value ($\sim 1000 \frac{kg}{m^3}$) comparable to the one of blood at 37° ($\sim 1060 \frac{kg}{m^3}$) [70].

Chapter 4

Results

One of the first accomplishment obtained during this project was the realization of fine size structures or microfluidic applications. As described in the experimental section, the first generation of chip was characterized by open to surface pillar chamber. This has made the chip problematic in the experimentation phases; however, it should be noticed the precision of the fabrication technique in the pillar realization. All pillars presented a good homogeneity in their dimension - $\sim 45 \mu\text{m}$ in diameter and $100 \mu\text{m}$ in height -, while the gaps, which spaced the pillar along the chamber – were divided in two bands: one ranged from $10 \mu\text{m}$ to $15 \mu\text{m}$ and the other was $\sim 50 \mu\text{m}$. These dimensions were quite uniform for the whole chip thanks to the particular etching technique that allowed the acid solution to enter not only from the accesses but even from the top. Furthermore, the pillars showed to be correctly positioned and resisted to the etching procedures – involving the use of ultrasounds, that could be critical for their solidity.

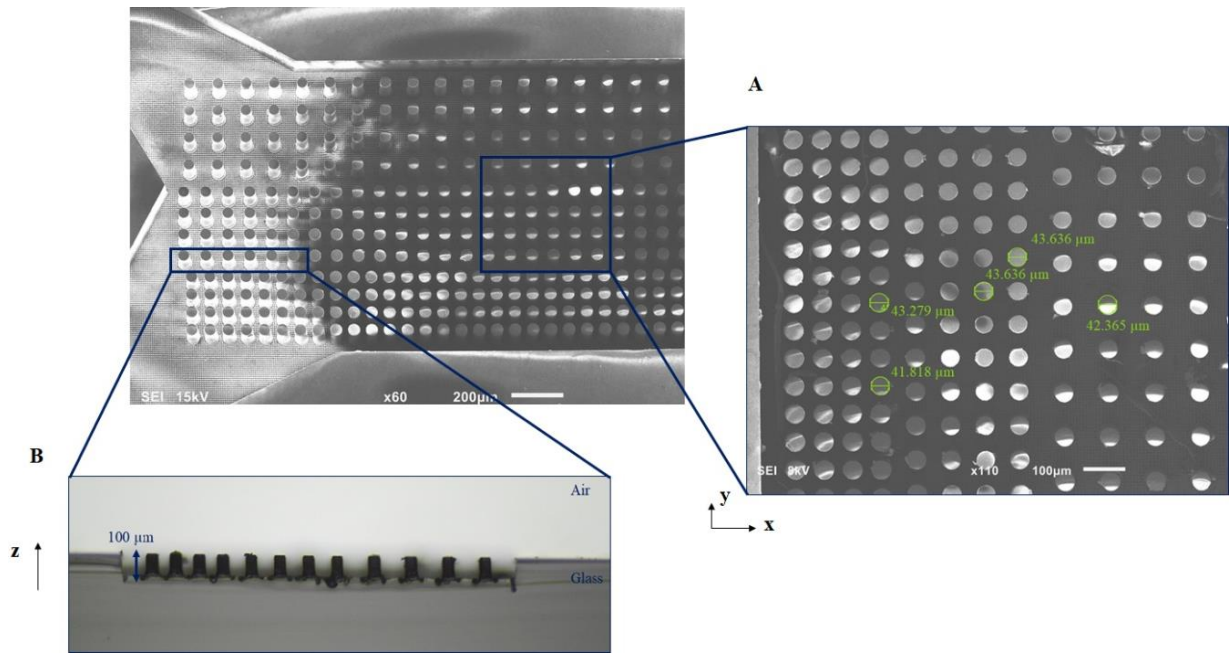


Figure 4.1: first generation chip characterized by pillar chamber open to surface. (A) top view: the pillar diameters showed a good homogeneity. (B) Side view: the pillars were uniform along the Z axis.

The result that could be indicated as remarkable was the realization of complex-shaped structures completely embedded in the substrate, without the need of further operations, like the sealing one. This opened the way to high pressure experimentations and, thus, allowed the design of high throughput devices. This accomplishment could be attributed to the successful combination of various techniques for the etching procedure with the innovative optimized-writing -i.e. the “patch” method – in the fabrication process. Thus, in addition, the embedded structures presented a good degree of precision.

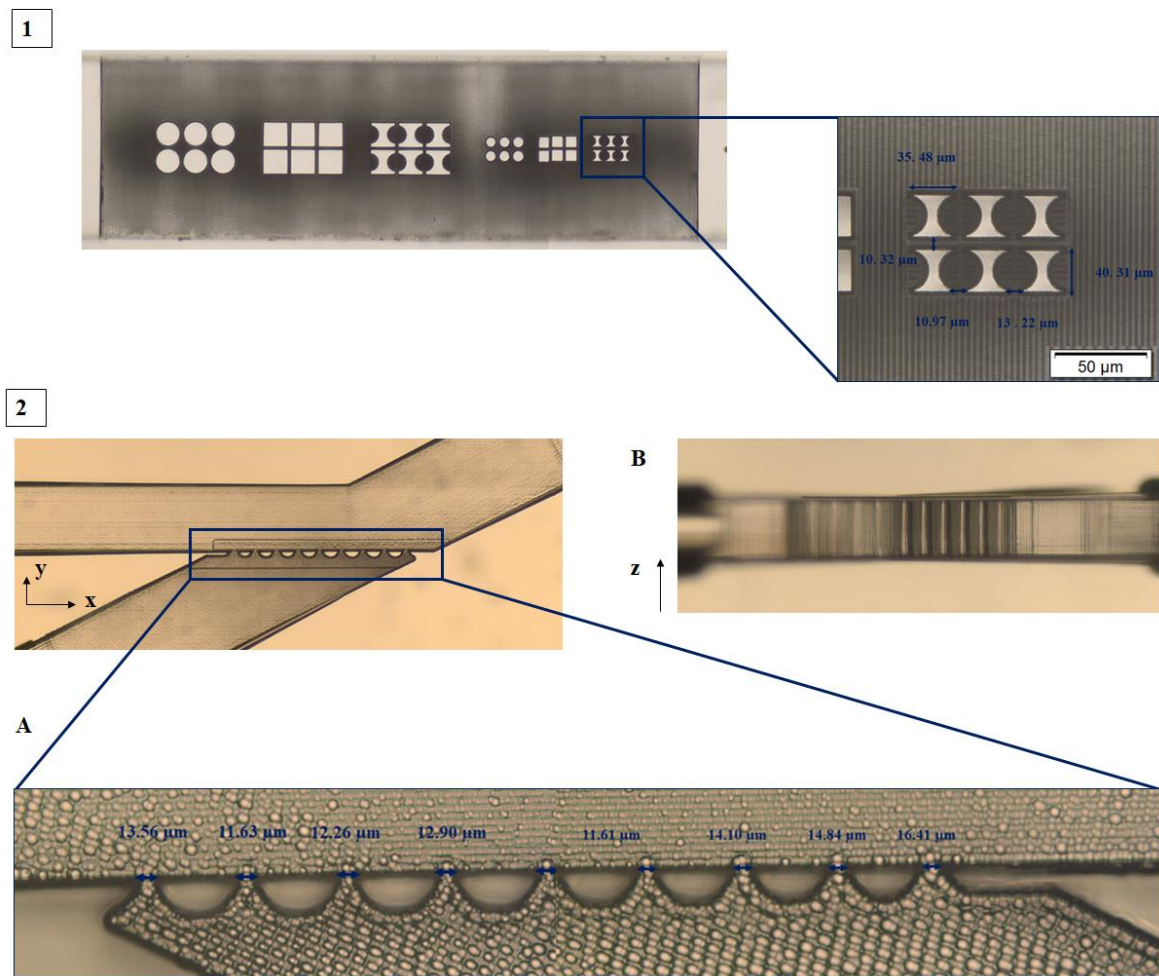


Figure 4.2.1: Complex and small shapes ($\sim 35 \mu\text{m}$) were obtained with a good precision degree embedded in the glass substrate.

4.2.2: Post-etching figure of the optimized chip version: (A) Very good precision was obtained in the reproducing of the software design. The gap size, the critical dimension of the chip – since if the separation is successful or not – has been designed to let pass only RBCs so values could be acceptable if in the range: $10 \mu\text{m} - 15 \mu\text{m}$. The obtained mean gap size was $13.41 \pm 1.56 \mu\text{m}$.

For the optimized version of the chip, it was reached, indeed, a mean gap size of $13.41 \pm 1.56 \mu\text{m}$.

As regards the experimentation phase of the **buried** devices, both showed a comparable behaviour in the separation task. As described in the experimental section, the fluidodynamics tests have been composed by two principal types. The first was carried on using a solution containing only small particles (diameter: $10 \mu\text{m}$) and both the geometries

showed the tendency to well separate these particles and to direct them toward the waste output. (fig. 4.3).

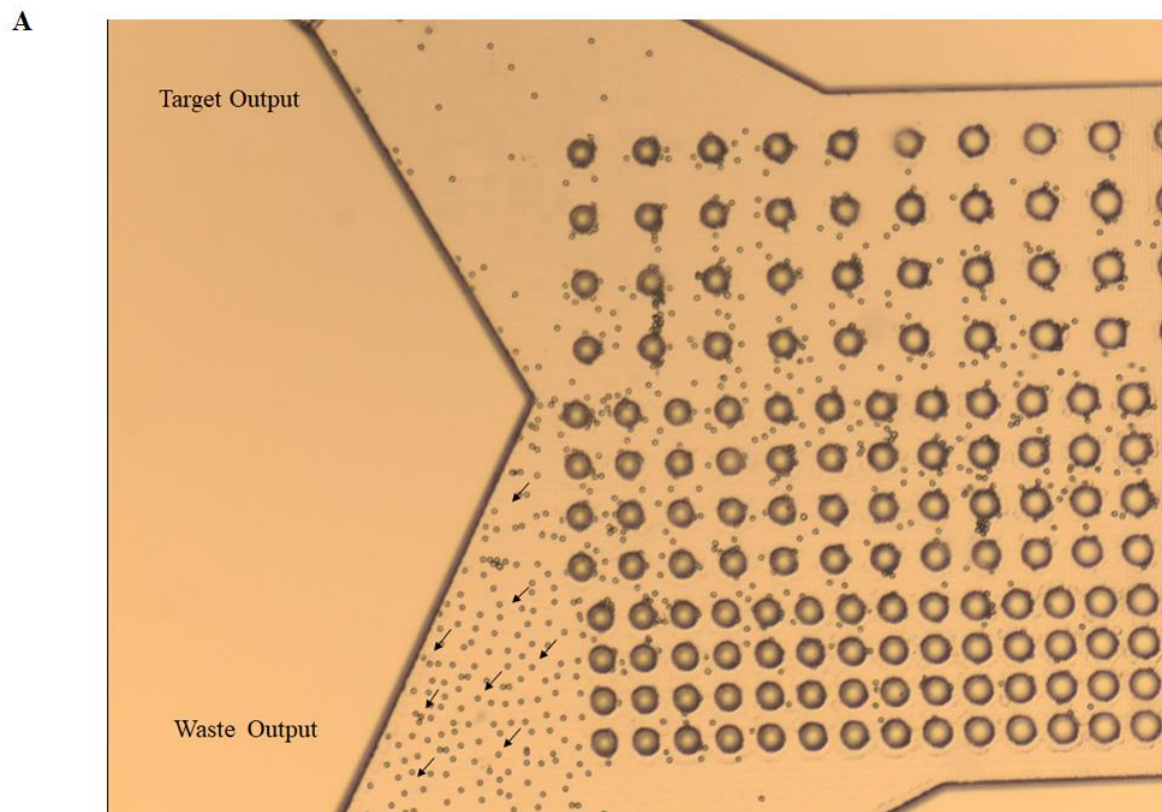


Figure 4.3 A: Figure taken in real-time during the tests of a buried device. (A) Test with a solution of only small particles ($10\ \mu\text{m}$): the device is correctly deviating in the waste outlet the small particles. A negligible number of them go in the target outlet -i.e. the wrong outlet.

B

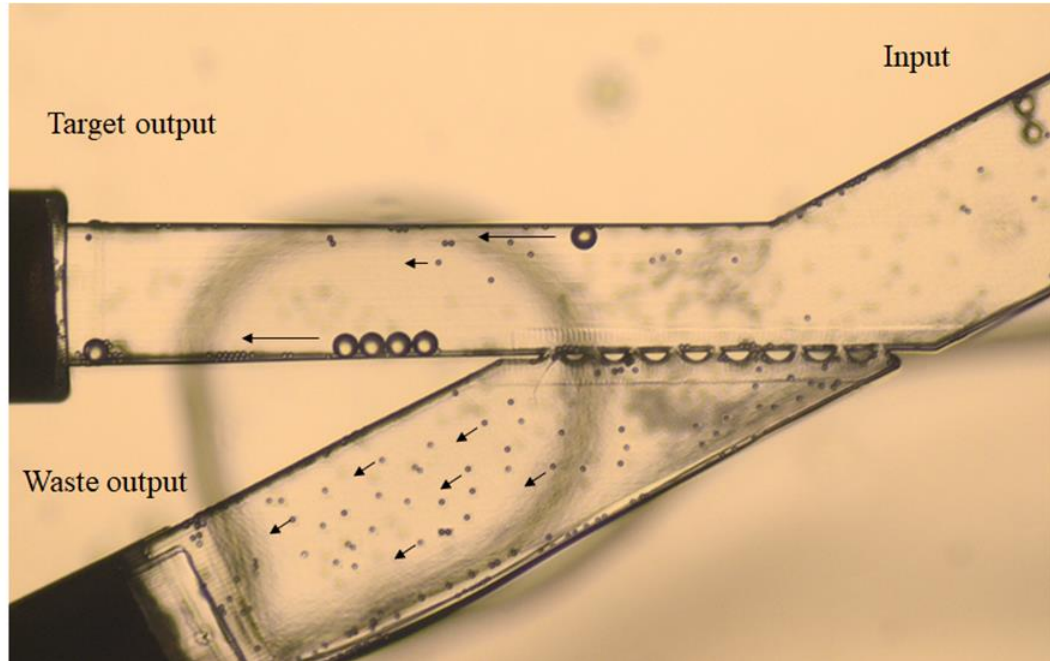
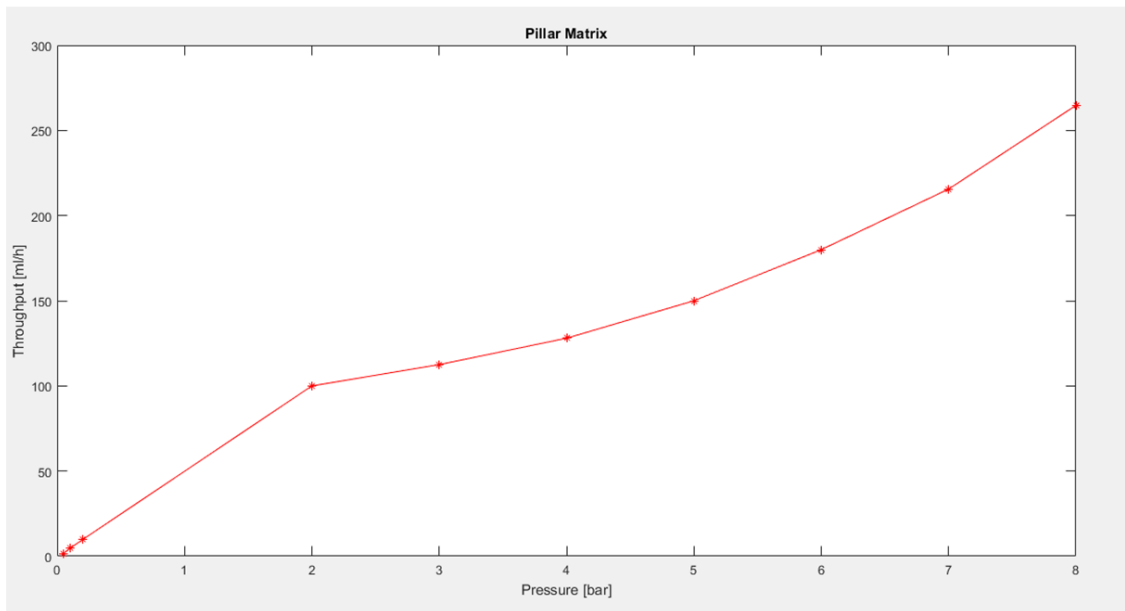
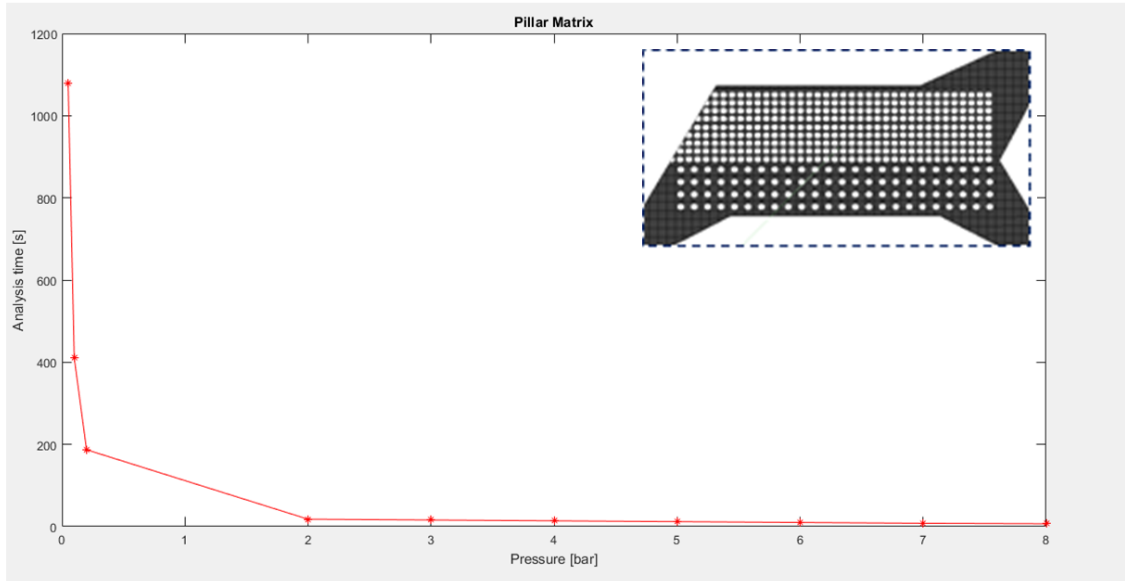


Figure 4.3 B: Figure taken in real-time during the tests of a buried device. Test with small and large particles: the large particles are well separated from the small ones and rightly directed toward the correct outlet. Few small particles, as noticed in the previous tests, go in the wrong direction

The second kind of experimentations involved the use of the combination of small and large ($40\ \mu\text{m}$) particles, suspended in a water solution. As far as the chips that were created are concerned, they both showed a good behaviour in this discrimination. Thanks to the structural barriers represented by the pillars, for all the conducted tests it was physically not possible for the large particles to cross over the post array.

Another type of tests was conducted during this project, not involving the separation task: it was meant to assess the capability of the devices to reach high pressures and high throughputs. Both the chip managed to withstand pressures up to 8 bars – i.e. the maximum reachable by the micropump system used to inject the sample in the devices -without showing signs of breakage or leakage. Measuring the amount of time required to process a fixed volume of water (0.5 ml) at different constant inlet pressures, it was possible to build the following graphs:

A



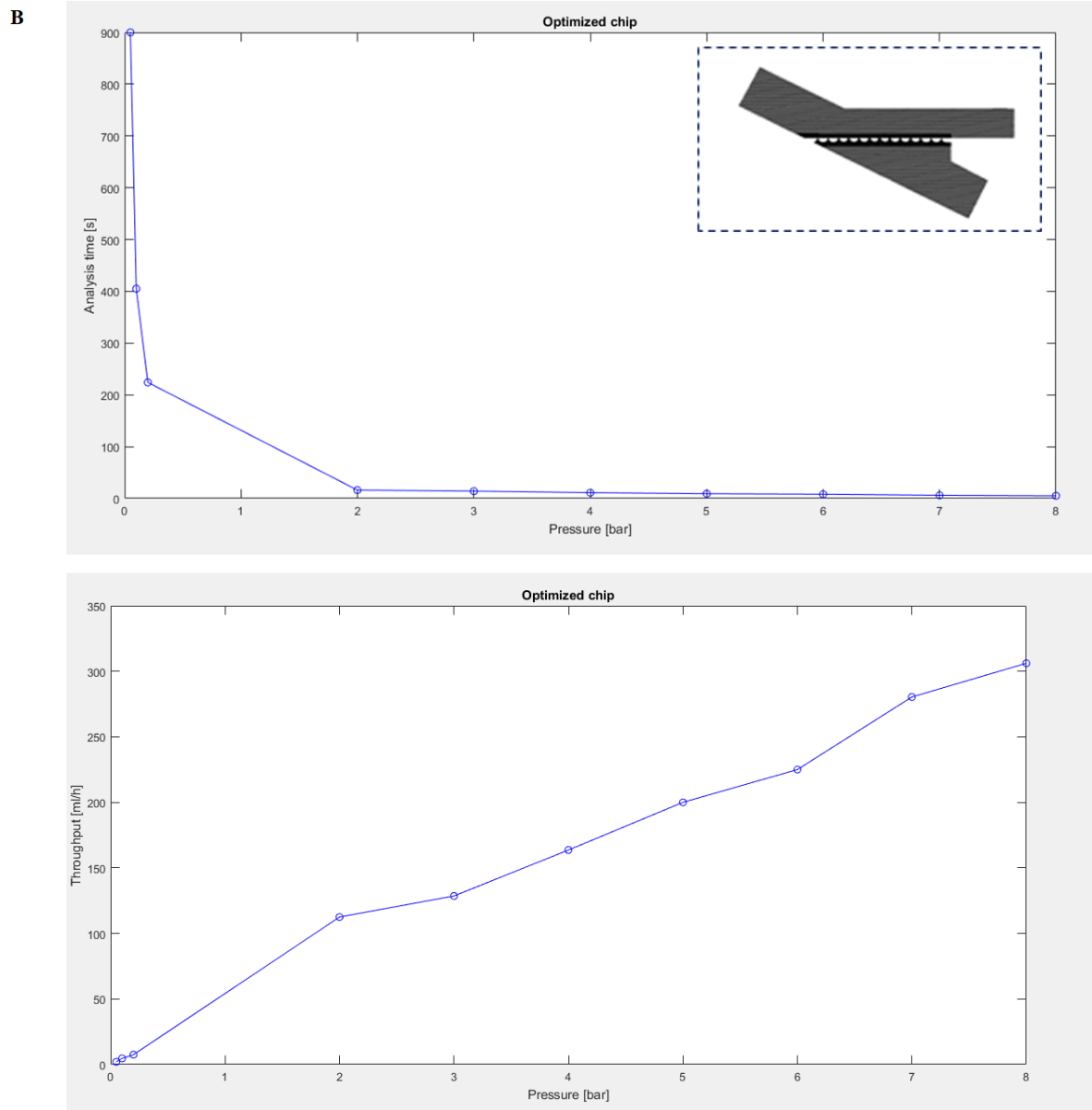


Figure 4.4: Graphs of the amount of time to process 0.5 ml of water at different constant inlet pressures (Up) and the relative throughput (Down) for (A) the pillar matrix chip and (B) the chip referred to as the “optimized version”.

By the comparison between the throughput values of the two geometries, it is straightforward to see that the optimized chip has a generally greater throughput.

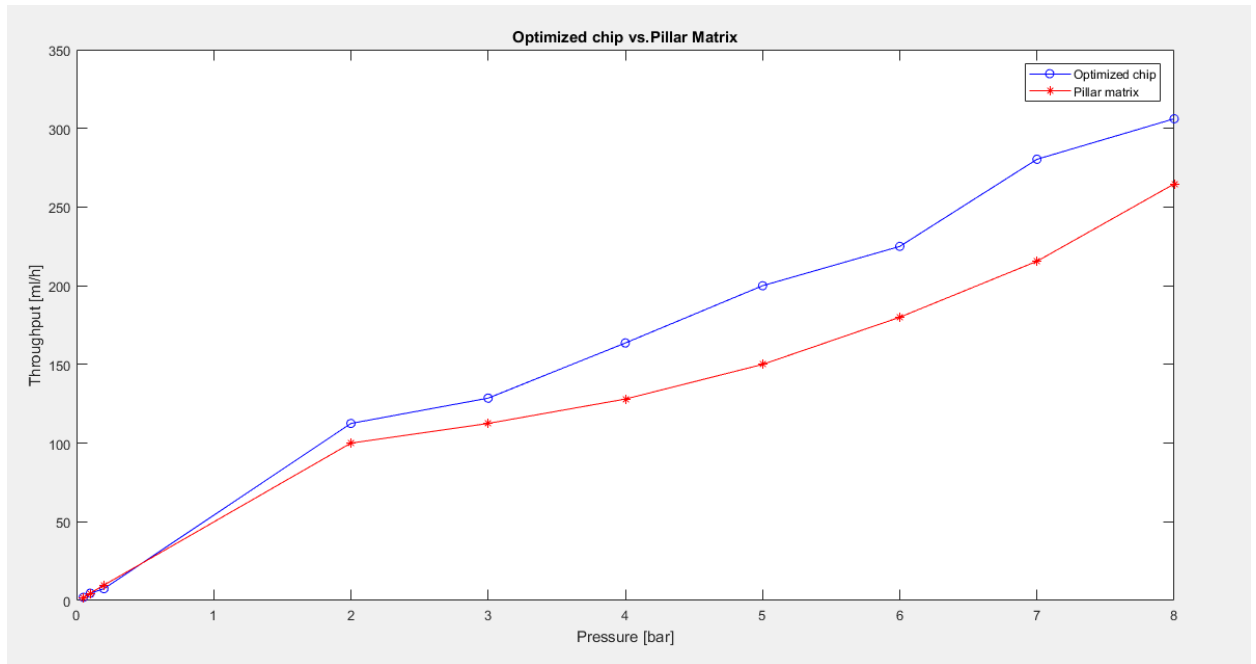


Figure 4.5: Throughput: optimized chip versus pillar matrix. (O) Optimized chip and (*) pillar matrix.

As foreseeable, the maximum throughput was reached by both the devices at a pressure of 8 bar: for the pillar matrix it was 264.72 ml/h and for the optimized chip 306.12 ml/h.

The values thus obtained are comparable with other DLD devices presented in the state of art and greater – of at least one order of magnitude of all the other non-DLD microfluidic devices, excepted the “membrane filtering” ones.

One of the reasons why the optimized chip reached a higher throughput value, in addition to a better fluidodynamic – i.e. not slowed down by the presence of too many pillars – could be found in the greater processing area: this means that, the optimized chip, thanks to its low number of pillars, shows a greater “free area” than the pillar matrix. In particular the area occupied from the pillars showed to be: ~70% for the matrix pillar and 25 % for the optimized chip – these values have been computed using equation (10) in the experimental section. Since the section area of the figure is constant, the reasoning stands also for the volumes.

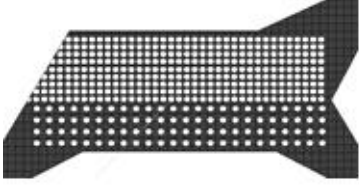
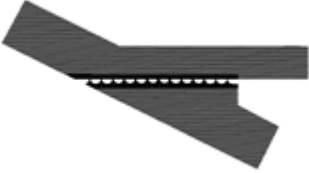
Device	Maximum throughput	“Free” Volume
	264.72 ml/h	30%
	306.12 ml/h	75%

Table 4.1: Resuming of the processing behaviour of the created devices, showing the maximum throughput reached for each geometry and the “free” volume - i.e. the volume, within the chip, not occupied by the pillars; it is calculated with respect the total volume of the device.

Chapter 5

Discussion and conclusions

The work done during this project has been verified by the obtained results: particularly, it could be said that this thesis represents a useful confirmation of innovative techniques in the field of laser micromachining and chemical etching. Thus, the fabricated devices can be seen as a validation of the hybrid etching approach and as an early application of an innovative technological expedient – i.e. KOH etching in ultrasound sonication - to increase further the etch-rate of this etchant. Also on the side of the writing technique there have been some improvements: the refining of the volume writing through designed planar section that, finally, led to the “patch” method, has proved its effectiveness in the obtaining of the presented structures, with such small dimensions and such precision. Therefore, the combination of these technologies has shown its own potential and has proved the existence of scope for further improvement. Thus, the 3D sample-embedded realization of devices can still face an additional increase in geometry complexity. There is still space, indeed, for the optimization of the latter technique: for instance, the effect of the variation of the writing power in the “patched” areas could be investigated as an additional parameter. But also new designing approaches could be studied. For example, the conversion in a plotting file - readable from the laser machine - of the slicing of software-designed 3D complex solids could open the way to the easily implementation of structures with a cross section that varies also along the Z axis. In this way, it should be obtained a new arbitrary 3D and high-resolution writing process that could take advantage of the control over the etching phase.

Regarding the current lab-on-chip application, this technique provided good results. The distance between pillar could be accepted if in the range from 10 μm to 15 μm . This size

window is imposed by the dimension of RBCs (8-10 μm) and the purpose of the device, that aims at their separation from a blood sample. Although the mean inter-pillar distance that resulted from the optimized chip ($13.41 \pm 1.56 \mu\text{m}$) is in the range of acceptance, with simple modifications in the geometry designing stage, it could be reached the desired range of 8-10 μm . Thus, proving the above-mentioned potentialities of this fabrication technique.

Looking at the experimentations results, the fact that not all the small particles were correctly separated could be not considered as an issue. The aim of the chip, indeed, is the first step filtration of the whole blood in order to remove as many erythrocytes as possible, thus increasing both the efficiency both the throughputs of the subsequent steps. The stages following to the first, as a matter of fact, can be considered as a “finer” filter: their aim, in particular that of the third stage, is to discriminate CTCs from WBCs. If the latter step is capable to do that operation, thus it would not have complications in distinguishing also CTCs from red blood cells. Therefore, if few RBCs would go through the wrong outlet it would not compromise neither the device functioning nor the efficiency of the analysis. On the contrary, regarding the experimentations with the small and large particles containing solution, it is crucial that not even one of the larger particles go in the wrong outlet – i.e. the waste output -; this has been appreciably verified and demonstrated. It should be kept in mind that the final aim of the whole device is the implementation of a clinical test for the detection of tumoral cells. Especially in the case of rare cells, such as CTCs, there is the need to be able to identify all the “events” that verifies. Otherwise the risk is to run into false negative, that should be completely avoid in a screening device. From this point of view, the working behaviour of the devices was remarkable. However, the drawback of such a strict barrier is the accumulation of particles on it, phenomenon known as clogging. In some cases, it has been possible to resolve this issue by suddenly increase the inlet pressures ($\sim 4-5 \text{ bar}$) and to flush away the block; in any case, more dilute solutions of particles could limit this problem. Thanks to the intrinsic structural resistance of a buried device, high pressures were reached without any leakage or damage of the chip. The result of these pressures was a very high sample processing speed. The obtained throughput values are thus remarkable as, from the literature, they result to be greater – of at least one order of magnitude - than most of the other CTC identification devices. Furthermore, these ones could be compared also with the literature values of the fastest chip, all implementing a filtering operation through DLD.

In conclusion, even if the principal goals of this thesis project were reached, few optimizations are still necessary to obtain an excellent filtration chip and future steps have already been evaluated and decided.

Although there is still work to be done to obtain an efficient chip for the filtering problem – completely eliminate the clogging problem and minimize the number of “unwanted” cells in the target output -, the work done in this thesis has laid the foundation that will allow to continue on this way. It gave also the proof that either the fabrication system, either the pillar-based geometry are valid methods to reach the goal, thus adding a very small brick to the technological development that, hopefully, will lead to consider a disease as cancer neither less terrible, nor less scary, but more attackable.

Bibliography

- [1] N. Hao and J. X. J. Zhang, “Microfluidic Screening of Circulating Tumor Biomarkers toward Liquid Biopsy,” *Sep. Purif. Rev.*, vol. 0, no. 0, pp. 1–30, 2017.
- [2] R. A. Harouaka, M. Nisic, and S.-Y. Zheng, “Circulating Tumor Cell Enrichment Based on Physical Properties,” *J. Lab. Autom.*, vol. 18, no. 6, pp. 455–468, 2013.
- [3] N. Takeishi, Y. Imai, T. Yamaguchi, and T. Ishikawa, “Flow of a circulating tumor cell and red blood cells in microvessels,” *Phys. Rev. E - Stat. Nonlinear, Soft Matter Phys.*, 2015.
- [4] D. S. Micalizzi, D. A. Haber, and S. Maheswaran, “Cancer metastasis through the prism of epithelial-to-mesenchymal transition in circulating tumor cells,” *Mol. Oncol.*, vol. 11, no. 7, pp. 770–780, 2017.
- [5] N. P. A. D. Gunasinghe, A. Wells, E. W. Thompson, and H. J. Hugo, “Mesenchymal-epithelial transition (MET) as a mechanism for metastatic colonisation in breast cancer,” *Cancer Metastasis Rev.*, vol. 31, no. 3–4, pp. 469–478, 2012.
- [6] T. W. Friedlander, G. Premasekharan, and P. L. Paris, “Looking back, to the future of circulating tumor cells,” *Pharmacol. Ther.*, vol. 142, no. 3, pp. 271–280, 2014.
- [7] A. M. C. Barradas and L. W. M. M. Terstappen, “Towards the biological understanding of CTC: Capture technologies, definitions and potential to create metastasis,” *Cancers (Basel)*, vol. 5, no. 4, pp. 1619–1642, 2013.
- [8] F. A. W. Coumans, S. T. Ligthart, J. W. Uhr, and L. W. M. M. Terstappen, “Challenges in the enumeration and phenotyping of CTC,” *Clin. Cancer Res.*, vol. 18, no. 20, pp. 5711–5718, 2012.
- [9] M. Cristofanilli *et al.*, “Circulating Tumor Cells, Disease Progression, and Survival in Metastatic Breast Cancer,” *N Engl J Med*, vol. 351, no. 8, pp. 781–791, 2004.
- [10] M. H. D. Neumann *et al.*, “Isolation and characterization of circulating tumor cells using a novel workflow combining the CellSearch?? system and the

- CellCelector???,” *Biotechnol. Prog.*, vol. 33, no. 1, pp. 125–132, 2017.
- [11] D. L. Adams *et al.*, “Cytometric characterization of Circulating Tumor Cells Captured by microfiltration and their correlation to the cellsearch® CTC test,” *Cytom. Part A*, vol. 87, no. 2, pp. 137–144, 2015.
- [12] S. T. Ligthart *et al.*, “Circulating Tumor Cells Count and Morphological Features in Breast, Colorectal and Prostate Cancer,” *PLoS One*, vol. 8, no. 6, p. e67148, 2013.
- [13] J. Chen, J. Li, and Y. Sun, “Microfluidic approaches for cancer cell detection, characterization, and separation,” *Lab Chip*, vol. 12, no. 10, p. 1753, 2012.
- [14] I. Cima *et al.*, “Label-free isolation of circulating tumor cells in microfluidic devices: Current research and perspectives,” *Biomicrofluidics*, vol. 7, no. 1, 2013.
- [15] W. S. Low and W. A. B. Wan Abas, “Benchtop technologies for circulating tumor cells separation based on biophysical properties,” *Biomed Res. Int.*, vol. 2015, 2015.
- [16] M. K. Jolly, “Implications of the Hybrid Epithelial/Mesenchymal Phenotype in Metastasis,” *Front. Oncol.*, vol. 5, no. July, pp. 1–19, 2015.
- [17] M. Yu *et al.*, “NIH Public Access,” vol. 339, no. 6119, pp. 580–584, 2013.
- [18] S. Wu *et al.*, “Classification of circulating tumor cells by epithelial-mesenchymal transition markers,” *PLoS One*, vol. 10, no. 4, pp. 1–14, 2015.
- [19] A. Satelli *et al.*, “Potential role of nuclear PD-L1 expression in cell-surface vimentin positive circulating tumor cells as a prognostic marker in cancer patients,” *Sci. Rep.*, vol. 6, no. July, p. 28910, 2016.
- [20] L. A. Diaz and A. Bardelli, “Liquid biopsies: Genotyping circulating tumor DNA,” *J. Clin. Oncol.*, vol. 32, no. 6, pp. 579–586, 2014.
- [21] M. Ilie *et al.*, “‘Sentinel’ circulating tumor cells allow early diagnosis of lung cancer in patients with Chronic obstructive pulmonary disease,” *PLoS One*, vol. 9, no. 10, pp. 4–10, 2014.
- [22] E. Crowley, F. Di Nicolantonio, F. Loupakis, and A. Bardelli, “Liquid biopsy: monitoring cancer-genetics in the blood,” *Nat. Rev. Clin. Oncol.*, vol. 10, no. 8, pp. 472–484, 2013.

- [23] T. Masuda, N. Hayashi, T. Iguchi, S. Ito, H. Eguchi, and K. Mimori, “Clinical and biological significance of circulating tumor cells in cancer,” *Mol. Oncol.*, vol. 10, no. 3, pp. 408–417, 2016.
- [24] D. F. Hayes *et al.*, “Circulating tumor cells at each follow-up time point during therapy of metastatic breast cancer patients predict progression-free and overall survival,” *Clin. Cancer Res.*, vol. 12, no. 14 Pt 1, pp. 4218–4224, 2006.
- [25] J. M. Jackson, M. A. Witek, J. W. Kamande, and S. A. Soper, “Materials and microfluidics: enabling the efficient isolation and analysis of circulating tumour cells,” *Chem. Soc. Rev.*, vol. 46, no. 14, pp. 4245–4280, 2017.
- [26] S. J. Cohen *et al.*, “Relationship of circulating tumor cells to tumor response, progression-free survival, and overall survival in patients with metastatic colorectal cancer,” *J. Clin. Oncol.*, vol. 26, no. 19, pp. 3213–3221, 2008.
- [27] J. S. De Bono *et al.*, “Circulating tumor cells predict survival benefit from treatment in metastatic castration-resistant prostate cancer,” *Clin. Cancer Res.*, vol. 14, no. 19, pp. 6302–6309, 2008.
- [28] M. P. Wong, “Circulating tumor cells as lung cancer biomarkers,” *J. Thorac. Dis.*, vol. 4, no. 6, pp. 631–634, 2012.
- [29] K. C. Andree, G. van Dalum, and L. W. M. M. Terstappen, “Challenges in circulating tumor cell detection by the CellSearch system,” *Mol. Oncol.*, vol. 10, no. 3, pp. 395–407, 2016.
- [30] J. Q. Yu and M. Cristofanilli, “Circulating tumor cells and PET,” *J. Nucl. Med.*, vol. 52, no. 10, pp. 1501–4, 2011.
- [31] K.-H. Han, A. Han, and A. B. Frazier, “Microsystems for isolation and electrophysiological analysis of breast cancer cells from blood,” *Biosens. Bioelectron.*, vol. 21, no. 10, pp. 1907–1914, 2006.
- [32] K. Ried, P. Eng, and A. Sali, “Screening for Circulating Tumour Cells Allows Early Detection of Cancer and Monitoring of Treatment Effectiveness: An Observational Study,” *Adv. Cancer Prev.*, vol. 2, no. 2, pp. 2275–2285, 2017.

- [33] M. Ignatiadis, M. Lee, and S. S. Jeffrey, “Circulating tumor cells and circulating tumor DNA: Challenges and opportunities on the path to clinical utility,” *Clin. Cancer Res.*, vol. 21, no. 21, pp. 4786–4800, 2015.
- [34] A. Alama, A. Truini, S. Coco, C. Genova, and F. Grossi, “Prognostic and predictive relevance of circulating tumor cells in patients with non-small-cell lung cancer,” *Drug Discov. Today*, vol. 19, no. 10, pp. 1671–1676, 2014.
- [35] J. H. Myung and S. Hong, “Microfluidic devices to enrich and isolate circulating tumor cells,” *Lab Chip*, vol. 15, no. 24, pp. 4500–4511, 2015.
- [36] J. F. Swennenhuis, G. van Dalum, L. L. Zeune, and L. W. M. M. Terstappen, “Improving the CellSearch® system,” *Expert Rev. Mol. Diagn.*, vol. 16, no. 12, pp. 1291–1305, 2016.
- [37] M. C. Miller, G. V. Doyle, and L. W. M. M. Terstappen, “Significance of Circulating Tumor Cells Detected by the CellSearch System in Patients with Metastatic Breast Colorectal and Prostate Cancer,” *J. Oncol.*, vol. 2010, pp. 1–8, 2010.
- [38] F. Simoni *et al.*, “Optofluidic Microlasers based on Femtosecond Micromachining Technology,” pp. 7–13, 2017.
- [39] M. M. Ferreira, V. C. Ramani, and S. S. Jeffrey, “Circulating tumor cell technologies,” *Mol. Oncol.*, vol. 10, no. 3, pp. 374–394, 2016.
- [40] S. Nagrath *et al.*, “NIH Public Access,” vol. 450, no. 7173, pp. 1235–1239, 2007.
- [41] M. M. X. Lin *et al.*, “Enrichment, detection and clinical significance of circulating tumor cells,” *Lab Chip*, vol. 14, no. 1, pp. 1–15, 2014.
- [42] A. Khamenehfar and P. C. H. Li, “Microfluidic devices for circulating tumor cells isolation and subsequent analysis,” *Curr. Pharm. Biotechnol.*, vol. 17, no. 9, 2016.
- [43] V. Murlidhar, L. Rivera-Báez, and S. Nagrath, “Affinity Versus Label-Free Isolation of Circulating Tumor Cells: Who Wins?,” *Small*, no. 33, pp. 4450–4463, 2016.
- [44] B. J. Green, T. Saberi Safaei, A. Mepham, M. Labib, R. M. Mohamadi, and S. O. Kelley, “Beyond the Capture of Circulating Tumor Cells: Next-Generation Devices

- and Materials,” *Angew. Chemie - Int. Ed.*, vol. 55, no. 4, pp. 1252–1265, 2016.
- [45] I.-F. Cheng, W.-L. Huang, T.-Y. Chen, C.-W. Liu, Y.-D. Lin, and W.-C. Su, “Antibody-free isolation of rare cancer cells from blood based on 3D lateral dielectrophoresis,” *Lab Chip*, vol. 15, no. 14, pp. 2950–2959, 2015.
- [46] C. M. Yousuff, E. T. W. Ho, I. Hussain K., and N. H. Hamid, “Microfluidic platform for cell isolation and manipulation based on cell properties,” *Micromachines*, vol. 8, no. 1, p. 15, 2017.
- [47] V. Gupta *et al.*, “ApoStream???, a new dielectrophoretic device for antibody independent isolation and recovery of viable cancer cells from blood,” *Biomicrofluidics*, vol. 6, no. 2, pp. 1–14, 2012.
- [48] M. Antfolk, C. Magnusson, P. Augustsson, H. Lilja, and T. Laurell, “Acoustofluidic, Label-Free Separation and Simultaneous Concentration of Rare Tumor Cells from White Blood Cells,” *Anal. Chem.*, vol. 87, no. 18, pp. 9322–9328, 2015.
- [49] J. Che *et al.*, “Classification of large circulating tumor cells isolated with ultra-high throughput microfluidic Vortex technology,” *Oncotarget*, vol. 7, no. 11, pp. 12748–60, 2016.
- [50] M. E. Warkiani *et al.*, “An ultra-high-throughput spiral microfluidic biochip for the enrichment of circulating tumor cells,” *Analyst*, vol. 139, no. 13, p. 3245, 2014.
- [51] M. S. Kim *et al.*, “SSA-MOA: a novel CTC isolation platform using selective size amplification (SSA) and a multi-obstacle architecture (MOA) filter,” *Lab Chip*, vol. 12, no. 16, p. 2874, 2012.
- [52] A. F. Sarioglu *et al.*, “HHS Public Access,” vol. 12, no. 7, pp. 685–691, 2016.
- [53] T. Krüger, D. Holmes, and P. V. Coveney, “Deformability-based red blood cell separation in deterministic lateral displacement devices-A simulation study,” *Biomicrofluidics*, vol. 8, no. 5, pp. 1–15, 2014.
- [54] C. Wyatt Shields IV, C. D. Reyes, and G. P. López, “Microfluidic cell sorting: a review of the advances in the separation of cells from debulking to rare cell isolation,” *Lab Chip*, vol. 15, no. 5, pp. 1230–1249, 2015.

- [55] J. A. Davis *et al.*, “Deterministic hydrodynamics: Taking blood apart,” *Proc. Natl. Acad. Sci.*, vol. 103, no. 40, pp. 14779–14784, 2006.
- [56] K. K. Zeming, S. Ranjan, and Y. Zhang, “Rotational separation of non-spherical bioparticles using I-shaped pillar arrays in a microfluidic device.,” *Nat. Commun.*, vol. 4, no. March, p. 1625, 2013.
- [57] K. Loutherbach, J. D’Silva, L. Liu, A. Wu, R. H. Austin, and J. C. Sturm, “Deterministic separation of cancer cells from blood at 10 mL/min,” *AIP Adv.*, vol. 2, no. 4, 2012.
- [58] E. S. Park *et al.*, “Continuous Flow Deformability-Based Separation of Circulating Tumor Cells Using Microfluidic Ratchets,” *Small*, vol. 12, no. 14, pp. 1909–1919, 2016.
- [59] Z. Liu *et al.*, “Rapid isolation of cancer cells using microfluidic deterministic lateral displacement structure,” *Biomicrofluidics*, vol. 7, no. 1, pp. 1–10, 2013.
- [60] J. P. Beech, S. H. Holm, K. Adolfsson, and J. O. Tegenfeldt, “Sorting cells by size, shape and deformability,” *Lab Chip*, vol. 12, no. 6, p. 1048, 2012.
- [61] P. N. Nge, C. I. Rogers, and A. T. Woolley, “NIH Public Access,” vol. 113, no. 4, pp. 2550–2583, 2014.
- [62] M. C. Béné, “Microfluidics in flow cytometry and related techniques,” *Int. J. Lab. Hematol.*, vol. 39, no. March, pp. 93–97, 2017.
- [63] G. Meineke, M. Hermans, J. Klos, A. Lenenbach, and R. Noll, “A microfluidic opto-caloric switch for sorting of particles by using 3D-hydrodynamic focusing based on SLE fabrication capabilities,” *Lab Chip*, vol. 16, no. 5, pp. 820–828, 2016.
- [64] J. Gottmann, M. Hermans, N. Repiev, and J. Ortmann, “Selective laser-induced etching of 3D precision quartz glass components for microfluidic applications-up-scaling of complexity and speed,” *Micromachines*, vol. 8, no. 4, 2017.
- [65] S. Lo Turco, R. Osellame, R. Ramponi, and K. C. Vishnubhatla, “Hybrid chemical etching of femtosecond irradiated 3D structures in fused silica glass,” *MATEC Web Conf.*, vol. 8, p. 5009, 2013.

- [66] V. Stankevič and G. Račiukaitis, “Formation of rectangular channels in fused silica by laser-induced chemical etching,” *Lith. J. Phys.*, vol. 54, no. 3, pp. 136–141, 2014.
- [67] S. Kiyama, S. Matsuo, S. Hashimoto, and Y. Morihira, “Examination of etching agent and etching mechanism on femtosecond laser microfabrication of channels inside vitreous silica substrates,” *J. Phys. Chem. C*, vol. 113, no. 27, pp. 11560–11566, 2009.
- [68] P. Liu, L. Jiang, J. Hu, X. Yan, B. Xia, and Y. Lu, “Etching rate enhancement by shaped femtosecond pulse train electron dynamics control for microchannels fabrication in fused silica glass,” *Opt. Lett.*, vol. 38, no. 22, pp. 4613–6, 2013.
- [69] K. Loutharback, K. S. Chou, J. Newman, J. Puchalla, R. H. Austin, and J. C. Sturm, “Improved performance of deterministic lateral displacement arrays with triangular posts,” *Microfluid. Nanofluidics*, vol. 9, no. 6, pp. 1143–1149, 2010.
- [70] O. Ogore, K. Sherpa, C. Baron, M. Zenouzi, D. Ph, and S. Krishnan, “Design of a Simplified Hemodialysis Simulation Using COMSOL,” pp. 1–12.
- [71] N. Saucedo-Zeni *et al.*, “A novel method for the in vivo isolation of circulating tumor cells from peripheral blood of cancer patients using a functionalized and structured medical wire,” *Int. J. Oncol.*, vol. 41, no. 4, pp. 1241–1250, 2012.